UNIVERSITY OF TURKU

IMAGING GLUCOSE METABOLISM, NEUROINFLAMMATION, AND CANNABINOID RECEPTOR 1 IN TRANSGENIC MOUSE MODELS OF ALZHEIMER'S DISEASE

Jatta Takkinen

TURUN YLIOPISTON JULKAISUJA – ANNALES UNIVERSITATIS TURKUENSIS
SARJA - SER. D OSA - TOM. 1418 | MEDICA - ODONTOLOGICA | TURKU 2019

UNIVERSITY OF TURKU

IMAGING GLUCOSE METABOLISM, NEUROINFLAMMATION, AND CANNABINOID RECEPTOR 1 IN TRANSGENIC MOUSE MODELS OF ALZHEIMER'S DISEASE

Jatta Takkinen

TURUN YLIOPISTON JULKAISUJA – ANNALES UNIVERSITATIS TURKUENSIS
SARJA - SER. D OSA – TOM. 1418 | MEDICA – ODONTOLOGICA | TURKU 2019

University of Turku

Faculty of Medicine
Clinical Physiology and Nuclear Medicine
Doctoral Programme in Clinical Research
Turku PET Centre
MediCity Research Laboratory

Supervisors

Adjunct Professor Merja Haaparanta-Solin, PhD
Turku PET Centre
University of Turku
Turku, Finland

Professor Olof Solin, PhD
Turku PET Centre
University of Turku
Turku, Finland

Professor Juha Rinne, MD, PhD
Turku PET Centre
Turku University Hospital
University of Turku
Turku Finland

Reviewers

Professor Heikki Tanila, MD, PhD
A.I. Virtanen Institute
University of Eastern Finland
Kuopio, Finland

Associate Professor Andrea Varrone, PhD
Department of Nuclear Medicine
Karolinska Institutet
Stockholm, Sweden

Opponent

Adjunct Professor Stina Syvänen, PhD
Department of Public Health and Caring Sciences
Uppsala University
Uppsala, Sweden

The originality of this publication has been checked in accordance with the University of Turku quality assurance system using the Turnitin OriginalityCheck service.

Cover image: Jatta Takkinen

ISBN 978-951-29-7601-0 (PRINT)
ISBN 978-951-29-7602-7 (PDF)
ISSN 0355-9483 (Print)
ISSN 2343-3213 (Online)
Painosalama Oy – Turku, Finland 2019

Make a plan.
Set a goal.
Work toward it.
But every now and then, look around.
Drink it in.
Breathe it out.
Smile.
Love.
Break the law.

Because this is it.
It might all be gone tomorrow.

To my past and present fluffies.

ABSTRACT

UNIVERSITY OF TURKU
Faculty of Medicine
Turku PET Centre
MediCity Research Laboratory
Jatta Takkinen: Imaging glucose metabolism, neuroinflammation, and cannabinoid receptor 1 in transgenic mouse models of Alzheimer's disease
Doctoral Dissertation, 176 pp.
Doctoral Programme in Clinical Research – Clinical Physiology and Nuclear Medicine
March 2019

The pathophysiological cascade leading to Alzheimer's disease is characterized by the accumulation of destructive β-amyloid in the brain. Convincing evidence has also shown that cerebral energy hypometabolism and an overproduction of translocator protein during neuroinflammation, as well as deficits in the endocannabinoid system, play major roles in progression of the disease. Monitoring temporal changes inside the diseased brain with non-invasive positron emission tomography (PET) would be a unique translational tool, bridging the gap between disease models and patients and aiding in the discovery of disease-modifying therapies against Alzheimer's disease.

The aim of this thesis was to evaluate the translational feasibility of cerebral glucose metabolism targeting PET tracer ^{18}F-FDG in APP_{swe}-PSI_{dE9}, Tg2576, and APP/PS1-21 mouse models of Alzheimer's disease. In addition, this thesis aimed to examine the suitability of neuroinflammation-specific protein targeting tracer ^{18}F-DPA-714 for longitudinal follow-up in aging APP/PS1-21 mice and whether it correlates with changes in glucose metabolism. Furthermore, the translational applicability of ^{18}F-FMPEP-d_2 was evaluated as a tool to assist in preclinical research targeting cannabinoid receptor 1 (CB_1R) in wild-type and APP/PS1-21 mice.

Of the tested models, APP/PS1-21 mice demonstrated the most aggressive β-amyloid pathology. Furthermore, repeated PET scans with ^{18}F-FDG and ^{18}F-DPA-714 detected progressive glucose hypometabolism and neuroinflammation in the APP/PS1-21 model as the mice aged. However in the APP_{swe}-PSI_{dE9} and Tg2576 mouse models, only a weak or non-altered glucose metabolism was observed. ^{18}F-FMPEP-d_2 was able to reveal altered CB_1R availability when aging APP/PS1-21 mice were followed with repeated PET scans.

This thesis work demonstrated that Alzheimer's disease mouse models differ in terms of amyloidosis and cerebral glucose metabolism, which creates challenges when comparing the research results between the models. The feasibility of ^{18}F-FDG small animal PET depends on the chosen disease model and environmental factors. In the APP/PS1-21 model, longitudinal ^{18}F-FMPEP-d_2 and ^{18}F-DPA-714 PET scans were able to demonstrate pathological features related to Alzheimer´s disease, which were confirmed by *ex vivo* examinations.

Keywords: Alzheimer's disease; positron emission tomography; small animal imaging; cerebral glucose metabolism; neuroinflammation; cannabinoid receptor; transgenic mouse model

TIIVISTELMÄ

TURUN YLIOPISTO
Lääketieteellinen tiedekunta
Turun PET-keskus
MediCity-tutkimuslaboratorio
Jatta Takkinen: Aivojen energia-aineenvaihdunnan, tulehduksen ja tyypin 1 kannabinoidireseptorin kuvantaminen Alzheimerin taudin muuntogeenisissä hiirimalleissa
Väitöskirja, 176 s.
Turun Kliininen tohtoriohjelma – Kliininen fysiologia ja isotooppilääketiede
Maaliskuu 2019

Alzheimerin taudin keskeisimmät aivomuutokset ovat sakkautuvien β-amyloidipeptidien muodostuminen plakeiksi, aivojen heikentynyt energia-aineenvaihdunta, tulehduksen lisääntyminen ja endokannabinoidijärjestelmässä tapahtuvat muutokset, jotka lopulta johtavat hermosolujen vaurioitumiseen ja tyypillisten kognitiivisten häiriöiden ilmentymiseen. Aivomuutoksia on mahdollista seurata elävässä tutkittavassa kajoamattoman positroniemissiotomografia (PET)-kuvantamisen avulla. Muuntogeenisten Alzheimerin taudin eläinmallien PET-kuvantaminen antaa ainutlaatuisen mahdollisuuden selvittää sairauden monimutkaisia patologisia tapahtumia ja seurata uusien lääkeaineiden vaikutusta ja turvallisuutta.

Tämän tutkimuksen tavoitteena oli arvioida aivojen glukoosiaineenvaihduntaa mallintavan ^{18}F-FDG-merkkiaineen soveltuvuutta muuntogeenisten APP_{swe}-PSI_{dE9}, Tg2576 ja APP/PS1-21 hiirimallien pieneläinPET-kuvantamiseen. Toisena tavoitteena oli arvioida tulehdusproteiiniin sitoutuvan PET-merkkiaineen, ^{18}F-DPA-714, soveltuvuutta aivoissa etenevän tulehduksen seuraamiseen muuntogeenisessä APP/PS1-21 hiirimallissa. Kolmantena tavoitteena oli tutkia tyypin 1 kannabinoidireseptori-PET-merkkiaineen, ^{18}F-FMPEP-d_2, soveltuvuutta pieneläinkuvantamiseen villityypin hiirillä ja Alzheimerin taudin reseptorimuutosten seuraamiseen APP/PS1-21 hiirimallilla.

APP/PS1-21 hiirimallin β-amyloidipatologia eteni muita malleja nopeammin. Lisäksi hiirimallin aivojen glukoosiaineenvaihduntaa mallintavan merkkiaineen kertymä heikentyi ja tulehdusproteiiniin sitoutuvan merkkiaineen määrä kasvoi, kun hiiriä kuvattiin toistuvasti PET-menetelmällä. Vastaavasti APP_{swe}-PSI_{dE9} ja Tg2576 hiirimalleilla havaittiin vain lievää tai olematonta glukoosiaineenvaihdunnan heikkenemistä. ^{18}F-FMPEP-d_2 PET-tutkimukset osoittivat alentunutta merkkiainekertymää APP/PS1-21 hiirimallissa verrattuna terveisiin eläimiin, ja soveltuvuutta tuleviin pieneläinkuvantamistutkimuksiin.

Tutkimustulokset osoittivat, että muuntogeeniset eläinmallit eroavat merkittävästi toisistaan, mikä asettaa haasteita tutkimustulosten vertaamiseen mallien kesken. Aivojen ^{18}F-FDG-kertymä vaihtelee tautimallin ja ympäristötekijöiden mukaan, mikä tuo rajoitteita pieneläinkuvantamisen toteuttamiseen. Sekä ^{18}F-DPA-714- ja ^{18}F-FMPEP-d_2-merkkiaineet pystyivät osoittamaan Alzheimerin taudille tyypillisiä aivomuutoksia APP/PS1-21 hiirissä, mitkä voitiin varmentaa *ex vivo* menetelmin hiirten aivoleikkeistä.

Avainsanat: Alzheimerin tauti; positroniemissiotomografia; pieneläinkuvantaminen; energia-aineenvaihdunta; tulehdus; kannabinoidireseptori; muuntogeeniset hiirimallit

TABLE OF CONTENTS

ABBREVIATIONS

^{11}C-PiB	^{11}C-labelled Pittsburgh Compound B
^{14}C-DG	^{14}C-2-deoxyglucose
^{18}F-FDG	2-deoxy-2-^{18}F-fluoro-D-glucose
^{18}F-FMPEP-d_2	((*3R*,*5R*)-5-((3-(^{18}F-fluoromethoxy-d2)phenyl)-3-((R)-1-phenyl-ethylamino)-1-(4-trifluoromethylphenyl)-pyrrolidin-2-one)
^{18}F-DPA-714	^{18}F-*N*,*N*-diethyl-2-(2-[4-(2-fluoroethoxy)phenyl]-5,7-dimethyl-pyrazolo[1,5-α]pyrimidine-3-yl)acetamide
2-AG	2-arachidonoylglycerol
%ID/g	normalized percentage of the injected radiotracer dosage per weight of the animal
γ	gamma
μ	micro
Aβ	β-amyloid
AD	Alzheimer's disease
AEA	N-arachidonoylethanolamide
am	ante meridiem
APOE	apolipoprotein E
APP	amyloid precursor protein
ATP	adenosine triphosphate
BC	before Christ
BSA	bovine serum albumin
CBR	cannabinoid receptor
CERARD	Consortium to Establish a Registry for Alzheimer's Disease
CNS	central nervous system
COX	cyclo-oxygenase
CSF	cerebrospinal fluid
CT	computed tomography
DTT	dithiothreitol
ECS	the endocannabinoid system
EO-FAD	early-onset familial Alzheimer's disease
FAAH	fatty acid amide hydrolase
fMRI	functional magnetic resonance imaging
glu	glucose
GABA	gamma-aminobutyric acid
GFAP	the glial fibrillary acidic protein
GLUT	glucose uptake transporter
HCl	hydrochloride
K_i	equilibrium constant
Iba1	ionized calcium-binding adapter molecule 1
IL	interleukin
IFN	interferon
IP	intraperitoneal
IV	intravenous
keV	kiloelectron volt
LOAD	late-onset Alzheimer's disease
LogP	partition coeffient

MAGL	monoacylglycerol lipase
MAPT	microtubule-associated protein tau
MAO-B	monoamine oxidase B
MCI	Mild Cognitive Impairment
MMSE	Mini-Mental State Examination
MRI	magnetic resonance imaging
mRNA	messenger RNA
mtDNA	mitochondrial DNA
mtRNA	mitochondrial RNA
NIA-AA	the National Institute on Aging and Alzheimer's Association
NFT	neurofibrillary tangle
p.i.	post injection
PET	positron emission tomography
pH	pondus hydrogenii
pm	post meridiem
PSEN	presenilin
PSL/mm^2	photostimulated luminescence intensity per square millimeter
p-tau	phosphorylated tau
R_f	retention factor
ROI	region of interest
ROS	reactive oxygen species
SDS	sodium dodecyl sulfate
SPM	statistical parametric mapping
SUV	standardized uptake value
SUV_{glu}	standardized uptake value corrected for the individual baseline blood glucose value
$T_{½}$	half-life
TBS-T	Tween Tris-buffered saline
TG	transgenic
TLC	thin-layer chromatography
TNF	tumor necrosis factor
T-tau	total tau
TREM2	the triggering receptor expressed on myeloid cells 2
TSPO	translocator protein
VOI	volume of interest
V_T	distribution volume
WT	wild-type
w/v	percentage of weight of solution in the total volume of solution

LIST OF ORIGINAL PUBLICATIONS

This thesis is based on the following three original publications, which are referred in the text according to their Roman numerals (**I-III**).

I Snellman A, **Takkinen JS**, López-Picón FR, Eskola O, Solin O, Rinne JO, Haaparanta-Solin M. *Effect of genotype and age on cerebral ^{18}F-FDG uptake varies between transgenic APP$_{Swe}$-PS1$_{dE9}$ and Tg2576 mouse models of Alzheimer's disease.* Submitted

II **Takkinen JS**, López-Picón FR, Al Majidi R, Eskola O, Krzyczmonik A, Keller T, Löyttyniemi E, Solin O, Rinne JO, Haaparanta-Solin M (2017) *Brain energy metabolism and neuroinflammation in ageing APP/PS1-21 mice using longitudinal ^{18}F-FDG and ^{18}F-DPA-714 PET imaging*. J Cereb Blood Flow Metab 37(8):2870-82

III **Takkinen JS**, López-Picón FR, Kirjavainen AK, Pihlaja R, Snellman A, Ishizu T, Löyttyniemi E, Solin O, Rinne JO, Haaparanta-Solin M (2018) *^{18}F-FMPEP-d_2 PET imaging shows age- and genotype-dependent impairments in the availability of cannabinoid receptor 1 in a mouse model of Alzheimer's disease*. Neurobiol Aging 69:199-208

In addition to the publications, unpublished data are also presented.

1 INTRODUCTION

Alzheimer's disease (AD) is the most common memory disorder in the aging population and is characterized by a progressive cognitive decline and loss of memory, eventually leading to the need for institutional care and the development of terminal secondary illnesses. In Finland, the number of people stricken with age-related dementia is estimated to be over 190 000, with that number increasing by approximately 14 500 new cases every year due to the increasing numbers of elderly (THL muistisairauksien yleisyys). AD is traditionally explained by an aggressive accumulation of abnormally formed β-amyloid (Aβ) peptide outside the cells and intracellular aggregation of hyperphosphorylated tau protein in paired helical filaments, eventually forming dense neuritic plaques and neurofibrillary tangles (NFTs), respectively, and leading to synaptic disruption and neuronal cell death (Braak and Braak 1997). Previously, these histopathological hallmarks were detected only via *post mortem* from brain autopsy samples dissected from deceased AD patients. In addition to the proteinopathological changes, years of in-depth research have produced a convincing body of evidence indicating that other pathological changes are involved in progression of the disease and, thus, in the cognitive decline. These complex signaling pathways include proinflammatory revival, mitochondrial dysfunction, altered cerebral glucose metabolism, and deficits in several aspects of the neurotransmitter machinery, including the endocannabinoid system (ECS), many of which are thought to be present decades before the first symptoms (Bedse et al. 2015; Clarke et al. 2018; Hansen et al. 2018). Currently, no single method is available that can help in making a reliable AD diagnosis, although several tools have been utilized for examining human memory and cognition, as well as revealing structural alterations in the brain, and changes in the levels of cerebrospinal fluid (CSF) biomarkers (Käypä Hoito A 2016).

Positron emission tomography (PET) is a nuclear medical imaging method that can be used for real-time monitoring of tissue metabolism or neurotransmitter function in a living human or animal. PET is based on the administration of tracers labelled with radioactive isotopes, which target a specific biological system. Consequently, PET has represented a noninvasive way to follow changes in cerebral energy metabolism or Aβ plaque formation inside the brain of a living AD patient. Even though PET is beneficial in clinical research, this imaging method is still too laborious to be used in routine diagnostics, although it is applied to examine borderline cases (Rabinovici et al. 2007; Foster et al. 2007; Minoshima et al. 2001; Bohnen et al. 2012). 2-Deoxy-2-^{18}F-fluoro-D-glucose (**^{18}F-FDG**) is a glucose analogue that can be used to detect *in vivo* decreases in cerebrocortical glucose metabolism, which are considered to be one of the major pathological hallmarks in the AD brain. The severity of the hypometabolic features has been correlated with the temporal pattern of cognitive decline. For this reason, ^{18}F-FDG PET findings have been included into the small pool of the AD diagnostic biomarkers (Jack et al. 2013 and 2018). However, disease models of AD have revealed fluctuating cerebral metabolism in response

to the variable methodological and analytical procedures, as well as genetic differences between the models. Nevertheless, the deterioration in glucose utilization within human neurons has been postulated to originate mainly from a functional impairment of *mitochondria*, the energy powerhouse of the cell. Mitochondrial respiration is thought to be detrimentally affected by the upregulation of *translocator protein* (TSPO; Papadopoulos et al. 2006). TSPO is abundantly present on the glial cell membrane in a known neuroinflammatory process in trauma and neurodegenerative diseases (Chen and Guilarte 2008). Currently, non-specific TSPO increase in AD cascade can be monitored by PET in clinical and preclinical research. One of the many radiotracers useful for this purpose is ^{18}F-*N*,*N*-diethyl-2-(2-[4-(2-fluoroethoxy)phenyl]-5,7-dimethyl-pyrazolo[1,5-α]pyrimidine-3-yl)-acetamide (**^{18}F-DPA-714**), which possesses useful characteristics, including the ability to discriminate AD patients from healthy controls (Hamelin et al. 2016). This differentiating property has also been demonstrated in an AD transgenic (TG) mouse model (Sérrière et al. 2015; Chaney et al. 2018). However, the search for a reliable PET imaging agent that targets neuroinflammation is still a work in progress, underlining the need for further evaluation studies with different tracers and neuroinflammation targets with respect to AD. *The type 1 cannabinoid receptor* (CB_1R) may be one of these targets; this system has been suggested to participate in the pathological pathways involving mitochondrial dysfunction and neuroinflammation. CB_1R is one of the most abundant receptors in the brain, and is present not only in the neuronal membranes but also at the mitochondrial membrane (Brailoiu et al. 2011). These receptors are part of the complex cerebral system that controls excitatory and inhibitory neurotransmitter release, synaptic plasticity, memory, and the immune system (Freund et al. 2003; Benard et al. 2012). Disturbances within this system have been shown to enhance proinflammatory responses via glia cells that may provide an indirect measurement of neuroinflammation in the diseased brain (Bedse et al. 2015). However, despite researchers investigating PET tracers targeting CB_1Rs for the past 10 years, progress has been slow, and monitoring changes in receptor availability in neurodegenerative diseases has been challenging. One of the most recently designed radioligands, ((*3R*,*5R*)-5-((3-(^{18}F-fluoromethoxy-d_2)phenyl)-3-((R)-1-phenyl-ethylamino)-1-(4-trifluoromethyl-phenyl)-pyrrolidin-2-one) (**^{18}F-FMPEP-d_2**), has demonstrated to possess superior tracer qualities, including reduced lipophilicity compared to the previously developed CB_1R PET ligands (Terry 2009a; Terry et al. 2010). Thus, the applicability of this tracer would be interesting to evaluate in laboratory mice and preclinical studies related to AD. If it proves capable of revealing temporal CB_1R changes in AD disease models then hopefully it could be applied in AD patients in the future.

Disease-modifying therapeutics are not yet available for AD. Anti-amyloid targeting drug discovery has been unsuccessful, perhaps because of the large number of unresolved questions regarding the neurodegeneration in both the human brain and animal models. Thus, there is an urgent need to clarify the pathogenic profile beyond amyloid plaques in a causal and temporal manner, and to unravel the interplay between different pathological pathways leading to AD.

Therefore, the aim of this thesis work was to evaluate the translational usability of cerebral glucose utilization, TSPO-based neuroinflammation, and CB_1Rs targeting PET radioligands for use in preclinical *in vivo* imaging studies in AD mouse models. Three TG mouse models (APP_{swe}-PSI_{dE9}, Tg2576, and APP/PS1-21) were evaluated using the cerebral glucose metabolism targeting PET tracer ^{18}F-FDG with cross-sectional APP_{swe}-PSI_{dE9} and Tg2576; Study **I**) or longitudinal (APP/PS1-21; Study **II**) study protocols. The longitudinal follow-up suitability of TSPO targeting tracer ^{18}F-DPA-714 (Study **II**) and CB_1R targeting tracer ^{18}F-FMPEP-d_2 (Study **III**) were examined in aging APP/PS1-21 mice. In addition, prior to the follow-up study in APP/PS1-21 mice, the applicability of ^{18}F-FMPEP-d_2 was evaluated in mice focusing on metabolism, distribution, and specificity with the respect of future preclinical *in vivo* imaging studies (Study **III**). The relationships between Studies **I**-**III** are illustrated in *Figure 1*.

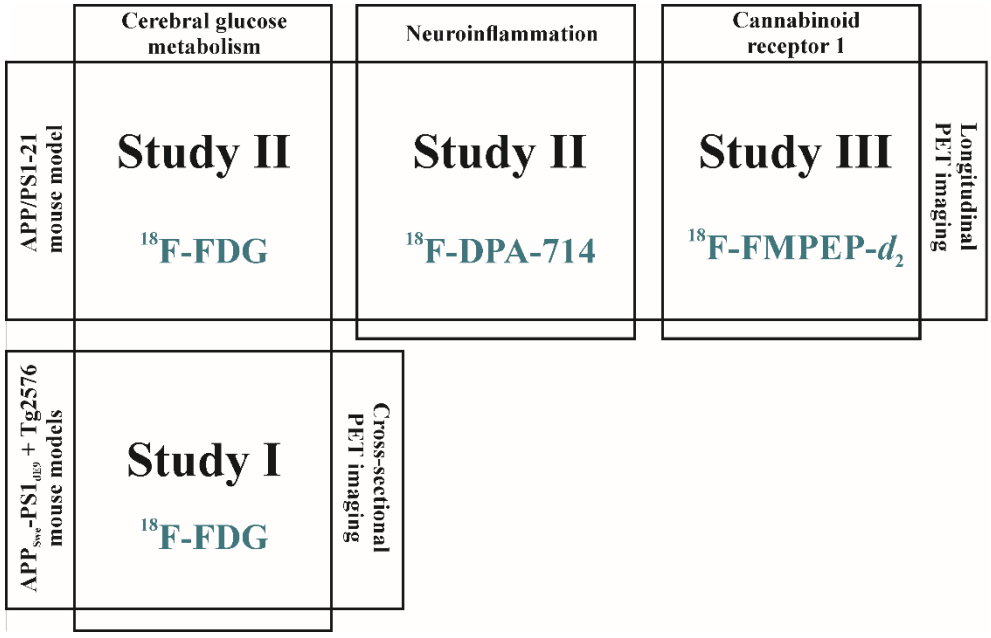

Figure 1. The interconnections between the Studies I–III.

2 REVIEW OF LITERATURE

2.1 FROM COGNITIVE DECLINE TO ALZHEIMER'S DISEASE

"Diseases of all kind dance around the old man in a troop. But worse than any loss in the body is the failing mind, which forgets the names of slaves, and cannot recognize the face of the old friend who dined with him last night, nor those of the children whom he has begotten and brought up."

Juvenal, 1st century

The history of dementia extends almost 3000 years back to the ancient Mediterranean cities. One of the oldest descriptions of human memory deficits originates from the ancient Egyptian maxim from the 8th century before Christ (BC), which further puzzled several famous Greek philosophers, Pythagoras, Plato, and Aristoteles. In the late era of the Greek-Roman medicine in the 2nd century BC, a famous doctor Galenos postulated the most popular theory for cognitive decline, *dementia senilis*, which referred to an inevitable cognitive decline due to aging (Berchtold and Cotman 1998; Haltia 2003). Unfortunately, many individuals with dementia were most often viewed as being mentally insane and therefore, were kept incarcerated in prisons. It was not until the beginning of the 19th century, when a French physician, Philippe Pinel, suggested that insanity was not a crime, but more often a disease. Ultimately, this humanitarian reform led to identification of different forms of mental disorders with dementia being subdivided into different categories (McGrew 1985). In late 19th century, the progress in clarifying the brain anatomy as well as advances in instrumentation and microscopy increased our understanding of the relationship between brain weight loss and arteriosclerotic atrophy with the symptoms of dementia. The German psychiatrist and neuropathologist, Alois Alzheimer, observed in the 1890's that atheromatous blood vessel degeneration accompanied with stroke was a crucial triggering event for the development of brain atrophy and senile dementia (Forstl and Howard 1991). In 1906, by applying recently developed staining methods, Alzheimer was able to reveal startling neuropathological features, such as abnormal fibrils and deposits, in the brain of his deceased 51-year-old patient, Auguste Deter. After years of following the progression of the cognitive impairment in his patient, and finally confirming that the abnormal histopathological brain changes were related to the symptoms, Alzheimer was able to publish the first clinical description of new brain disease, which we currently recognize as AD.

Cognitive decline and dementia

Cognition is a process in which knowledge and understanding are involved when a person is thinking, feeling, or experiencing. Subtle declines in cognition are a common feature during healthy aging in terms of learning, remembering, or performing executive functions (Salthouse 2012), however the kinds of declines in cognitive functions that affect an individual's everyday life, are considered as abnormal and feared. Abnormal cognitive decline consists of impairments in inductive reasoning, spatial orientation, perceptual speed, and abilities in numeric and verbal

understanding (Ray and Davidson 2014). One of the stops on the continuum of the cognitive decline is Mild Cognitive Impairment (MCI) with healthy aging at one end of the spectrum and diagnosed dementia at the other. The prevalence of MCI is between 10% to 20% in adults aged 65 or over, and it is a clinical stage, in which although a cognitive impairment is evident, it does not interfere with the person's abilities to perform everyday life tasks (Knopman and Petersen 2014; Plassman et al. 2008). In contrast, clinical dementia is a progressive heterogenic syndrome that is composed of a complex deterioration in cognitive function caused by a variety of different diseases or brain injuries (*Figure 2*). The most characteristic dementia symptoms are memory loss, an inability to manage straightforward tasks, and changes in mood and personality. To date, there are over 100 causative forms of dementia, with the most common being AD, vascular dementia, dementia with Lewy bodies, Parkinson's dementia, and frontotemporal dementia; all of these diseases cause temporal brain damage and loss in memory via different mechanisms with different disease onsets. Currently, 50 million people worldwide have been diagnosed with some kind of clinical dementia, but it is believed that many more are never diagnosed. It is projected that the total number of dementia patients will reach nearly 152 million by 2050, and the majority, approximately 60−70% of all dementia cases are attributable to AD (Patterson 2018; WHO 2018 Dementia).

AD is an irreversible, progressive neurodegenerative syndrome that abnormally affects the aging brain by destroying cognition, deteriorating episodic memory, causing abnormal behavior and mood, and increasing the difficulties in coping with everyday life. While the disease progresses, the ability to recognize time and place becomes impossible (Jack et al. 2018). Traditionally, AD has been divided in the clinic into three different phases according to the symptoms: preclinical, prodromal, and AD dementia. *Preclinical AD* refers to a stage where pathological processes in the brain have begun to progress but there is no signs of symptoms crossing any clinical diagnostic threshold. Only recently, preclinical AD has been divided further into three sub-stages according to CSF biomarkers, which include abnormal amyloid markers (stage 1), with a combination with tau markers (stage 2), and the presence of a subtle cognitive decline (stage 3) (Sperling et al. 2011). *Prodromal AD* refers to a predementia phase, where mild cognitive alterations have already occurred with confirmed brain imaging markers. The differentiation between prodromal AD and MCI is suggested to be somewhat mercurial, since in both cases, there is a decline in one or more distinguished cognitive domains. In *AD dementia*, cognitive impairments have become so obvious that they pass the threshold for a clinical diagnosis since individual's abilities to perform simple daily duties have become evidently restricted (Dubois et al. 2014). Not surprisingly, these stages might overlap with one and another, and the different stages are difficult to distinguish. Thus, the recent proposals issued by the National Institute on Aging and Alzheimer's Association (NIA-AA) state that AD should regarded as a continuum, and not separated into distinct stages (Vos et al. 2013; Dubois et al. 2014; Jack et al. 2018).

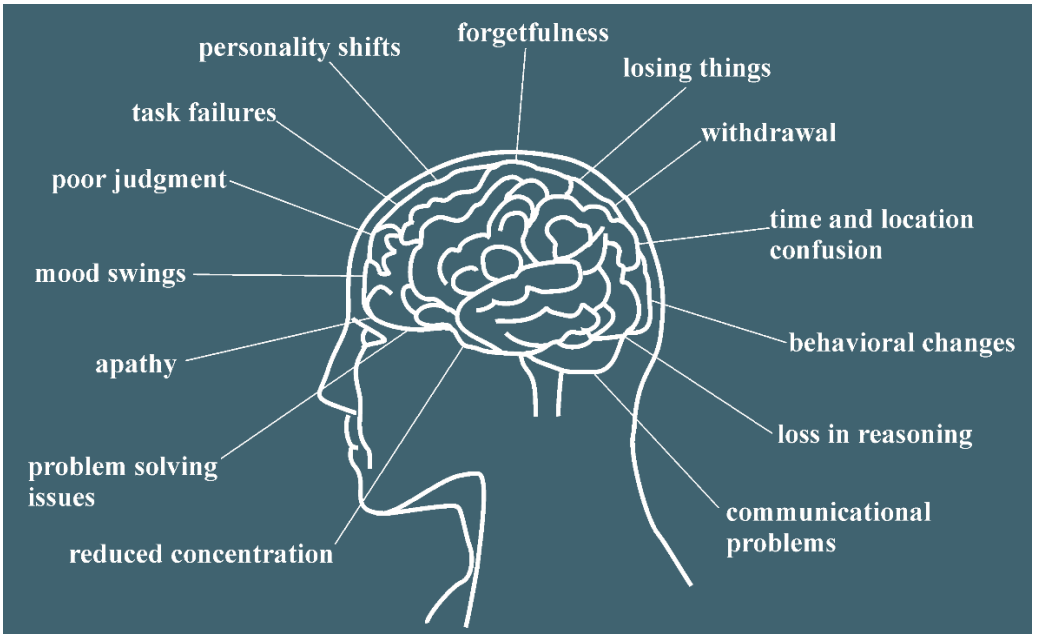

Figure 2. Typical warning signs related to dementia syndromes. Characteristical symptoms may become evident already at the early disease phase or during progressed dementia.

In histopathological aspect, the most known characteristic findings in the AD brain are a shrinkage in the cortical and hippocampal gray matter, and an enlargement of the ventricles. These pathological hallmarks progress for decades, and start long before there are signs of cognitive decline. In neuropathological level, AD is characterized by an abnormal aggregation of extracellular Aβ peptide fragments and intracellular NFTs of paired helical filaments composed of hyperphosphorylated tau proteins (Braak and Braak 1997). Temporally, Aβ pathogenesis begins in the neocortex, then extends to the subcortical structures and cerebellum as the disease progresses, whereas NFTs have been shown to originate from the transentorhinal cortex and extend to the hippocampus and neocortical area (Braak and Braak 1997; Thal et al. 2002).

This review of literature will focus on AD, especially on the risk and protective factors of the disease, and then proceed to examine the complex pathophysiological mechanisms behind the cognitive dysfunctions. Finally, in conjunction with the expanding knowledge of current AD diagnostics and the potential of using PET for this task, we will justify the thinking behind the experiments conducted and described in the original publications.

Risk factors

The causality of AD is still a matter of debate even though it has been investigated for decades. While age is known to be the greatest risk factor for developing AD, there are also numerous genetic and environmental risk factors involved with the disease. Since AD is a heterogenic

disease with no curative treatment available, confirming the potential risk factors would enable the early detection in the establishment of the disease in individuals even before irreparable damage had occurred. In the end, this could open new vistas for drug discoveries.

Genetic risks

The characteristic differentiation into either early-onset familial (EO-FAD) or late-onset AD (LOAD) is based on an evaluation of risk factors of the disease - age and genetic background. Only 1–5% of the patients have an EO-FAD profile, which affects individuals already at an age between 30 to 60 years (Reltz 2011). EO-FAD is considered to be a more severe and aggressive form of the disease and is usually linked with autosomal dominant mutations in one of the three genes: Amyloid precursor protein (*APP*, in chromosome 21), presenilin-1 (*PSEN1*, in chromosome 14) or presenilin-2 (*PSEN2*, in chromosome 1). These genes encode APP and presenilin proteins 1 (PS1) and 2 (PS2) that are involved in the proteolytic processes, which eventually lead to the Aβ peptide production, the principal compound in the protein aggregates found in the brains of AD patients (Goate et al. 1991; Sherrington et al. 1995; Levy-Lahad et al. 1995). Mutations in *PSEN1* represent the majority of the EO-FAD cases, while *APP* and *PSEN2* mutations are rarer (Tanzi 2012). Furthermore, recent findings also suggest that there are different risk genes other than *APP*, *PSEN1*, or *PSEN2* involved in the heritability of AD (Rademakers et al. 2005; Ostojic et al. 2004), and a protective *APP* gene variant against amyloid pathology exclusively among Icelandic and Scandinavian people (Jonsson et al. 2012).

The majority of the AD patients are considered to have LOAD i.e. a sporadic profile, with the symptoms usually developing after the age of 65. From the clinical point-of-view, EO-FAD and LOAD are generally agreed to be the same disease, although there are distinguishable differences in the underlying temporal pathogenesis. Although the origin of LOAD is still unresolved, there is a convincing body of evidence that the onset of the disease is composed of complex interactions between genetic risk factors and the environmental risks and lifestyle choices, which together determine the lifetime risk for developing clinical AD (Tanzi 2012). It is apparent that no specific gene is responsible for the establishment of LOAD, however, one gene variant, an ε4 allele of the apolipoprotein E gene (*APOEε4*, in chromosome 19) has been demonstrated to increase the LOAD risk (Strittmatter et al. 1993; Tanzi 2012). A single ε4 allele increases the risk by approximately 3-fold, whereas two copies elevates the risk for AD nearly by 16-fold. However, the precise mechanism by which *APOEε4* elevates the AD risk is not totally understood, but the presence of this allele is not considered to be necessary for developing LOAD since not all *APOEε4* carriers are destined to suffer AD (Myers et al. 1996). In addition to *APOEε4*, numerous genome-wide association studies have shown that there are other risk gene variants involved in the pathogenesis of LOAD, such as neuronal sortilin-related receptor gene (Rogaeva et al. 2007), the clusterin gene, the complement component (3b/4b) receptor encoding gene, the PI-binding clathrin assembly protein encoding gene (Harold et al. 2009; Lambert et al. 2009), and the

bridging integrator 1 gene (Tan et al. 2013). Furthermore, the discovery of an AD-variant of the triggering receptor expressed on myeloid cells 2 gene (*TREM2*) as being highly expressed by microglia cells in the AD brain emphasized the crucial role of neuroinflammatory markers in AD onset (Guerreiro et al. 2013; Jonsson et al. 2013; Reltz 2011; Onyango 2018).

Environmental risks

Several environmental risk factors and lifestyle choices have been linked to the dementia pathway, affecting the disease etiology or the overall outcome. *Figure 3* represents the wheel of the potential modifiable dementia risk factors, which are collected from several epidemiological cohort studies and reported annually by the global Alzheimer's Disease International federation (www.alz.co.uk). *Females* are more likely than males to develop sporadic AD; this difference has been speculated to be related to the *APOEε4* allele, metabolic factors, and estrogen interaction during the menopause (Duarte et al. 2018). *Traumatic brain injury*, *depression*, *physical inactivity*, midlife *obesity*, and *low educational attainment* have shown to further exert an impact on overall health and the prevalence of AD (Fleminger et al. 2003; Hartman et al. 2002; Franz et al. 2003; Norton et al. 2014; Reitz and Mayeux 2014), together with *alcohol overconsumption* and *smoking* (Harwood et al. 2010; Norton et al. 2014; Käypä Hoito A 2016). *Cerebrovascular impairments* in response to severe vascular disorders, such as ischemic stroke, atherosclerosis, mid-life *hypertension*, and cardiac diseases, have also been shown to be linked to dementia by increasing the overall risk (Kivipelto et al. 2001; Whitmer et al. 2005; Morović et al. 2009; Viswanathan et al. 2009; De la Torre 2009; Skoog and Gustafson 2003). In addition, there is evidence emphasizing the strong relationship between *type 2 diabetes* and AD, indicating that insulin resistance or impairments in insulin signaling promote neurodegenerative pathology and double the risk for disease prevalence (Takeda et al. 2010; Leibson et al. 1997; Mehla et al. 2014) via neuroinflammatory or oxidative stress related mechanisms (Bharadwaj et al. 2017). Consequently, according to a population-based and proof-of-concept randomized controlled trial, risk factors involved in *midlife obesity* and *hypertension*, *type 2 diabetes*, *smoking*, *depression*, and *low education* could potentially be prevented if an individual was better informed, motivated, or treated (Ngandu et al. 2015; Reitz and Mayeux 2014). *Exercise* might assist controlling the body weight as well as promoting mental and brain health. Physical activity triggers continuous oxidative stress that induces a series of counteractive mechanisms enhancing mitochondrial function to combat the effects of reactive oxygen species (ROS) (Onyango et al. 2010; Radak et al. 2016). Some *dietary choices*, such as a diet rich in vegetables, fruits, and polyunsaturated fatty acids but low in red meat and added sugar, have been shown to reduce the incidence of metabolic disorders and thus, AD (Scarmeas et al. 2006). Other beneficial factors preserving health and cognition include an *active social network and lifestyle*, and *high education* (Reitz and Mayeux 2014).

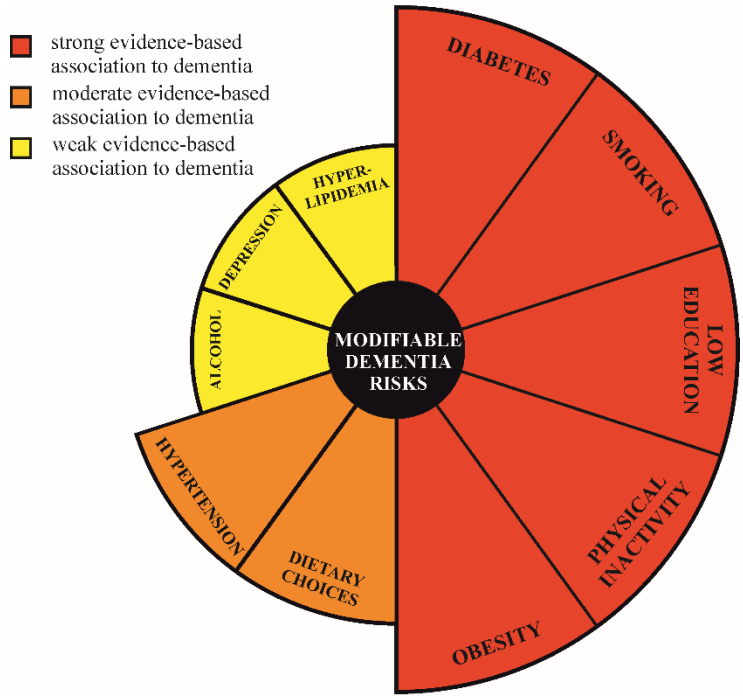

Figure 3. Wheel of the evidence-based, modifiable dementia risk factors targeted especially to middle-aged people. Strongest evidence of the association to dementia risk has been found with the type 2 diabetes, smoking, low education, physical inactivity, and mid-life obesity. Moderate association to dementia risk has been identified with mid-life hypertension and unfavorable dietary choices. Weak evidence-based association has been demonstrated with alcohol overconsumption, suffered depression, and hyperlipidemia for overall dementia risk. Modified from the World Alzheimer's Report 2014.

2.2 ALZHEIMER'S DISEASE – PATHOGENESIS

The complexity of AD pathophysiology has been investigated for decades, yet the origin of the disease is still a mystery, emphasizing the complexity of the undiscovered mechanisms behind the pathological processes of this disease. It is, however, recognized that AD is not due to a single culprit, which is responsible for the neuronal cell loss, instead several mechanisms have been shown to play a role in the etiology of AD. Therefore, the ongoing AD research has concentrated on seeking new mechanisms in addition to the well-known amyloid cascade.

2.2.1 Proteinopathies

The amyloid cascade hypothesis has greatly influenced AD research such as the search for therapeutic interventions, perhaps due to its undoubted benchmark status in the etiology of AD. According to the original hypothesis, the amyloid cascade consists of a complex series of events in which the production and accumulation of pathological microaggregates of $A\beta_{1\text{-}42}$ lead to the formation of hyperphosphorylation of tau, and eventually to neuronal cell loss and the appearance

of clinical dementia (Hardy and Higgins 1992; Hardy and Selkoe 2002).

Type I glycosylated transmembrane protein APP is involved in several neuronal functions including neural stem cell development, neuronal survival and repair, and synaptic plasticity (Dawkins and Small 2014) even though the main physiological function of APP remains unknown. The *APP* gene is located in chromosome 21, and the corresponding APP protein is considered to be the precursor of the main pathological component of amyloid plaques in AD, **Aβ peptide**. APP is synthetized in the endoplastic reticulum from where it is first transported to the trans-Golgi-network and then to the cell surface (Zhang et al. 2011), where it is cleaved by α-secretase (*non-amyloidogenic pathway*) or β-secretase (*amyloidogenic pathway*). Cleavage by α-secretase produces soluble APP ectodomains (sAPPα), which have been linked to neuronal plasticity and cell survival, whereas cleavage by β-secretase forms APP ectodomains releasing soluble APPβ, which have been shown to mediate neuronal cell death (Nikolaev et al. 2009). After the cleavage by β-secretase, the remaining carboxyl terminal fragment of APP (CTFβ) in the cell membrane is further cleaved by γ-secretase, which is composed of active PS1 and PS2, and generates soluble $A\beta_{1\text{-}40}$ and $A\beta_{1\text{-}42}$ while releasing the intracellular APP domain (AICD) (*Figure 4*). $A\beta_{1\text{-}42}$ is more prone to fibril formation and further aggregation into soluble Aβ oligomers. An $A\beta_{1\text{-}42}$ or $A\beta_{1\text{-}42}/A\beta_{1\text{-}40}$ ratio increase will trigger the formation of Aβ amyloid fibrils, which further develop into senile plaques. This event is suggested to be the main cause in the establishment of neurotoxicity and tau pathology, as well as neuronal cell death, oxidative stress, and glia cell activation (Hardy and Higgins 1992; Zhang et al. 2011; Kametani and Hasegawa 2018).

The amyloid cascade hypothesis has been supported by the discovery of autosomal dominant mutations in three genes *APP*, *PSEN1*, and *PSEN2*, all of which enhance the production of Aβ in EO-FAD. However, this hypothesis has faced criticism with regard to the biased pathological mechanisms and their relationship to the disease onset and cognition (Aizenstein et al. 2008; Mintun et al. 2006), and thus, evidence emerging in the last two decades has brought new perspectives into our understanding of AD. Aβ peptide, while being the key component in neuritic plaques in AD, is also a typical APP secretion product during normal cellular metabolism (Haass et al. 1992). It has also been postulated that insoluble $A\beta_{1\text{-}42}$ fibrils would not be responsible for the synaptic dysfunction, but instead the culprits are the soluble Aβ oligomers that are impossible to detect in amyloid plaque immunohistochemical stainings (Selkoe 2000; Hardy and Selkoe 2002). Furthermore, some evidence has proposed that Aβ accumulation and tau pathology are two interacting independent series of events (Duyckaerts 2011). This proposal is supported with the fact that genetic mutations in Aβ production lead to clinical AD, whereas a genetic tauopathy does not cause AD (Goate et al. 1991; Hutton et al. 1998). Aβ accumulation has been shown to impair cerebral blood flow, which lowers the availability of glucose within the neurons, further worsening the cerebral blood flow and activating neuronal cell death (Popa-Wagner et al.

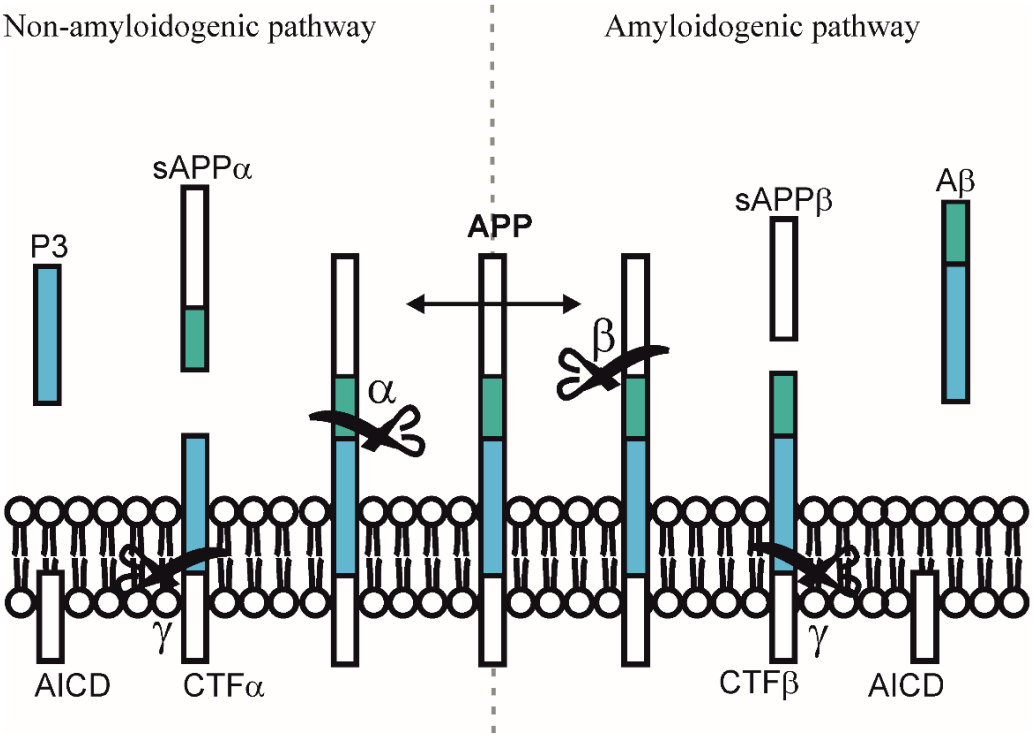

Figure 4. Amyloid precursor protein (APP) processing by two different pathways. In non-amyloidogenic pathway, a cleavage by α- and γ-secretase will produce secreted (sAPPα) and intracellular (AICD) APP domains. In the amyloidogenic pathway, the cleavage by β- and γ-secretase will produce an intracellular APP domain (sAPPβ), but also a variety of β-amyloid (Aβ) peptides of different lengths, of which $A\beta_{1\text{-}40}$ and $A\beta_{1\text{-}42}$ are related to Alzheimer's disease. The figure was inspired by Fig. 1 in Amtul 2016.

2015). Indeed, Aβ is known to speed up the AD pathogenesis, however, on its own, it might be unable to trigger neurodegeneration or cognitive decline (Jack et al. 2018). The most recent data from a longitudinal follow-up study with asymptomatic at-risk individuals for AD indicated that Aβ should not be considered as a cause of AD, but rather as one of the risk factors (Dubois et al. 2018). These discrepancies in the amyloid cascade hypothesis might partly explain the failures of anti-amyloid treatment clinical trials, and emphasize the need to examine the possible benefits of non-amyloid treatment approaches.

Neurodestructive **tau** depositions, i.e. intracellular NFTs in the brain, are the earliest neuropathological feature and a hallmark of the AD pathogenesis, being detectable as early as before the age of ten (Braak and Del Tredici 2011). It has been suggested to be one of the variants leading to cognitive impairment in later adulthood, because studies have revealed a correlation between NFT and gray matter atrophy loci, i.e. neurodegeneration, seen in the early AD (Braak et al. 2006). NFTs are formed from aggregates of filamentous tau protein, which is an unfolded protein that binds to the axonal (Binder et al. 1985) or dendritic (Tashiro et al. 1997; Klein et al. 2002) microtubules in order to stabilize the cell structure. Tau has a total of six isoforms, which

are expressed as three (3R) or four (4R) replicates and produced via alternative splicing of microtubule-associated protein tau gene (*MAPT*) in chromosome 17 (Goedert et al. 1989). The microtubule binding properties of tau are dependent on its phosphorylation status and the resulting conformation, as well as being linked with the activities of the related kinases and phosphatases (Hanger et al. 2009). Excessive phosphorylation of tau as a result of conformational changes, *MAPT* mutations, or interactions with other proteins, such as Aβ, is speculated to lead to neuronal dysfunction and eventually to its accumulation and aggregation into paired helical filament structures (Braak and Braak 1997; Lewis et al. 2000). The tau hypothesis in AD, on the other hand, differs from the mainstream amyloid hypothesis; it postulates that the dendritic accumulation of tau makes neurons more vulnerable to Aβ depositions, and thus, accelerates the pathogenetic processes leading to AD (Kametani and Hasegawa 2018). This hypothesis is supported by the evidence of the appearance of the tau lesions preceding earlier than amyloid deposition (Braak and Del Tredici 2014; Bennett et al. 2004).

2.2.2 Neurodegeneration

Synaptic impairment and neuronal cell loss are very early events in the pathogenesis of AD, being present in the preclinical stage of the disease. The cell loss progresses to gray matter atrophy, which initiates in the hippocampal cell layer CA1 and entorhinal cortex layer 2 (Bali 1977; Gómez-Isla et al. 1996). Atrophy further spreads to the temporal gyrus, and frontal and parietal cortices (Coleman and Flood 1987), and during the late stage of the disease, to the entire brain. Synaptic loss and neuronal damage are thought to be derived from several factors, such as synaptic protein malfunction or decreased mitochondrial RNA (mtRNA) levels (Callahan et al. 1999; Gylys et al. 2004) but most prominently from the accumulation of NFTs, which correlates well to the gray matter atrophy and progressive cognitive decline (Jack et al. 2013). In contrast, convincing evidence for a correlation between neuronal loss and Aβ pathology is still missing (Jack et al. 2018).

2.2.3 Metabolic impairments

The indisputable causal role of the abnormal protein aggregation in the EO-FAD poorly explains the underlying causes for sporadic AD. Thus, alternative hypotheses have emerged in response to the growing body of evidence postulating that AD is far more complex than being simply a proteinopathy. Findings from clinical and animal studies have revealed that a variety of metabolic impairments begin to develop within several biological systems related to energy production and insulin-related activities (Clarke et al. 2018). The metabolic disturbances related to obesity and diabetes have also been shown to be associated with AD, sharing many similar biological features (Bharadwaj et al. 2017; De Felice 2013; De Felice and Ferreira 2014). In normal circumstances, neuronal energy metabolism and brain glucose utilization include mitochondrial-generated

oxidative phosphorylation, insulin signaling pathways, and glucose transporter mediated energy uptake. Together these form a complex of synergistic and symbiotic processes involving multiple signaling pathways, metabolites, enzymes, transporters, and other compounds, which all work in parallel to maintain neuronal functionality. In terms of energy metabolism, AD is traditionally characterized by decreased neuronal glucose uptake, impaired insulin signaling, and altered receptor functions related to energy production or transfer; these will be briefly discussed in the following chapters (Yin et al. 2016; Clarke et al. 2018).

During normal cell homeostasis, **mitochondria** play a key role in energy metabolism and apoptosis, transferring and storing the energy that cells need via adenosine triphosphate (ATP). It is vital for the cell survival that these organelles function efficiently and there is an equilibrium between mitochondrial fusion and fission reactions. This ensures steady energy production, cell homeostasis, Ca^{2+} signaling, normal production of ROS, and regulation of apoptosis (Chan 2006; Chen et al. 2005; McBride et al. 2006; Yu et al. 2006). In neurons, mitochondria have been demonstrated to be involved in neurotransmission by regulating the ATP levels in the nerve endings (Smith et al. 2016; Pathak et al. 2015). Thus, not surprisingly, impairments in this crucial energy metabolic system lead to disruption of neuronal function and structure.

Mitochondrial dysfunction and oxidative stress are early signs in the pathogenesis of AD, which are considered to be consequence behind the glucose dysmetabolism detected in both AD patients and disease models (Yao et al. 2009; Du et al. 2010; Sultana et al. 2011; Reddy 2011). This important finding has encouraged researchers to speculate on the causes of sporadic AD. The best known explanation, the **mitochondrial cascade hypothesis**, postulates that in LOAD, bioenergetic dysfunction as a result of genetic mutations in mitochondrial DNA and environmental factors, together with the impact of age, determine the rate of the pathological mitochondrial changes (Swerdlow and Khan 2004; Swerdlow et al. 2014; Stewart and Chinnery 2015). These detrimental mitochondrial changes can lead to overexpression of oxidative stress markers, tau phosphorylation, inflammasome activation, alterations in APP processing, and the synthesis of $A\beta_{1\text{-}42}$ (Blass et al. 1990; Zhou et al. 2011; Swerdlow et al. 2014). Oxidative stress further increases the production of ROS and reactive nitrogen species including superoxide radical anions, nitric oxide, and peroxynitrile to levels capable of triggering the neurodegeneration while decreasing the production of ATP (Tönnies and Trushina 2017) (*Figure 5*). In contrast to the hypothesis explaining metabolic impairments in LOAD, Aβ is thought to be the key mediator leading to mitochondrial impairments in EO-FAD as a consequence of the autosomal dominant mutations causing mitochondrial impairments, which further trigger the characteristic series of metabolic events leading to AD. However, the mitochondrial cascade may not be the complete story since previous studies with cells, disease models, and *post mortem* samples related to AD have shown that Aβ accumulates into the mitochondrial compartment, which may result in mitochondrial dysfunction and further neuronal cell death (Devi et al. 2006;

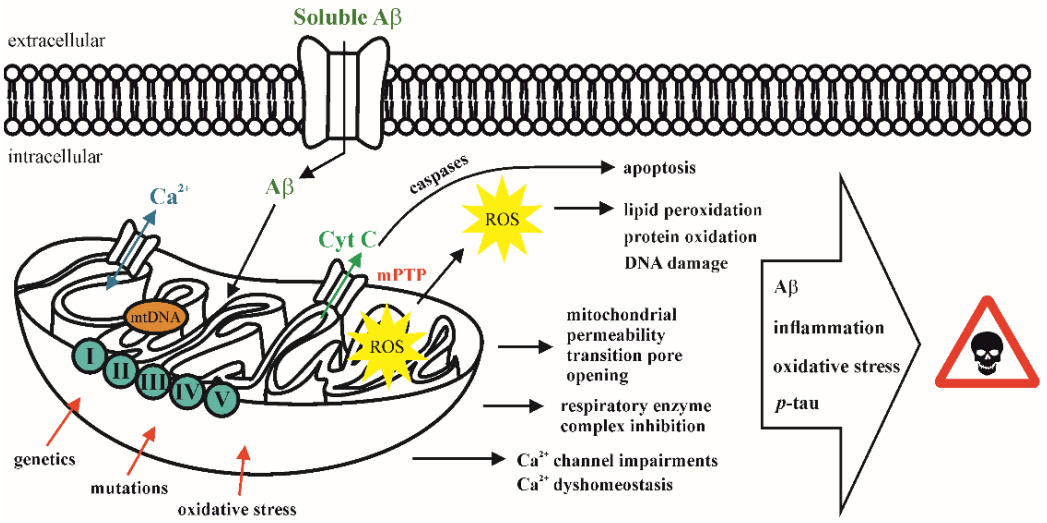

Figure 5. Mitochondrial dysfunction in Alzheimer's disease. Mitochondrial cascade is suggested to be originated from the intracellular β-amyloid (Aβ) accumulation, inherited and unfavorable genetic factors, mutations in mitochondrial DNA (mtDNA), or oxidative stress induced from the environmental factors. Mitochondrial dysfunction is suggested to manifest pathological events related to apoptosis, production of reactive oxygen species (ROS), Ca^{2+} channel impairments, opening in mitochondrial permeability transition pore (mPTP), and inhibition of respiratory enzyme complex, which are further increasing oxidative stress, inflammatory signaling, and abnormal proteinopathies including Aβ and phosphorylated tau (*p*-tau). Eventually, these changes enhance neuronal cell damage. *Cyt C*, cytochrome C.

(Anandatheerthavarada and Devi 2007). Even though there is no consensus about the main reason in evoking metabolic impairments in AD, i.e. Aβ or mitochondrial deficits, mitochondria are known to be structurally and functionally altered in AD (Burte et al. 2015; Cai and Tammineni 2016; Onyango 2018). *Post mortem* experiments have further shown that mitochondrial enzymes are underexpressed, mitochondrial mass is decreased, and the amount of mitochondrial DNA (mtDNA) increased in the intracellular fluid (Terni et al. 2010; Maurer et al. 2000; Clarke et al. 2018). Mitochondrial dysfunction has further shown to be accompanied by a release of pro-apoptotic proteins via Ca^{2+}-induced events, which leads to cellular apoptosis and vascular defects, and metabolic disturbances (Moreira et al. 2001 and 2002).

In addition to energy metabolic impairments, brain **insulin signaling** has been reported to be impaired in AD not only in the human brain but also in the TG disease models (De Felice 2013; De Felice and Ferreira 2014; Talbot et al. 2012; Sancheti et al. 2013). Brain insulin resistance has been shown to be an early marker in AD pathogenesis with a characteristic features related to altered signaling pathways promoting tau hyperphosphorylation and synaptic destruction (Liu et al. 2011; Grillo et al. 2015). Insulin and insulin-like growth factor receptors are highly expressed in the brain, especially in the hippocampus and neocortex, where they participate in neuroprotective processes and mediate mitochondrial function. Unfortunately, AD-related insulin resistance and its underlying mechanisms are still poorly understood but they bear resemblances with the biomechanical disturbances encountered in type 2 diabetes, and are accompanied by

mitochondrial dysfunction (Bonfirm et al. 2012; Ott et al. 2011; Pitt et al. 2017; de la Monte and Wands 2005). Altered insulin signaling has also been demonstrated to be derived from inflammatory and stress related signaling activations, which might contribute to the impairments in memory (Yoon et al. 2012; Bonfirm et al. 2012).

Glucose is transported passively or actively into the cell depending on the metabolic demands of the cell. Active uptake is conducted with the help of **glucose uptake transporters** (GLUTs). In *post mortem* AD studies, reductions in the levels of GLUT1 and GLUT3 have been observed in different brain regions. These changes have been associated with altered glucose metabolism and correlated with hyperphosphorylation of tau (Simpson et al. 1994; Liu et al. 2008). TG disease models have also revealed reduced GLUT1, GLUT3, and GLUT4 expression in specific brain regions in relation to disease model and gender (Hooijmans et al. 2007; Sancheti et al. 2013). Deficits in the signaling pathway regulating glucose transportation system are not well characterized, however, it is possible that there are complex interactions between the mitochondrial and insulin related pathological cascades.

2.2.4 Neuroinflammation

Neuroinflammation is involved in the vicious cycle in the pathogenesis of AD, which triggers a destructive pathway characterized by protein accumulation, activation of resident phagocytes known as *glia cells*, and release of inflammatory mediators leading to disease progression. Several types of immune cells have been associated with neuroinflammation, such as lymphocytes, monocytes, and macrophages in the hematopoietic system, and glial cells in the central nervous system (CNS). Neuroinflammation can be divided into acute and chronic inflammation. *Acute neuroinflammation* refers to the activation of the resident immune cells, which eventually leads to destruction of damaged cells in order to limit the injury within the tissue. In contrast, *chronic neuroinflammation* is a deleterious, self-perpetuating response, which persists long after the initial tissue injury. A chronic neuroinflammatory cycle refers to a sustained response in which peripherally infiltrated cluster of differentiation 4 –positive T cells (Goverman 2009) accompanied by *microglial and astroglial activation* in the CNS exert amplified destructive effects on neurons. These events cause further release of inflammatory mediators through the mitogen-activated protein kinase activation and nuclear factor κB cascade (Munoz and Ammit 2010), which eventually lead to damage within the nervous tissue (Cai et al. 2014).

Microglia have a central role in the inflammatory processes during aging and neurodegenerative diseases. In normal circumstances, microglia are resident, but extremely motile phagocytic macrophages that comprise nearly 15% of the total cells in the CNS. Their primary mission is to support and maintain neuronal plasticity, to protect and remodel synapses, and to destroy and clear foreign material via an innate immune response utilizing phagocytic and cytotoxic mechanisms (Cai et al. 2014). Microglial phagocytosis and proliferation are stimulated by the cell

surface receptor TREM2, which has also been shown to be involved in the uptake of Aβ (Takahashi et al. 2005). Alois Alzheimer was the first to describe the abnormalities within the microglial structure in the AD brain (Hansen et al. 2018). Now, after decades of research, microglia are recognized to have a dual-edged function in the AD pathway, even though their ability to bind soluble and fibrillar Aβ is considered to be one of the key processes triggering inflammatory mechanisms (Perry and Teeling 2013). During the very early stages of the disease, microglia are considered to be neuroprotective rather than proinflammatory as they promote Aβ clearance from the neuronal tissues. However, abnormal microglial activation and disturbances in their morphology and proliferation due to their enhanced sensitivity to inflammatory stimuli eventually prevents the microglia from acting in a neuroprotective manner. The dual role of activated microglia has been explained by the proportion of the proinflammatory (M1) and non-inflammatory (M2) microglial cell phenotypes (Varrone and Nordberg 2015), i.e. an overexpression of the M1 activation state is thought to be related to the worsening of AD. However, recent evidence has revealed a novel protective subtype of microglia, which express genes in a spatial manner to modify the lipid metabolic pathway and microglial inflammatory actions, at first without and then via TREM2 both in mouse and human AD brain (Keren-Shaul et al. 2017).

In AD, Microglial activation is a dynamic procedure, in which overexpression of microglial-related proteins is fundamentally affected by the microglial phenotype stage among other AD factors (*Figure 6*). Binding to Aβ triggers the microglia cells into an activation mode via cell-surface receptors known as cluster of differentiation 36 and Toll-like receptors 4 and 6, resulting in the release of free radicals and thus of various inflammatory molecules such as interleukins (ILs) 1 and 6, interferon γ (IFN-γ), tumor necrosis factor α (TNF-α), complement components, and chemokines that contribute Aβ production and accumulation (Sochocka et al. 2013; Li et al. 2013; McGeer and McGeer 2010; Veerhuis et al. 1999). The ongoing Aβ formation and sustained exposure of inflammatory mediators further activate proinflammatory factors, which eventually evoke a chronic neuroninflammatory cycle (Bianca et al. 1999; Stewart et al. 2010). Microgliosis further leads to the establishment of the abnormal expression and function of several other components during neuroinflammation. Among different molecules, the expression of 18-kDa **TSPO** (formerly known as the peripheral benzodiazepine receptor) has been shown to be elevated during inflammatory revival and glial activation. TSPO is an outer mitochondrial membrane protein in glial cells that has been identified both in periphery and CNS at relatively low levels in non-pathological circumstances. The exact pharmacological functions of the peripheral and brain TSPO are yet to be elucidated. However, TSPO has been associated with a variety of different cellular functions such as cell growth and proliferation, calcium flow, apoptosis, and cholesterol transport (Papadopoulos et al. 2006; Veenman et al. 2007; Chen and Guilarte 2008; Gulyás et al. 2009). Therefore, the upregulation of TSPO in the neuroinflammatory pathway leading to AD is considered to affect also mitochondrial respiration

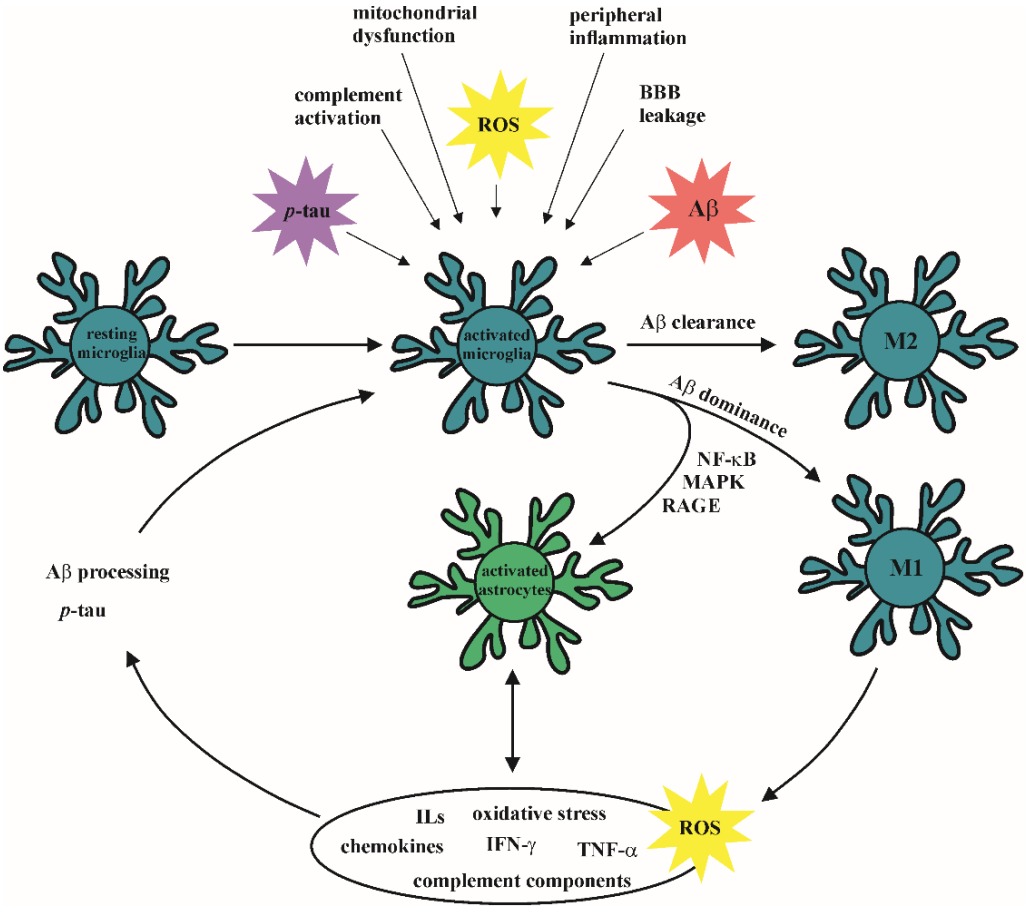

Figure 6. Microglial activation in chronic neuroinflammation related to Alzheimer's disease. Microglial function has suggested to have dual-faced role during inflammatory processes, in which resting microglia cells become activated, and the proinflammatory phenotype (M1) takes over the anti-inflammatory features (M2). Factors influencing this cascade are suggested to be involved in mitochondrial dysfunction, overproduction of reactive oxygen species (ROS), abnormal proteinopathies including β-amyloid (Aβ) and phosphorylated tau (*p*-tau) dominance, and peripheral inflammation leakage through blood-brain barrier (BBB). As a result, activated microglia and astrocytes trigger proinflammatory component production, which further manifests Aβ and *p*-tau processing.

and ROS production since the protein is part of the mitochondrial permeability transition pore. In contrast, it has been suggested that TSPO and inflammatory factors, such as ILs and TNF-α, can interact with each other, enhancing each other's pathological pathways (Bourdiol et al. 1991; Oh et al. 1992; Choi et al. 2002). In addition to that of TSPO, upregulation of the microglial purinergic receptor $P2X_7$ ($P2X_7R$) expression has also been demonstrated in AD patient-derived cells, in an Aβ-infused rat model, and in a mouse model of AD (McLarnon et al. 2006; Parvathenani et al. 2003). $P2X_7R$ is an ATP-gated ion channel that controls Ca^{2+} and Na^{+} influx and K^{+} efflux. In pathological conditions, these receptors play an important role in inflammatory signaling, e.g. overactivation of $P2X_7Rs$ results in the formation and release of IL-1β, and this

further increases Ca^{2+} levels in the cytoplasm, elevating oxidative stress, and evoking a neuronal injury (Hide et al. 2000).

Neuroinflammation is not only characterized by the presence of activated microglia but also of **astrocyte** hyperthrophy and atrophy, which might be triggered by the accumulation of Aβ and microglia (*Figure 6*). In the presence of an abnormal trigger, reactive astrocytes overproduce proinflammatory cytokines and chemokines, and increase the expression of glial fibrillary acidic protein (GFAP) (Heneka et al. 2015). Overexpression of TSPO has also been detected in the reactive astrocytes, however, the contribution to the overexpression of TSPO during inflammation between astrocytes and microglia is yet to be confirmed. Nonetheless in non-pathological conditions, astrocytes maintain neuronal function and Aβ clearance, which they mediate via *APOE* expression (Koistinaho et al. 2004). Furthermore, astrocytes are part of the energy supply to the neurons via glucose transportation and the regulation of cerebral blood flow (Morgello et al. 1995; Magistretti and Pellerin 1999). However in AD, when they are activated in the neuroinflammatory pathway, astrocytes are known to contribute to neurodegeneration, oxidative stress, and destruction of the signaling between glia cells and neurons (Acosta et al. 2017). Due to the pathogenic activation by increased levels of proinflammatory markers, there has also been reported to be elevated expression levels of monoamine oxidase B (MAO-B) enzyme within the activated astrocytes that is considered to be one of the astrogliotic biomarkers of neuroinflammation (Gulyás et al. 2011).

2.2.5 Endocannabinoid deficits

The ECS has attracted strong interest as a promising therapeutic target in AD due to the convincing evidence that it is one of the key mediators in the brain. The ECS acts at many levels for the cerebral function, many of which seem to be altered in AD (Aso and Ferrer 2014; Bedse et al. 2015). In general, the ECS is an endogenous lipid signaling system, which mediates the neurotransmitter release and regulates the functions of ion channels and other neuronal activities (Piomelli 2003). This complex system is composed of G-protein coupling cannabinoid receptors (CBRs), the endogenous ligands targeting the receptors, and the enzymes required for ligand biosynthesis and degradation. The ECS ligands are very lipophilic molecules that have crucial roles in regulating or controlling neurotransmission, e.g. the receptors are involved in neuroprotection, immune system, memory, synaptic plasticity, emotions, and even appetite and pain (Eljaschewitsch et al. 2006; Kano et al. 2009; Marsicano et al. 2002; Martin et al. 2002; Piomelli 2003). The endogenous ligands are postsynaptically produced from membrane phospholipids and released only via an on-demand request. These agents can modulate synaptic plasticity and promote neuronal activation. Upon release, they act in a retrograde manner to activate synaptic CBRs, which reduce either the short- or long-term neurotransmitter release at excitatory and inhibitory synapses. The two most abundant ECS ligands in the brain are 2-

arachidonoylglycerol (2-AG) and N-arachidonoylethanolamide (AEA) (Mechoulam et al. 1995; Devane et al. 1992); these compounds are synthetized in various cells types such as macrophages, glial cells, endothelial cells, and adipocytes (Walter et al. 2003; Gonthier et al. 2007). 2-AG is a full agonist, i.e. receptor activating ligand, for the cannabinoid receptors **CB_1R** and **CB_2R**, whereas AEA is a partial agonist for only CB_1R (Sugiura et al. 2000). Both 2-AG and AEA are very sensitive to enzymatic breakdown; their actions in neurotransmission signaling are terminated via cellular intake and enzymatic hydrolysis by serine hydrolases. The principal enzymes involved in metabolizing 2-AG and AEA are the presynaptic monoacylglycerol lipase (MAGL) and postsynaptic fatty acid amide hydrolase (FAAH). 2-AG is also metabolized to a lesser extent by FAAH, serine hydrolases α/β hydrolase domain 6 and 12, and cyclo-oxygenase 2 (COX2) (Hwang et al. 2010). The ECS receptors are seven-transmembrane domain proteins that, after a stimulus, trigger an intracellular cascade of protein inhibition or activation and ion channel function, ultimately affecting virtually every neuronal and cellular function. CB_1Rs are found throughout the body but are mainly localized in the brain both intracellularly in the endosomes and also in excitatory and inhibitory presynaptic terminals as well as to a lesser extent in postsynaptic terminals and mitochondrial membranes (Mackie 2005; Onaivi et al. 2012; Brailoiu et al. 2011). The brain can be said to be replete with these receptors; they are present within the neurons and glia cells and are principally localized in the cerebral cortex, cerebellum, hippocampus, and basal ganglia with low levels in the thalamus, pons, and medulla, but absent in the white matter (Herkenham et al. 1990). The CB_1Rs alter neurotransmitter inhibition in several ways i.e. adenylate cyclase inactivation, inhibition of calcium influx, and regulating mitochondrial activity (Freund et al. 2003; Benard et al. 2012). In contrast, CB_2Rs are widely expressed in the immune system and CNS, but seem to be only detectable within the microglia and astrocytes after an inflammatory signal (Onaivi et al. 2006; Stella 2009).

The ECS has been linked both causally and temporal manner to AD, however, a complete understanding of the complex mechanisms within this interaction is still missing. The ECS seems to possess a double-edged role in AD, i.e. exerting neuroprotective actions via CB_1R signaling mechanisms in the early disease stage, but as the AD progresses, pathological abnormalities within the ECS lead to decreased CB_1Rs levels, and overproduction and overactivation of the CBRs and ECS ligands, which can trigger inflammatory processes via microglial activation (*Figure 7*). Both *in vitro* and *in vivo* animal studies have shown that endogenous cannabinoids, synthetic receptor agonists, and the ECS reuptake inhibitors are able to diminish the Aβ-triggered destruction and neuroinflammatory mechanisms (Chen et al. 2011; Ramirez et al. 2005; Milton 2002; Esposito et al. 2007; Ehrhart et al. 2005). However, the role of CB_1Rs in AD is somewhat contradictory according to previous reports from investigations of AD patients and preclinical data: Human *post mortem* AD studies have demonstrated unchanged levels of CB_1Rs and CB_1R messenger RNA (mRNA) in the brain (Westlake et al. 1994; Benito et al. 2003; Mulder et al. 2011; Lee et al. 2010), but also reduced CB_1R agonist autoradiographical binding in the

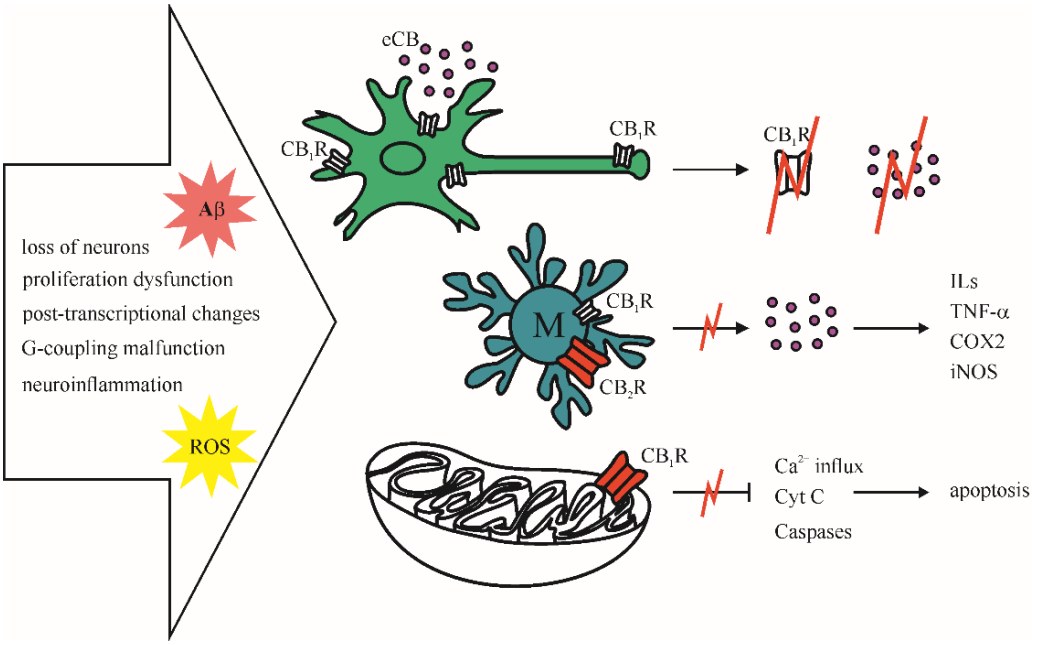

Figure 7. Type 1 cannabinoid receptor (CB_1R) involvement in the pathogenesis of Alzheimer's disease. CB_1Rs are suggested to be affected by the pathological events related to neuroinflammation, β-amyloid (Aβ) accumulation, post-transcriptional or proliferation changes, and receptor G-coupling dysfunction that cause abnormalities within the receptor signaling system. In neurons, levels of CB_1Rs and endocannabinoids (eCBs) have shown to be decreased, which prevents the CB_1R neuroprotective actions. In microglia, due to the proinflammatory response, the function of eCBs via CB_1Rs seems to be limited, which triggers the production of proinflammatory markers, such as interleukins (ILs), tumor necrosis factor α (TNF-α), cyclo-oxygenase 2 (COX2), and inducible nitric oxide synthase (iNOS). In mitochondria, due to the overexposure for reactive oxygen species (ROS), CB_1R-mediated functions are shown to be limited, which increases the function of caspases, Ca^{2+} influx, and cytochrome C (Cyt C) production that promotes abnormal apoptosis.

hippocampus, substantia nigra, and globus pallidus (Westlake et al. 1994), as well as decreased CB_1R expression levels in the cerebral cortex (Ramirez et al. 2005; Solas et al. 2013). However, increased CB_1R activation (Manuel et al. 2014) and density (Farkas et al. 2012) have been reported in the prefrontal cortex and hippocampus in the early disease stage, but this seems to decline in the advanced AD stages. In TG animal models for AD, decreased hippocampal CB_1R levels in association with proinflammatory elevations (Kalifa et al. 2011) or unchanged receptor-dependent G_i-protein activation (Kärkkäinen et al. 2012) have been observed in the hippocampus of the APP_{swe}-PSI_{dE9} mouse model, whereas in the 3xTg-AD mice, CB_1R protein levels were markedly decreased (Bedse et al. 2014). In an $A\beta_{1-42}$-insulted rat model, decreases in the levels of cerebral CB_1R and its mRNA have also been demonstrated (Esposito et al. 2007), suggesting that amyloid pathology alters the ECS. In contrast to the conflicting reports with CB_1Rs, CB_2Rs are clearly upregulated following microglial activation in response to the brain injury, with these changes being detected in *post mortem* AD brain sections. In more detail, cortical protein and mRNA levels of CB_2R have been shown to be upregulated both in *post mortem* AD human and APP_{swe}-PSI_{dE9} mouse brain (Benito et al. 2003; Ramirez et al. 2005; Solas et al. 2013; Horti et al.

2010; Nunez et al. 2008). Abnormal changes in the expression levels of ECS ligands and enzymes have also been reported: the FAAH activity appears to be elevated around neuritic Aβ plaques, a process associated with reactive astrocytes and microgliosis of *post mortem* AD brain samples (Benito et al. 2003; Jung et al. 2012; Nunez et al. 2008). Reduced AEA levels in the cortical *post mortem* AD human (Jung et al. 2012) and striatal APP_{swe}-PSI_{dE9} brain (Maroof et al. 2014) have been detected, whereas there are increases in AEA and 2-AG levels in the PS1/AβPP mouse brain (Piro et al. 2012). The 2-AG association with AD has further produced somewhat conflicting results, since its levels seem to be unchanged in the *post mortem* AD brain (Jung et al. 2012). Hence, there is increasing evidence that the ECS could be a promising interventional target for AD, and pharmacological approaches targeting this system have exerted both neuroprotective and anti-inflammatory effects, and resulted in reduced Aβ neurotoxicity (Milton 2002) and inflammation (Benito et al. 2012; Pihlaja et al. 2015), as well as increased Aβ clearance (Bachmeier et al. 2013) with these effects mediated through several synaptic and signaling pathways (Bedse et al. 2015). *In vitro* and *in vivo* proof-of-principle findings on the neuroprotective, anti-inflammatory, and antioxidant effects of the ECS ligand and a non-psychoactive phytocannabinoid, *cannabidiol*, have shown that it should be considered as a primary candidate for evaluation in an ECS-based treatment strategy to combat AD (Watt and Karl 2017).

2.3 ALZHEIMER'S DISEASE – DISEASE MODELS

Artificially manifested disease models can be enlightening in revealing the pathological events underpinning disease progression at the cellular level. Disease models represent a valuable tool in drug discovery research as well as in the evaluation of novel PET radioligands. Many disease models for AD have been developed during the past 25 years in attempts to create the perfect model, which would capture the typical pathological changes in the brain of human AD patients. According to the Alzforum Research Model Database, there are 156 murine and 4 rat models available for AD research (Alzforum). Mice have been the favored species since they reproduce easily, and they have a short lifespan and modifiable genomes, which make them inexpensive and effective research animals (Kitazawa et al. 2012). At present, AD models have been predominantly developed as single- or multitransgene-driven murine models based on mutating the genes postulated to be involved in the amyloid cascade hypothesis in EO-FAD, i.e. *APP*, *PSEN1*, and *PSEN2*. As a result, the majority of the models exhibit overexpression of human *APP* carrying familial AD mutations to promote the Aβ pathology in the brain together with the other characteristical features, including glial activation and behavioral changes (Epis et al. 2010; Gulyaeva et al. 2017).

Mouse models expressing human mutant form of *APP* have been generated by employing one or more of the common types EO-FAD mutations into the human transgene; these are

implemented into the target model genome under the control of a specific promoter that is required for regulating the spatial and temporal transgene expression (Haruyama et al. 2009). The most common *APP* mutations from the dozens of recognized ones are the double KM670/671NL "*Swedish"* (Mullan et al. 1992), V717I "*London*" (Goate et al. 1991), V717F "*Indiana*" (Murrell et al. 1991), and E693G "*Arctic*" (Nilsberth et al. 2001) mutations, which have displayed temporal Aβ pathology together with the increases in the $A\beta_{1\text{-}42}/A\beta_{1\text{-}40}$ proportion in the TG murine brain as well as subtle gliosis and impairments in the cognitive abilities of the animals. Dense-core Aβ plaques start to develop in these type of TG models at different times – 6 months (**APP23**, Sturchler-Pierrat et al. 1997 and **PDAPP**, Games et al. 1995), 11-13 months (**Tg2576**, Hsiao et al. 1996), or 13-18 months (**APP_{V717I}**, Moechars et al. 1999). *APP* mouse models have also revealed increases in the TSPO and MAO-B PET radioligand uptake in the brain when the uptake results were compared to age-matched wild-type (WT) control mice (Maeda et al. 2011; Rodriguez-Vieitz et al. 2015; James et al. 2015; López-Picón et al. 2018). The other EO-FAD genes, *PSEN1* and *PSEN2*, have also been mutated and used to prepare humanized transgenes, but the mouse models generated exclusively from these transgenes, such as **$PS1_{M146L}$** (Duff et al. 1996) have not demonstrated AD-like pathology in terms of plaque formation or hypometabolism (Poisnel et al. 2012). Subsequently, human *APP* and *PSEN* mouse models have been crossed in order to produce double TG mouse models, which display an aggressive Aβ aggregation pathology (Epis et al. 2010) as an initial signs of Aβ pathology already at the age of 6 weeks (**APP/PS1-21**, Radde et al. 2006) and 6 months (**APP_{swe}-$PS1_{dE9}$**, Jankowsky et al. 2001; **PS2APP**, Ozmen et al. 2009; **TASTPM**, Howlett et al. 2004), together with gliosis, neuronal cell loss, and impairments in cognition. The implementation of *PSEN* gene might proceed the AD pathology, which *APP* does not seem to be able to drive alone. The amount of mutated genes lowers the amyloid burden in the murine brain if both *APP* and *PSEN* are targeted, as has been observed in **5xFAD** mouse models, which express *Swedish*, *Florida*, and *London* mutations in human *APP* together with two human *PSEN1*-mutations (Oakley et al. 2006). However, even though amyloid mouse models have offered a robust and relatively reliable reproduction of many AD-related features, none of them is a direct replicate of the human AD. The current models mimic the human inherited EO-FAD form, which represents only a minor proportion of the total number of the cases without focusing on LOAD, which is the disease suffered by the vast majority of patients. Furthermore, models tend to fail to manifest some crucial pathological changes, which are encountered in the human disease i.e. evidence of neurodegeneration such as the formation of NFT, subsequent neuronal cell loss, and gross atrophy. The different levels of Aβ depositions present in some TG murine brain do not seem to be sufficient to induce other pathological processes nor cause the extent of neuronal loss seen in the human AD brain. These failures might be attributed to the differences in the Aβ sequencing and thus, the dissimilar pathologies present in the different strains (Epis et al. 2010). Examining cognitive decline with behavioral murine studies on AD models must also be carefully considered and evaluate the reliability of the possible

study outcomes compared to human disease. Hence, even though the production of AD-like features with human EO-FAD mutations has been a gold standard, other approaches have been applied with respect to the pathogenesis of LOAD, proceeding to the establishment of more realistic AD disease models. As a conclusion, mutations in *MAPT* variant have been utilized either alone to investigate tauopathy or combined with the human *TREM2*, *APP*, *PSEN1*, and/or *PSEN2* mutations to study AD pathogenesis in a more sophisticated way. Combination models, such as **3xTg-AD** (Oddo et al. 2003) with human *APP Swedish*, *MAPT* P301L, and *PSEN1* M146V mutations and **TauPS2APP** with human *APP Swedish*, *MAPT* P301L, and *PSEN*2 N141I, have demonstrated early cerebral Aβ pathology as well as late NFT accumulation together with cognitive impairments at a very early disease stage, which seems to mirror the prognosis of human AD (Grueninger et al. 2010). Introduction of AD **rat models** have enhanced the research methods and analysis, including ease of arterial blood sampling for biomarker quantification, due to larger body size. The **APP+PS1** rat model expresses *Swedish* and *Indiana* mutations in human *APP* and a single L166P mutation in *PSEN1*; these animals show cerebral amyloid depositions at 19 months of age, whereas the **APP21** rat mode, which has similar *APP* mutations without *PSEN1*, does not show any amyloidosis, although there are some signs of neurodegeneration (Agca et al. 2016). Much more recent rat models that express aggressive Aβ pathology, homozygous **McGril-R-Thy1-APP** (Leon et al. 2010) and **TgF344-AD** (Cohen et al. 2013), have also demonstrated temporal increases in amyloidosis and microgliosis from 6 months of age, with significant neuronal loss and a cognitive decline in much older animals. The TgF344-AD model further displays NFT formation at 15 months of age via *Swedish APP* and delta exon 9 mutation in *PSEN1* without genetic mutations on *MAPT*.

Animals with genetic manipulation of known LOAD risk genes, such as *TREM2* and *APOEε4*, have also been generated; these show reduced *TREM2* expression around Aβ plaques in 4-month-old **TREM2 R47H KI x APP/PS1-21** mice (Cheng-Hathaway et al. 2018) and delayed Aβ pathology in **E4FAD** mice (Youmans et al. 2012). Furthermore, rodent models involving an infusion of Aβ (Van Dam and De Deyn 2011), endotoxin (Hauss-Wegrzyniak et al. 1998), synthetic double-stranded RNA (Krstic et al. 2012), or proinflammatory cytokines (Wenk et al. 2003) have been studied extensively. These animals display novel evidence about the involvement of neuroinflammation in the induction of both Aβ and tau. However, these experiments will require further validation and standardization especially in minimizing procedural artefacts before they can become reliable research models for AD (Van Dam and De Deyn 2011).

2.4 ALZHEIMER'S DISEASE – BIOMARKER-BASED DIAGNOSIS

Probable AD is traditionally diagnosed by the clear presence of gradually progressing symptoms, such as memory problems and difficulties in performing daily tasks, for at least of 6 months. The

current AD diagnosis relies on the NINCDS-ADRDA criteria (Mckhann et al. 1984), which with respect to probable AD, highlight the importance of exclusion of other reasons for a progressive cognitive decline. Nowadays, clinical observations include tests on cognition and memory, such as Consortium to Establish a Registry for Alzheimer's Disease (CERARD) and Mini-Mental State Examination (MMSE) in more advanced stages (Käypä Hoito A 2016), which are used to obtain an initial test score at the onset of the symptoms and to follow the rate of decline for several years. However, the certainty of clinical *in vivo* diagnosis of probable AD might be lower than 70%, and a clear diagnosis still needs to be verified by *post mortem* confirmation with neuropathological findings of protein aggregation (Wang et al. 2016; McKhann et al. 2011). This emphasizes the importance of finding ways to improve the accuracy of the present clinical diagnostics.

2.4.1 Cerebrospinal fluid biomarkers

The symptom-based diagnosis has been refined by the knowledge that there are novel biological markers, which associate with AD decades before the clinical onset (Jack et al. 2010 and 2013). Alterations in the levels of three CSF biomarkers, i.e. decreases in $A\beta_{1\text{-}42}$, and increased total tau (T-tau) and phosphorylated tau (*p*-tau), were the first measurable markers, which could help to confirm the symptomatic diagnosis of probable AD (Käypä Hoito A 2016; Blennow and Zetterberg 2018). CSF $A\beta_{1\text{-}42}$ changes are more common than CSF tau, and are associated with the fibrillar Aβ deposits in the brain. Similarly, increases in the amounts of CSF *p*-tau reflect abnormal NFT burden in the AD brain. Even though alterations in CSF $A\beta_{1\text{-}42}$ begin to develop 5−10 years before cognitive decline, changes in the CSF $A\beta_{1\text{-}42}$ levels are found also in cognitively normal people, which has raised criticisms of this biomarker. Therefore, the CSF $A\beta_{1\text{-}42/1\text{-}40}$ ratio has been considered to be more reliable biomarker for AD due to its stronger diagnostic accuracy than CSF $A\beta_{1\text{-}42}$ (Lewczuk et al. 2017). Hence recently, there has been a rising interest in finding more reliable biomarkers for AD, including synaptic biomarkers (Blennow and Zetterberg 2018), including the dendritic spine protein neurogranin (Reddy et al. 2005), the presynaptic terminal synaptosomal-associated protein 25 (Brinkmalm et al. 2014), and the presynaptic plasma protein synaptotagmin-1 (Öhrfelt et al. 2016) that have been studied extensively, since their levels in CSF have been shown to be drastically changed in AD.

2.4.2 Magnetic resonance imaging biomarkers

Magnetic resonance imaging (MRI) is based on mapping the location of the protons, i.e. hydrogen atoms, which exist abundantly in water and fat rich regions of the body. By introducing a strong magnetic field with a resonating frequency via an MRI device, the hydrogen atoms begin to spin and emit radiosignals according to the frequency pulses. The MRI device detects the equilibrium phase of the excited atoms, producing digitized MRI images showing contrast differences

between different tissues according to the rate of changes in this balance stage (Vlaardingerbroek and Boer 2003).

One of the main findings for probable AD is clear gray matter atrophy in the medial temporal lobes and hippocampus, which can be detected with structural MRI. The extent of gray matter atrophy correlates with both neuronal loss and tau-related neurodegeneration (Jack et al. 2013). Recent evidence has further demonstrated disturbances in the task-associated functional brain networks, detected with task-free functional MRI (fMRI), not only in AD, but also in MCI, asymptomatic *APOEe4* carriers, and asymptomatic individuals carrying high amyloid burden (Sperling et al. 2009). Furthermore, findings from different MRI experiments, such as perfusion-weighted MRI, have also yielded additional information about the heterogeneity of AD pathology in terms of changes in cerebral blood flow (Luckhaus et al. 2008), hypoperfusion in multiple brain regions (Alsop et al. 2000), and their association with vascular brain injuries (Riekse et al. 2004).

2.4.3 Positron emission tomography biomarkers

PET is a quantitative molecular imaging method, which can be utilized for noninvasive image measurements of biological functions in a living individual. The PET method relies on short-lived radioisotope-labelled molecules, i.e. *radioligands* or *tracers*, which are targeted exclusively to the desired compound, protein, or receptor of interest in the body. The most common radioactive isotopes are ^{11}C (half-life $T_{½}$ = 20.4 min), ^{15}O ($T_{½}$ = 2.04 min), and ^{18}F ($T_{½}$ = 109.8 min), and they have to be produced in cyclotrons. In brief, the presence of a high-energy beam in a strong magnetic field causes positively charged particles to collide with a stable atomic nucleus, producing a positron emitting radioactive isotope with an extra *proton*. The radioactive isotope is then incorporated into a specific molecule i.e. it is called a radiolabeled *tracer*, which is then administered to the living subject intravenously (IV), intraperitoneally (IP), or in an inhalation form (Phelps 2000). Immediately after the irradiation, the radioactive isotope begins to decay through positron emission or via electron capture. In electron capture, the added *proton* captures an intraelectron of the atom, becoming converted into a *neutron* while releasing one *electron neutrino*. In contrast, in **positron emission**, the additional *proton* inside the radioisotope nucleus is converted into a *neutron*, releasing a *positron* and an undetectable *electron neutrino*. After the radioligand administration, the *positron* travels in matter only for a short distance of under 1 mm while the total kinetic energy of the *positron* is consumed. At this point, the *positron* is able to interact with its antiparticle, i.e. an *electron*, causing an event called *annihilation*. The collision of *positron* and *electron* annihilates the masses producing an emission of an electromagnetic energy in the form of two gamma photons (á 511 keV) moving co-linearly in opposite directions (*Figure 8*). The emission of the photons is detected by the scintillators in the detector ring of the PET imaging device, and since the energy burst is a two-directional event, the spatial location of the annihilation can be determined (Phelps 2000; Cherry and Dahlblom

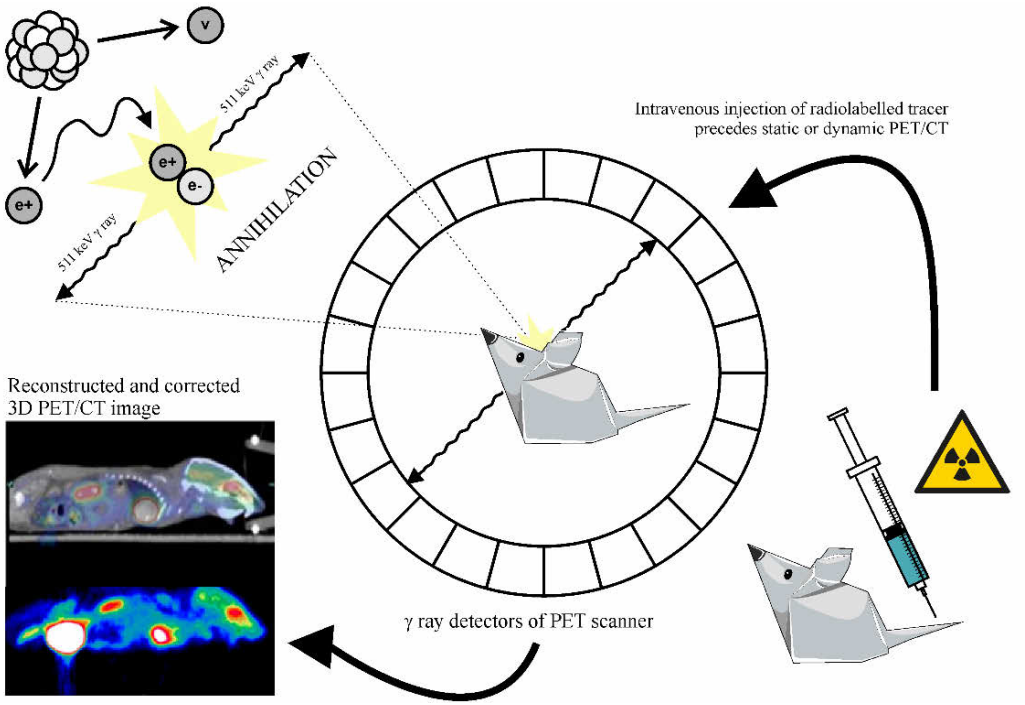

Figure 8. Annihilation. Positron emitting radionuclides are introduced into a living subject in a tracer formula, e.g. via intravenous injection. The radionuclide emits a positron (e+) when it travels a few millimeters in a tissue while consuming its total kinetic energy. At this point, the positron is able to interact with its antiparticle, an electron (e-), causing an event called *annihilation*. This reaction produces two 511 keV photons, which can be detected at nearly 180° inside the detector ring of the PET imaging device. The line of response can be defined via co-incidence of the registered annihilations, and a 3D PET/computed tomography (CT) image of the radioactivity distribution can be obtained via corrections and reconstructions.

2004). The PET imaging device can register up to 10^{10} coincident events during the PET scan, which are corrected according to the attenuation and scatter post scan. The imaging data is reconstructed into three dimensional tomographic images of voxels, in which the annihilation signal intensity is proportional to the amount of the tracer within the voxel (Cherry and Dahlblom 2004).

PET isotopes can be incorporated into biologically active molecules being administered to a living biological system. This feature can be considered to be one of the greatest advantages of PET compared to other imaging techniques. PET is a highly *sensitive* and *selective* modality, i.e. it can be utilized to select a specific target of choice, and measure very low concentrations of radioactivity. These features increase the image quality with a relatively small spatial resolution, but also lessen the radiation dose to which the subject is exposed and reduce the scanning time.

The typical spatial resolution in clinical PET device ranges between 4–6 mm, whereas in preclinical µPET, the spatial resolution can be even below 1.5 mm (Saha 2016). Spatial resolution is the best known limiting factor for reliable PET imaging. Spatial resolution is clearly limited by

detector-dependent factors, but also by the *positron range* and the annihilation *acollinearity* (Moses 2011; Saha 2016). The *positron range* is an isotope-dependent event in which different annihilation positions create a blurring effect of the radioactivity decay, and *acollinearity* is caused from the standard deviation of two-tailed 0.25% from the theoretical 180° angle of the annihilated γ rays (Moses 2011). Furthermore, achieving a proper PET scan faces also other challenges. A successful PET ligand should possess some beneficial characteristics in order to be an applicable imaging tool for clinical and research purposes: Radiolabeling should be straightforward and fast to save the radioactivity of the short-lived isotopes. The radioligand should possess a high radioactivity concentration, high molar activity, and a reliable and high target uptake. The safety of the compound must also be investigated, and its selectivity for the target must be studied carefully. In addition, a *high signal-to-noise ratio*, and *low non-specific binding* are characteristics of a good radioligand. In neuroreceptor imaging, the radioligand should have *reversible binding* to the target and the capability of *washing out* from the target within a reasonable time. A successful PET tracer should not be metabolized into radioactive compounds that would confound the quantification (Terry 2009a; Pike 2009) nor be too lipophilic to the cost of feasible brain penetration. Lipophilicity is most often expressed as a LogP value, which corresponds to the partition coefficient between n-octanol and water. Radiotracer lipophilicity is usually reported as the corresponding distribution coefficient at physiological pH and termed as D7.4. Thus in general, a successful tracer should possess a LogD7.4 value between 2.0 and 3.5, since this should enable passive brain penetration and prevent excessive blood protein binding. However, some tracers that express higher lipophilicity than the above range have been shown to enter the brain without causing any undesirable side effects (Pike 2009; Donohue et al. 2008a; Terry et al. 2008).

Glucose PET findings

With the advances in molecular imaging, researchers have been able to monitor and quantify molecular and biological processes of interest in the brain of living subjects. Imaging biomarkers can be utilized to identify underlying pathology regardless of the symptomatic stage of the neurodegenerative disease. Molecular imaging biomarkers are also tools for monitoring disease progression and possible intervention efficacy in disease-modifying trials by applying a longitudinal assessment. Therefore, PET has been incorporated into the diagnostic criteria of AD, primarily utilizing the most widely used tracer **^{18}F-FDG**. ^{18}F-FDG is a measure of cerebral glucose uptake, i.e. energy consumption metabolism and it is a derivative of one of the earliest radioligands, ^{14}C-labelled 2-deoxyglucose (**^{14}C-DG**) (Sokoloff et al. 1977), which is a reversible competitive inhibitor of glucose-6-phosphate in a complex glycolytic pathway. The distinctive pattern of altered regional glucose metabolism has been demonstrated in multiple neurodegenerative diseases, such as dementia with Lewy Bodies, frontotemporal dementia, and AD. For diagnosing AD, ^{18}F-FDG PET has become established feature as being able to detect

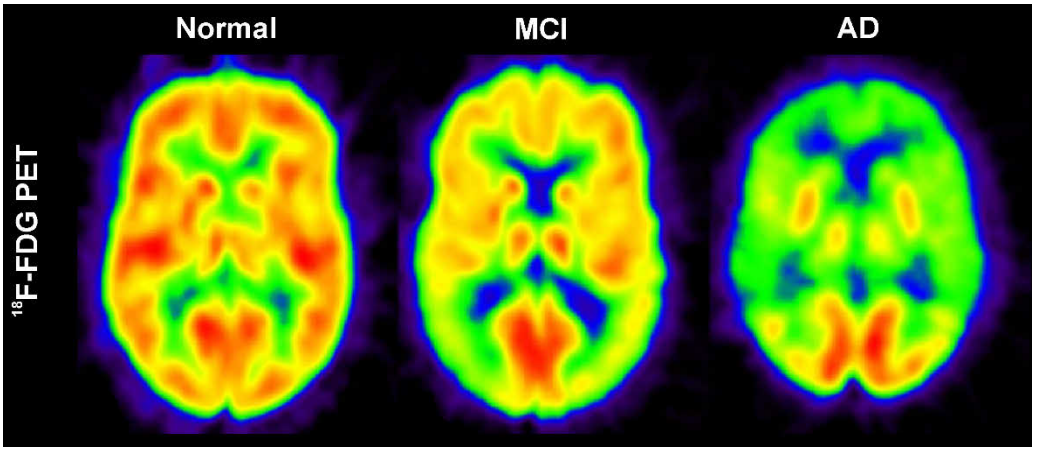

Figure 9. Changes in cerebral ^{18}F-FDG retention in a dementia continuum. A cognitively asymptomatic (normal) individual (*left*) has greater tracer retention in the brain compared to an individual with mild cognitive impairment (MCI; *center*). Decreases in the ^{18}F-FDG retention can be detected in the posterior cingulate cortex at early disease stage. In a patient with diagnosed Alzheimer's disease (AD) dementia (*right*), the ^{18}F-FDG retention has further declined in the bilateral temporo-parietal and frontal lobes, and basal ganglia compared to individual with MCI. Modified from Rice and Bisdas 2017.

regional metabolic changes reflecting glucose utilization. ^{18}F-FDG PET measurement provides also an indirect detection of regional synaptic and neuronal activity, since glucose is the primary energy substrate used by this system. The most characteristic PET distribution pattern is a regional hypometabolism visualized primarily in the posterior cingulate cortex during the early disease stage, and in the bilateral temporo-parietal and frontal lobes, and basal ganglia in advanced AD (Garibotto et al. 2017) (*Figure 9*). With respect to the hippocampus, which is one of the earliest sites experiencing AD pathology, the spatial resolution of PET imaging scanner is not sufficient to allow detection of a hypometabolic pattern within this region (Chételat et al. 2008). The pattern in the occipital cortex, which usually demonstrates significant hypometabolism in dementia with Lewy Bodies, is preserved in AD (Garibotto et al. 2017).

The diagnostic accuracy of ^{18}F-FDG PET is well examined; it has been proved to be able to distinguish AD patients from healthy controls with a pooled sensitivity of 86% and a specificity of 84% (Data pooled from the meta-analysis in Frisoni et al. 2013). Changes in the glucose metabolism correlate well with the cognitive decline and symptoms in AD progression. Thus, the regional hypometabolic pattern can predict the prognosis from MCI to AD (Villemagne et al. 2011; Ito et al. 2015; Zhang S et al. 2012) and distinguish AD from other forms of dementia (Foster et al. 2007; Minoshima et al. 2001; Bohnen et al. 2012). Therefore, ^{18}F-FDG PET has met the criteria for being a suitable biomarker for AD. However recently, this technique has been subjected to increasing criticism; it has been claimed that cerebral dysmetabolism is not sufficiently specific to be a biomarker for AD since other neurodegenerative diseases demonstrate similar phenomena, and thus, it represents a poor indicator of the underlying brain pathogenesis.

In addition, ^{18}F-FDG uptake in the brain has been speculated to reflect the progressive loss of *neuropils* (i.e. interwoven complex of dendrites, axons, and glial cells without soma, Braak 1986), rather than the metabolic impairments within the neurons, which may account for some of the conflicting results from imaging studies. However, due to the strong body of evidence supporting both the specificity and the accuracy of ^{18}F-FDG PET imaging in terms of AD diagnosis, and since ^{18}F-FDG provides additional information about the pathological stage during AD onset, NIA-AA recommends that it can keep its status as a neurodegenerative biomarker (Jack et al. 2018). In contrast, preclinical ^{18}F-FDG studies have yielded problematic outcomes, which will be further discussed in detail in Chapter 2.5.1.

Amyloid PET imaging

According to the most recent suggestions, a positive amyloid PET finding should be included into the future diagnostic criteria for AD (Jack et al. 2018). Currently, amyloid PET imaging is mostly only utilized for research purposes, although a positive amyloid burden detected with *in vivo* imaging is considered as a supporting feature for probable AD (Käypä Hoito A 2016). Amyloid PET can also be used for distinguishing AD from other forms of dementia, such as frontotemporal dementia, where Aβ is not a pathological feature (Rabinovici et al. 2007).

The first amyloid PET tracer, ^{11}C-labelled Pittsburgh Compound B (**^{11}C-PiB**) demonstrated excellent binding properties for insoluble fibrillary forms of $A\beta_{1\text{-}40}$ and $A\beta_{1\text{-}42}$ in human brain (Klunk 2001 and 2004). The typical ^{11}C-PiB PET finding in AD patients is an increased tracer retention in frontal cortex, and to a lesser extent in the parietal and lateral temporal cortices, along with binding in the striata (Rice and Bisdas 2017). The binding loci have been shown to correlate significantly with the *post mortem* histopathological findings of high amyloid burden (Thal et al. 2002; Leinonen et al. 2008). At present, three ^{18}F-labelled tracers, **^{18}F-florbetabir**, **^{18}F-flutemetamol**, and **^{18}F-florbetaben**, have been approved for clinical use by the Food and Drug Administration of the United States Department of Health and Human Services and the European Medicines Agency in regard to sufficiently sensitive (88%) and specific (85%) outcome of amyloid PET imaging to allow it to be used as an early diagnostic biomarker for AD (Pooled meta-analysis in accordance of Frisoni et al. 2013). However, even though these tracers have successfully discriminated AD patients from healthy controls, and predicted the MCI progression to AD with great specificity and sensitivity in multiple studies (Clark et al. 2012; Rowe et al. 2008; Vandenberghe et al. 2010), they have also demonstrated off-target binding to cerebellar white matter, limiting a more comprehensive clinical application (Vandenberghe et al. 2010). Several studies have further observed contradictory results on whether amyloid detected by PET appropriately correlates with the temporal course of the cognitive decline (Engler et al. 2006; Strodant et al. 2009; Aizenstein et al. 2008), since the amyloid pathology eventually plateaus while hypometabolism, as detected with ^{18}F-FDG, continues to progress (Förster et al. 2012; Landau et al. 2012). Criticism has also been aimed at whether amyloid tracers would be able to

detect AD variants that are characterized predominantly by diffuse plaques, and of the fact that approximately 25–35% of elderly individuals older than 75 years carry a high amyloid burden that is not accompanied by brain atrophy or cognitive problems (Mintun et al. 2006; Villemagne et al. 2013 and 2018), while conversely, some diagnosed AD patients may show negative amyloid PET retention in the brain (Cairns et al. 2009). Thus at present, for a possible AD diagnosis, amyloid PET imaging becomes relevant only in unclear cases; it is not an appropriate tool to diagnose those who are asymptomatic and cognitively normal subjects, individuals with normal cognition and tested autosomal dominant mutation in one of the AD-associated genes, nor in lieu of meeting the primary criteria for possible AD. Nevertheless, amyloid targeting PET imaging offers a valuable tool for early AD diagnosis, especially if anti-amyloid therapeutics capable of preventing disease progression become available in the future, as these would hopefully reduce the costs to society of the burgeoning AD epidemic.

Tau PET imaging

Noninvasive tau PET imaging is the newest modality added to the AD research battery; cortical binding of tau tracer has been postulated to be a biomarker for fibrillar tau according to the newest proposal for AD diagnostic criteria (Jack et al. 2018). This seems reasonable since the presence of amyloid deposits and paired helical filament tau deposits are both required to fulfill the neuropathological AD criteria (Montine et al. 2012; Hyman et al. 2012). Unfortunately, the heterogeneous isoformic phenotype and rather low tau concentration in the brain pose challenges in finding a suitable radioligand target region within the tau conformation. The current tau tracers are used exclusively for research purposes, requiring validation for *in vivo* purposes. The first-generation tau tracer **^{18}F-flortaucipir** has been shown to be specific for the 3R/4R isoform of tau deposits, and its binding correlates with the NFT staging by Braak and CSF tau levels (Chien et al. 2013; Marquié 2017b; Brier et al. 2016). Unfortunately, it suffers from high off-target binding in regions devoid of tau and there have been discrepancies noted between *in vitro* and *in vivo* human imaging results (Marquié et al. 2015; Lowe et al. 2016), as well as between *ante mortem* and *post mortem* findings (Marquié 2017a and 2017b). **^{18}F-THK5351**, **^{18}F-THK5317**, and **^{11}C-PBB3,** have been shown to possess similar limiting features including low binding affinity, low binding site concentration and as a result, an undetectable threshold for the PET scanner, and high non-specific binding to MAO-B (Villemagne et al. 2018). Fortunately, the second-generation tau tracers have improved characteristics, including reduced off-target binding (**^{18}F-RO69558948**) or no off-target binding (**^{18}F-MK6240** and **^{18}F-PI2620)** at all (Walji et al. 2016; Gobbi et al. 2017; Stephens 2017). As a summary, tau PET imaging has revealed that NFTs are in a tight association with the other neurodegeneration biomarkers, such as lower ^{18}F-FDG uptake and cortical gray matter atrophy (Xia et al. 2017; Chiotis 2018), and together they can be considered to be an excellent biomarker for disease progression. In contrast to amyloid pathology, from the neuropathological point-of-view, tau levels do not seem to be as crucial as the topographical

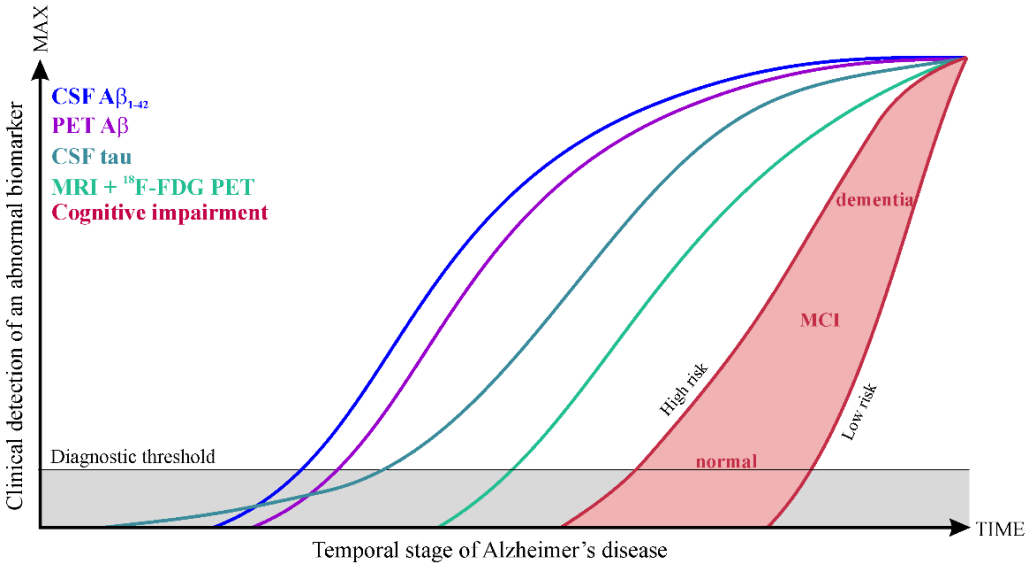

Figure 10. Temporal course of dynamic biomarkers during the cascade of Alzheimer's disease. Abnormal detection of β-amyloid (Aβ) as $A\beta_{1-42}$ cerebrospinal fluid (CSF) biomarker and positron emission tomography (PET) findings are the earliest events to be measured in Alzheimer's disease diagnosis that precede CSF tau changes, ^{18}F-FDG PET findings on hypometabolism or magnetic resonance imaging (MRI) findings in hippocampal atrophy (Lo et al. 2011). However, *post mortem* experiments have shown that tau pathology precedes Aβ pathology, and thus, it should be viewed as the initial benchmark in the pathophysiological cascade of Alzheimer's disease (Braak and Braak 1997; Braak and Del Tredici 2011). Hence, Aβ markers are considered as the initial detectable biomarkers, which are followed by biomarkers of neurodegeneration – tau, gray matter atrophy, and glucose hypometabolism - and finally by the cognitive decline. Modified from Jack 2013.

distribution of the neurofibrillary tau deposits (As discussed by Royall 2007; Swerdlow 2007).

Aforementioned biomarkers of AD become abnormal at different times during the disease progression and the manifestation of symptoms. Decades of evidence from patient samples have produced a hypothetical model of the dynamic relationship between AD biomarkers during the temporal course of the disease (Jack et al. 2013). The hypothesis is not ideal for all forms of LOAD, but it does indicate the clinical threshold at which an abnormal biomarker can be detected and this may well differ from the actual underlying pathogenesis (*Figure 10*). Furthermore, the rate of change of the pathological biomarkers varies between individuals and changes in a non-linear manner during the temporal course of the disease. Hence, more studies are needed, especially to confirm the temporal course of CSF tau, ^{18}F-FDG PET and structural MRI, as well as the development of better PET radioligands both in AD patients and disease models.

2.5 TRANSLATIONAL PET FOR ALZHEIMER'S DISEASE

AD offers a variety of alternative targets for PET radioligand development, including proteins, enzymes, and brain receptors, some of which also represent promising medical intervention targets to combat the disease. Proteins like α-synuclein and β-secretase, the former being

significantly overexpressed in AD and the latter involved in processing APP to Aβ, have been a focus of interest in PET imaging technology as possible *in vivo* targets (Mathis et al. 2017; Zhang L et al. 2018). Furthermore, according to the *AD metal hypothesis*, the concentrations of certain metal ions, such as Zn^{2+}, are abnormally increased at the site of accumulated Aβ plaques (Bush 2008). These pathological findings have stimulated the search for ligands targeting metal, such as the ion chelator clioquinol (Vasdev et al. 2012). On the other hand, the *cholinergic hypothesis* postulates that declines in acetylcholine release and the degeneration of cholinergic neurons result in neuronal cell loss and cognitive decline (Bartus et al. 1982). The current treatment strategy for AD is based on this hypothesis, and three drugs targeting cholinergic and one glutamate neurotransmission are in clinical use to temporally alleviate the symptoms (Käypä Hoito B 2016). Thus, not surprisingly, PET ligands modified from acetylcholinesterase inhibitors, including ^{11}C-donepezil (De Vos et al. 2000), or acetylcholine esters, such as ^{11}C-PMP (Snyder et al. 1998), have been developed for imaging the *in vivo* abnormalities within this neurotransmitter system; these have enjoyed some significant successes when administered to AD patients (Iyo et al. 1997; Mochida et al. 2017). In addition to the acetylcholine system, the evidence of the involvement of the neuronal metabotropic glutamate receptors, muscarinic acetylcholine receptors, nicotinic acetylcholine receptors, and gamma-aminobutyric acid (GABA) subtype A receptors in AD brain has been utilized in the development of novel PET radioligands (Holland et al. 2014). Next, the applications and current research knowledge of translational PET targeting brain glucose hypometabolism, neuroinflammation, and CB_1Rs in relation to AD will be discussed in depth.

2.5.1 Targeting brain glucose metabolism

^{18}F-FDG is the only available *in vivo* radioligand targeting glucose energy metabolism; it was initially derived directly from glucose and 2-DG by labelling the second carbon atom of cyclohexane structure of glucose with fluorine-18 instead of hydroxyl (*glucose*) or hydrogen (*2-DG*). This substitution does not change the desired functions of the compound nor prevent its passage through the blood-brain barrier (*Figure 11*) (Sokoloff 1979). The biochemical features of ^{18}F-FDG mimic those of glucose i.e. it can access the metabolic pathway utilizing glucose as an energy source for cells called *glycolysis*: After the initial delivery into the body, both glucose and ^{18}F-FDG are phosphorylated by hexokinase. Glucose is then transformed into glucose-6-phosphate, metabolized into fructose-6-phosphate by phosphohexose isomerases, and eventually pyruvate, ATP, and nicotinamide adenine dinucleotide molecules remain as total end-products that can be stored as energy sources by cells. However, ^{18}F-FDG is only metabolized up to the hexokinase-catalyzed reaction (*Figure 12*), after which it does not proceed down the glycolytic pathway. Instead, the accumulated phosphorylated ^{18}F-FDG is further metabolized to radioactive metabolites, especially in aggressive sarcomas (Suolinna et al. 1986; Rokka et al. 2017) and trapped intracellularly emitting the radioactive signal, which can be detected by the PET scanner (Fowler and Ido 2003).

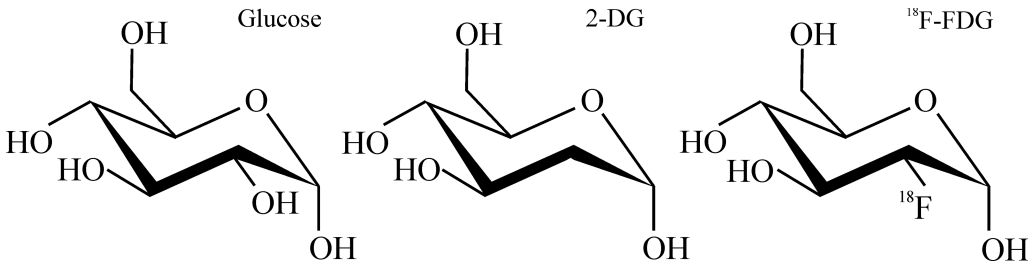

Figure 11. Molecular chair structures for glucose, 2-deoxyglucose (2-DG), and 2-deoxy-2-^{18}F-fluoro-D-glucose (^{18}F-FDG).

Table 1 represents in chronological order previous *in vivo* ^{18}F-FDG µPET studies with different AD mouse models from the past decade. Reductions of cerebral glucose metabolism in the posterior temporoparietal and later in the frontotemporal lobes in AD are well established features in clinical ^{18}F-FDG imaging, and these can also be correlated with the level of brain glutamatergic synaptic activity, i.e. neuronal loss in AD (Sibson et al. 1998). Replication of the detected regional hypometabolism with ^{18}F-FDG µPET has, unfortunately, proved to be challenging. According to the previous studies, **TASTPM** (Waldron et al. 2015a and 2017; Deleye et al. 2016) and **APP/PS1-21** (Waldron et al. 2015b; Deleye et al. 2017) models have successfully replicated the hypometabolic pattern in the AD brain, as demonstrated in the clinical ^{18}F-FDG outcome. Six-month-old TASTPM mice, which have been fasted for 8–12 hours in each study, displayed decreased ^{18}F-FDG retention in several brain regions when assessed as the individually normalized percentage of the injected radiotracer dosage per weight of the animal (%ID/g) or as standardized uptake values (SUVs) to blood glucose. In the APP/PS1-21 mice, hypometabolism have been measured in thalamus and striata at 12-month-old TG mice with prolonged fasting of 8–12 hours (Waldron et al. 2015b), whereas overall genotype-dependent decrease in the ^{18}F-FDG retention was quantified in untreated TG mice in a combinational intervention PET study (Deleye et al. 2017). In contrast, increased ^{18}F-FDG retention has been reported in **APP$_{751SL}$/PS1$_{M146L}$** (Poisnel et al. 2012) and **PS2APP** (Brendel et al. 2016) mouse models compared to WT littermattes. In these studies, SUVs relative measures to the individual cerebellar radioactivity showed enhanced tracer levels in the forebrain (Brendel et al. 2016), and cerebral cortex and hippocampus (Poisnel et al. 2012), which might have originated from an artefact attributable to the use of cerebellum as a reference region.

Some models have shown controversial results on the temporal course of the glucose metabolism in the brain: **Tg2576** mice have displayed no differences in the ^{18}F-FDG uptake compared to age-matched WT mice (Kuntner et al. 2009; Coleman et al. 2017), whereas at 7 months, it has been reported that there are hypermetabolic brain regions including hippocampus, thalamus, and cortical lobes, which was converted into a WT-like metabolic profile at 19 months of age (Luo et al. 2012).

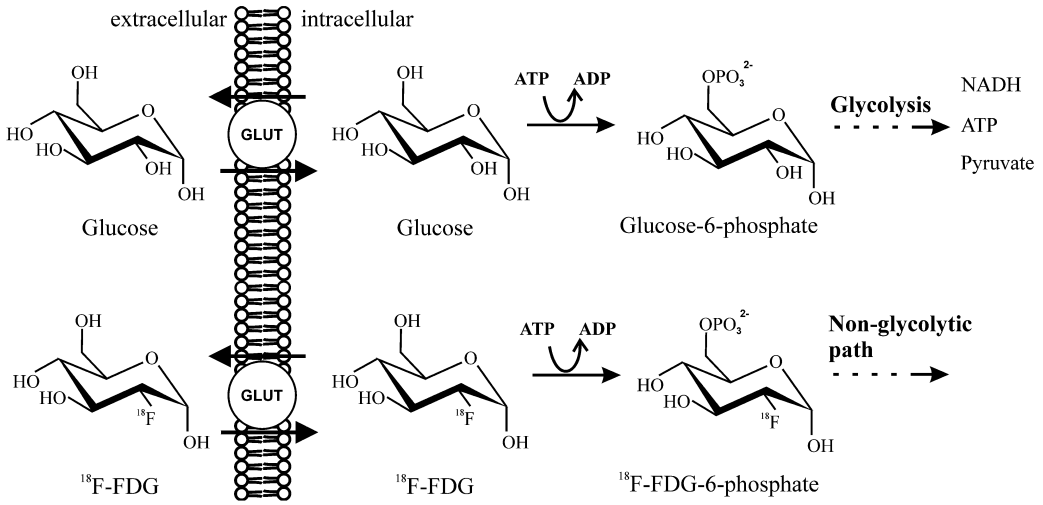

Figure 12. Utilization of glucose and 2-deoxy-2-^{18}F-fluoro-D-glucose (^{18}F-FDG) in the intracellular glycolytic pathway. Glucose or ^{18}F-FDG are actively transported inside the cell via glucose transporters (GLUT), and then metabolized into 6-phosphate forms. Glucose-6-phosphate further metabolizes in the glycolytic path that produces adenosine triphosphate (ATP), nicotinamide adenine dinucleotide (NADH), and pyruvate, whereas ^{18}F-FDG-6-phosphate radiometabolizes into tissue-specific metabolites, which does not follow the glycolytic pathway.

Similarly, 10- to 11-month old **5×FAD** mice have displayed increased (Rojas et al. 2013) or alternatively decreased glucose metabolism both at 5 months (DeBay et al. 2017) and 13 months of age (Macdonald et al. 2014). **PLB1$_{triple}$** mice have exhibited regional differences, with either a hyper- or hypometabolic pattern present at 5 months of age, but these changes had disappeared at 17 months of age (Platt et al. 2011). The **APP$_{swe}$-PS1$_{dE9}$** model has also demonstrated brain hypermetabolism as regional radioactivity measurements relative to the cerebellar radioactivity 2 to 8 months in different regions (Li et al. 2016), but unchanged glucose retention in 9-month-old female mice (Liu et al. 2017). These controversial results in specific models might be attributable to the obvious differences in methodological and quantification procedures (*Table 1*).

2.5.2 Targeting neuroinflammation

Neuroinflammation is a complex progressive event involving various cell types, which form an interactive, net-like signaling pathway in which, surprisingly, microglial TSPO expression has a small role. Nevertheless, current *in vivo* neuroinflammation imaging relies heavily on targeting TSPO, since its upregulation has been found to be selective and measurable in several brain diseases including in patients with stroke and AD. Thus, TSPO may not only be a potential diagnostic biomarker but it may also be a therapeutic target for neuroinflammatory-based brain diseases. In healthy brain tissue, the expression level of TSPO in glial and endothelial cells is relatively low, whereas in AD, enhanced TSPO expression has been found in several brain regions affected by amyloid depositions and hypometabolism in the *post mortem* AD brain (Papadopoulos et al. 2006; Cosenza-Nashat et al. 2009; Venneti et al. 2009a). Furthermore, TSPO

Table 1. Regional glucose retention detected with small animal ^{18}F-FDG µPET in transgenic mouse models of Alzheimer's disease.

Strain	Age (mo)	Sex	Fasting	Blood glucose control	Injection	Anesthesia maintenance	PET	^{18}F-FDG uptake	Target brain region	QU	Reference
Tg2576	13-15	M, F	8h	No	IV in anesthesia	1.5% isoflurane	60-90 min stat	NS	NA	%ID/ kg/g + VOI/B	Kuntner et al. 2009
$PLB1_{triple}$	5, 17	M, F	Over-night	No	IP awake	Vetalar, Medet., Domitor	55-95 min stat	5 mo (-), 5 mo (+)	CTX, STR, THA	SPM	Platt et al. 2011
APP_{751SL}/ $PS1_{M146L}$	3, 6, 12	F	No	Yes	IV in anesthesia	1–1.5% isoflurane	60 min dyn	6 + 12 mo (+)	HIP, CTX	SUVR CB	Poisnel et al. 2012
Tg2576	7, 19	F	6h	No	IV in anesthesia	Medet., ketamine	60 min dyn	7 mo (+), 19 mo (-)	HIP, CTX, THA	SUV	Luo et al. 2012
5×FAD	10-11	NA	No	No	IV in anesthesia	1.5% isoflurane	50-80 min stat	(+)	CTX	VOI/CB	Rojas et al. 2013
5×FAD	2, 5, 13	M	No	No	IV awake	1.5 –2% isoflurane	30-60 min stat	13 mo (-)	B, THA, HYPO, CB	SUV	Macdonald et al. 2014
TASTPM	13.5	M	8-12h	Yes	IV awake	2% isoflurane	45-65 min stat	(-)	THA, brain stem	%ID/g × glu, SPM	Waldron et al. 2015a
APP/PS1-21	12	F	8-12h	Yes	IV awake	2% isoflurane	45-65 min stat	(-)	THA, STR	%ID/g × glu, SPM	Waldron et al. 2015b
PS2APP	5, 8, 13, 16	NA	NA	NA	NA	NA	30-60 min stat	(+)	Forebrain	SUVR CB	Brendel et al. 2016

Note: (-) Decreased ^{18}F-FDG uptake in transgenic Alzheimer mice compared to wild-type mice; (+) increased ^{18}F-FDG uptake in transgenic Alzheimer mice compared to wild-type mice; Abbreviations: *B*, brain; *CB*, cerebellum; *CTX*, cortex; *dyn*, dynamic; *F*, female; *glu*, glucose; *HIP*, hippocampus; *HYPO*, hypothalamus; *IP*, intraperitoneal; *IV*, intravenous; *M,* male; *mo*, months; *NA*, not applicable ; *NS*, non-specific; *QU*, quantification unit; *SPM,* statistical parametric mapping; *stat*, static; *STR*, striatum; *SUV*, standard uptake value; *SUVglu*, glucose-corrected SUV; *THA*, thalamus

Continuum of Table 1. Regional glucose retention detected with small animal ^{18}F-FDG µPET in transgenic mouse models of Alzheimer's disease.

Strain	Age (mo)	Sex	Fasting	Blood glucose control	Injection	Anesthesia maintenance	PET	FDG uptake	Target brain region	QU	Reference
TASTPM	+14	NA	10/20h	Yes	IV awake	2% isoflurane	45-65 min stat	(-) or NS	All	%ID/g, SUV, SUVR CB, glu	Deleye et al. 2016
APP_{swe}-$PS1_{dE9}$	2, 3.5, 5, 8	F	+6h	No	IV awake	2% isoflurane	40-63 min stat	(+)	CTX, HIP, FC, THA, STR	SUVR CB	Li et al. 2016
APP/PS1-21	6-15	M, F	90 min	Yes	IV in anesthesia	2.5% isoflurane	60 min dyn	6 > 12 mo (-)	HIP, CTX, THA, STR, CB	SUV	**II**
TASTPM	6-15	M	8-12h	Yes	IV awake	2% isoflurane	45-65 min stat	(-)	All	SUVglu	Waldron et al. 2017
5×FAD	5	M	No	No	IV awake	1.5–2% isoflurane	30-60 min stat	(-)	All, except CB	SUV	DeBay et al. 2017
APP_{swe}-$PS1_{dE9}$	9	F	12h	Yes	IP awake	NA isoflurane	40- X min stat	NS	NA	%ID/g	Liu et al. 2017
Tg2576	+18	M, F	24h	Yes	IP awake	2.5% isoflurane	60-120 min stat	NS	NA	SUVglu	Coleman et al. 2017
APP/PS1-21	1.5-1.75, 4, 7-8, 12-13	F	10-14h	Yes	IV awake	2% isoflurane	45-65 min stat	(-)	THA, HIP	SUVglu	Deleye et al. 2017
APP_{swe}-$PS1_{dE9}$, Tg2576	6, 12, 17	F	3	Yes	IV in anesthesia	2.5% isoflurane	60 min dyn	(-) or NS	B, FC, HIP, STR, THA, CB	SUV, SUVglu	**I**

Note: (-) Decreased ^{18}F-FDG uptake in transgenic Alzheimer mice compared to wild-type mice; (+) increased ^{18}F-FDG uptake in transgenic Alzheimer mice compared to wild-type mice; Abbreviations: *B*, brain; *CB*, cerebellum; *CTX*, cortex; *dyn*, dynamic; *F*, female; *FC*, frontal cortex; *glu*, glucose; *HIP*, hippocampus; *HYPO*, hypothalamus; *IP*, intraperitoneal; *IV*, intravenous; *M,* male; *mo*, months; *NA*, not applicable; *NS*, non-specific; *QU*, quantification unit; *stat*, static; *STR*, striatum; *SUV*, standard uptake value; *SUVglu*, glucose-corrected SUV; *THA*, thalamus

PET imaging can be utilized for monitoring trans-synaptic glial cell activation in relation to physiological neuroplasticity and synaptic remodeling (Banati et al. 2001).

PET ligands targeting TSPO

The first PET ligand to target TSPO was an isoquinoline carboxamide **^{11}C-(*R*)-PK11195**, which demonstrated to be selective for TSPO and revealed glial activation through the TSPO elevation pattern in the AD brain (Junck et al. 1989; Cagnin et al. 2001). The development of new radioligands with similar short ^{11}C half-lives, but with more specific binding and better blood-brain barrier permeability, such as the *N*-benzyl-*N*-(2-phenoxyaryl)acetamides **^{11}C-DAA1106** and **^{11}C-PBR28** (Maeda et al. 2004; Brown et al. 2007) and an alpidem derivative **^{11}C-DPA-713** (James et al. 2005), have been able to improve the signal intensity and affinity to TSPO in the brain. However, the short half-life of the ^{11}C-labelled radioligands has practical limitations, which prevents tracer production for broader commercial utilization or within research centers without on-site radiochemistry. Thus, a variety of ^{18}F-labelled TSPO PET tracers have been developed, and their applicability in imaging of TSPO in animal models and human brain has been studied extensively. Many candidates, such as *N*-benzyl-*N*-(2-phenoxyaryl)acetamides, **^{18}F-PBR06** (Briard et al. 2005), **^{18}F-FEDAA1106** (Zhang et al. 2004), **^{18}F-FEMPA** (Varrone et al. 2015), **^{18}F-FEPPA** (Wilson et al. 2008), and tricyclic indoles **^{18}F-GE-180** (Wadsworth et al. 2012) and **^{11}C-ER176** (Ikawa et al. 2017), have, by far, proved to be applicable for imaging TSPO *in vivo* (Extensively reviewed in Cumming et al. 2018 and Edison et al. 2018). Furthermore, one of the alpidem derivatives (*Figure 13*), **^{18}F-DPA-714**, has shown to possess high specific binding and rapid brain uptake in non-human primates and rats with an affinity of K_i as 7.0 (0.4) nM (James et al. 2008). ^{18}F-DPA-714 has also displayed superior features compared to ^{11}C-PK11195 in terms of binding potential in an acute inflammation rat model (Chauveau et al. 2009), as well as good stability and a rapid clearance rate during the first 30 min with a peak uptake at 5 min after the tracer injection in the first in-human evaluation *in vivo* experiment (Arlicot et al. 2012). In mice, no radioactive metabolites have been detected in the brain 60 min after injection (Vicidomini et al. 2015; Keller et al. 2017), whereas in rat brain, a carboxylic acid radiometabolite constitutes 15% of the total ^{18}F-radioactivity (Peyronneau et al. 2013). Recently, a structural fluoroaryl analogue of ^{18}F-DPA-714, named as **^{18}F-FDPA**, has been developed and evaluated in WT rats (Keller et al. 2017) and in the APP/PS1-21 mouse model of AD (Keller et al. 2018), demonstrating fast washout and superior sensitivity for detecting activated glia cells in the AD mouse brain.

TSPO PET findings in AD patients

The feasibility of the gold standard TSPO tracer, **^{11}C-(*R*)-PK11195**, was examined for the first time in AD patients by Cagnin et al. (Cagnin et al. 2001). The tracer was able to to differentiate AD and MCI patients from healthy controls, a finding further confirmed by other investigators

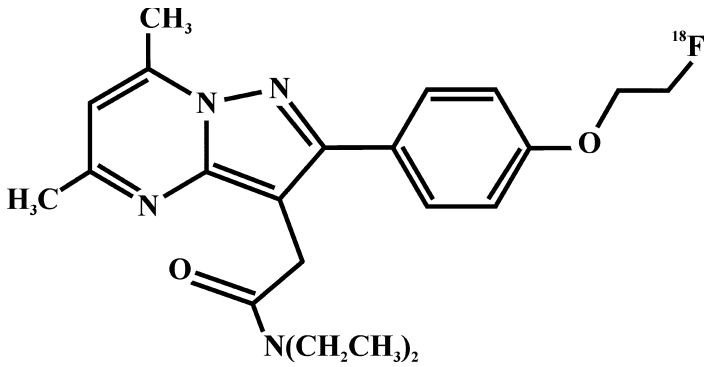

Figure 13. Molecular structure of ^{18}F-*N*,*N*-diethyl-2-(2-[4-(2-fluoroethoxy)phenyl]-5,7-dimethyl-pyrazolo[1,5-α]pyrimidine-3-yl)-acetamide (^{18}F-DPA-714).

(Edison et al. 2008; Fan et al. 2015; Parbo et al. 2017; Passamonti et al. 2018). In the recent imaging study, increased binding of ^{11}C-PK11195 was demonstrated to overlap with the cortical brain atrophy, and thus it has been suggested to be associated more tightly with neuronal loss (Kreisl et al. 2017). In contrast, other studies have shown no differences in the ^{11}C-PK11195 binding potentials between AD patients and healthy volunteers, nor did it correlate with cognitive scores (Schuitemaker et al. 2013; Parbo et al. 2018). In terms of the potential utilization of **^{11}C-DAA1106** and **^{18}F-FEDAA1106** in human imaging, the former has revealed significantly greater uptake in AD and MCI patients as compared to healthy controls (Yasuno et al. 2008a), whereas the latter compound failed to distinguish AD patients from the controls perhaps due to the slow washout from the brain (Varrone et al. 2013). Nonetheless, increased **^{11}C-PBR28** binding in the cerebral cortical regions has been successfully measured in the brain of genotype-corrected AD patients as compared to MCI and cognitively healthy controls (Kreisl et al. 2013; Lyoo et al. 2015). Genotype examinations in patients have been conducted prior to TSPO PET scans, because there is a genetic polymorphism in the TSPO gene rs6971, which affects the radioligand binding properties and thus, the data interpretation. Sensitivity to TSPO polymorphism is a characteristic of most of the second generation TSPO tracers except for ^{11}C-PK11195 and ^{18}F-GE-180, which show no or little sensitivity towards rs6971 (Largeau et al. 2017). In a consequence for the genetic stratification method, novel TSPO tracers, **^{18}F-FEMPA** and **^{18}F-FEPPA**, have displayed elevations in the tracer binding in AD patients as compared to healthy controls (Varrone et al. 2015; Suridjan et al. 2015).

One of the quantification method for analyzing human TSPO PET data has been the kinetic two-tissue compartment model with arterial input function; this has yielded promising results for **^{18}F-GE-180** (Fan et al. 2016; Feeney et al. 2016) and **^{18}F-DPA-714**. For ^{18}F-GE-180, the imaging applicability in the human brain has been evaluated in non-diseased conditions, yielding a poor distribution volume (V_T) and restricted penetration into the brain compared to ^{11}C-PBR28 (Zanotti-Fregonara et al. 2018). On the contrary, significantly increased **^{18}F-DPA-714** uptake has

been reported in high and mixed affinity binders in AD patients compared to controls after rs6971 genotyping (Hamelin et al. 2016), which was not shown in an older study, which might have been attributable to the lack of genotyping of the subjects (Golla et al. 2015).

TSPO PET findings in AD animal models

The most widely used AD mouse models express an upregulated form of *APP* and thus of Aβ pathology, representing a perfect disease model for amyloidosis in the prognosis of AD. However, neuroinflammation is not genetically implemented into these models, but previous preclinical imaging and histology data have revealed that TSPO-related microgliosis is an ongoing event in the TG mouse brain, preceding the accumulation of Aβ (López-Picón et al. 2018). *Table 2* shows in chronological order the *in vivo* μPET studies targeting neuroinflammation using TSPO radioligands in different AD mouse models. Studies using the first generation TSPO ligands, such as ^{11}C-AC-5216, have revealed increased TSPO levels in the hippocampal and cortical regions in **APP23** and **APP$_{E693d}$** mice older than 23 months of age (Maeda et al. 2011), whereas ^{11}C-PK11195 studies have shown that 13-month-old **APP$_{swe}$-PS1$_{dE9}$** mice exhibited undetectable TSPO alterations in the brain (Rapic et al. 2011), but at 16 to 19 months of age, the TSPO levels were remarkably increased (Venneti et al. 2009a). Others groups have also employed the same mouse model, and similar increases in the regional TSPO tracer uptake have been detected using longitudinal ^{18}F-DPA-714 (Sérrière et al. 2015; Chaney et al. 2018) and cross-sectional ^{18}F-GE-180 imaging (Liu et al. 2015). In the longitudinal ^{18}F-DPA-714 studies, the brain regions affected have been cerebral cortex in the 12- to 19-month-old **APP$_{swe}$-PS1$_{dE9}$** mice (Sérrière et al 2015), whereas in over 18-month-old mice, significant differences have been detected in hippocampus, cortical region, and thalamus of TG mice (Chaney et al. 2018). In both studies, the results were obtained by normalizing the regional radioactivity levels with a pseudo-reference region – cerebellum. Liu et al. utilized ^{18}F-GE-180 for the quantification using a unit of %ID/ml, which has not been used in newer studies with **PS2APP** (Brendel et al. 2016 and 2017b) and **APP23** (López-Picón et al. 2018) models with the same tracer. In these studies, the white matter region including cerebellum and cerebellum alone were used as pseudo-reference regions, respectively, and increased TSPO levels were detected at 5 months in the forebrain (Brendel et al. 2016 and 2017b) and in the cortical, hippocampal, and thalamic regions between 17 to 26 months of age (López-Picón et al. 2018). Furthermore, young 6-month-old **5×FAD** mice have exhibited significantly higher ^{11}C-PBR28 uptake in their brains as compared to WT mice (Mirzaei et al. 2016), whereas **APP$^{L/S}$** have displayed increases in the ^{18}F-PBR06 uptake in cerebral cortex and hippocampus only at the age of 15-16 months (James et al. 2015).

Table 2. Regional TSPO tracer retention detected with small animal μPET in transgenic mouse models of Alzheimer's disease.

Strain	Age (mo)	Sex	Tracer	Injection	Anesthesia	PET	Tracer uptake	Target brain region	QU	IHC	Reference
APP_{swe}/ $PS1_{dE9}$	13-19	NA	^{11}C-PK11195	IV in anesthesia	Isoflurane	60 min dyn	(+)	B at 16-19 mo	%ID/kg x g	Iba1+, GFAP+	Venneti et al. 2009
APP23, APP_{E693d}	23-29, 25	NA	^{11}C-AC-5216, ^{18}F-FEDAA11106, ^{11}C-AC-5216	IV in anesthesia	Isoflurane	60/90/60 min dyn	(+) / NS	HIP, CTX	VOI/STR	TSPO+	Maeda et al. 2011
APP/PS1	13	F	^{11}C-PK11195	IV in anesthesia	Isoflurane	30 min dyn	NS	NS	%ID/cc, SUV	CD11+	Rapic et al. 2013
APP_{swe}/ $PS1_{dE9}$	6-19	M	^{18}F-DPA-714	IV in anesthesia	Isoflurane	50 min dyn	(+)	CTX 12 + 19 mo, HIP 19 mo	SUVR CB	CD38+ at 19 mo	Sérrière et al. 2015
APP_{swe}/ $PS1_{dE9}$	4, 26	M	^{18}F-GE-180	IV in anesthesia	Isoflurane	120 min dyn	(+)	B, HIP	%ID/ml, B/THA	TSPO+, CD38+, CD40+ at 26 mo	Liu et al. 2015
$APP^{L/S}$	5-6, 9-10, 15-16	NA	^{18}F-PBR06	IV in anesthesia	Isoflurane	60 min dyn	(+)	CTX, HIP	VOI/muscle, VOI/B, %ID/g	CD38+, TSPO+ from 9 mo	James et al. 2015
5×FAD	6	F	^{11}C-PBR28	IV in anesthesia	Isoflurane	60 min dyn	(+)	B	VOI/heart, SUV, AUC	Iba1+	Mirzaei et al. 2016

Note: (+) increased TSPO tracer uptake in transgenic Alzheimer mice compared to wild-type mice; +, positive staining result; Abbreviations: *AUC*, area under the curve; *B*, brain; *CB*, cerebellum; *CTX*, cortex; *dyn*, dynamic; *F*, female; *HIP*, hippocampus; *IHC*, immunohistochemistry; *IV*, intravenous; *M*, male; *mo*, months; *NA*, not applicable; *NS*, non-specific; *QU*, quantification unit; *STR*, striatum; *SUV*, standard uptake value; *THA*, thalamus; *VOI*, volume of interest

Continuum of Table 2. Regional TSPO tracer retention detected with small animal μPET in transgenic mouse models of Alzheimer's disease.

Strain	Age (mo)	Sex	Tracer	Injection	Anesthesia	PET	Tracer uptake	Target brain region	QU	IHC	Reference
APP/PS1-21	6-15	M, F	^{18}F-DPA-714	IV in anesthesia	Isoflurane	60 min dyn	(+)	CTX, HIP, THA, STR	VOI/CB	Iba1+	**II**
PS2APP	5, 8, 13, 16	NA	^{18}F-GE-180	IV in anesthesia	Isoflurane	90 min dyn	(+)	Forebrain at 5 mo	Forebrain/CB, Forebrain/WM	Iba1+, TSPO+	Brendel et al. 2016
PS2APP	5, 8, 13, 16	F	^{18}F-GE-180	IV in anesthesia	Isoflurane	90 min dyn	(+)	Forebrain at 5 mo; B with SPM	Forebrain/CB, Forebrain/WM	Iba1+, TSPO+	Brendel et al. 2017
APP/PS1-21	1.5-1.75, 4, 7-8, 12-13	F	^{18}F-PBR111	IV awake	Isoflurane	40-60 min stat	(+)	CTX, THA, HIP	SUV	Iba1+, GFAP+	Deleye et al. 2017
APP_{swe}/ $PS1_{dE9}$	6, 12, 18	M	^{18}F-DPA-714	IV in anesthesia	Isoflurane	60 min dyn	(+)	HIP, subCTX at 18 mo	VOI/CB	GFAP+, TSPO+, CD11b+	Chaney et al. 2018
APP23	17-23	M, F	^{18}F-GE-180	IV in anesthesia	Isoflurane	60 min dyn	(+)	FC, PTC at 17 mo, HIP at 20 mo, THA at 26 mo	VOI/CB, SUV	Iba1+ at 26 mo	López-Picón et al. 2018
APP/PS1-21	4.5-19	M, F	^{18}F-FDPA	IV in anesthesia	Isoflurane	60 min dyn	(+)	FC, B, HIP at 12 mo	SUV	Iba1+	Keller et al. 2018

Note: (+) increased TSPO tracer uptake in transgenic Alzheimer mice compared to wild-type mice; +, positive staining result; Abbreviations: *B*, brain; *CB*, cerebellum; *CTX*, cortex; *dyn*, dynamic; *F*, female; *FC*, frontal cortex; *HIP*, hippocampus; *IHC*, immunohistochemistry; *IV*, intravenous; *M*, male; *mo*, months; *QU*, quantification unit; *stat*, static; *STR*, striatum; *SUV*, standard uptake value; *THA*, thalamus; *VOI*, volume of interest; *WM*, white matter.

Despite the successful imaging results gained from the aforementioned experiments, a criticism has been raised against TSPO - it should not be considered as a marker for overall neuroinflammation. TSPO tracers have also demonstrated several limitations, including high non-specific binding, low brain uptake, susceptibility to human polymorphism, and inabilities to discriminate between the activation stages of the glial cells (Janssen et al. 2018), which is accompanied with the limitations of the target itself. Furthermore, TSPO is differently expressed between species; it shows 9-fold increases in rodents, but not in humans (Owen et al. 2017). Therefore, other radioligands targeting different aspects of neuroinflammation have been explored due to the complex nature of the inflammatory pathway. Targets with great interest include MAO-B, COX2 (Shukuri et al. 2016), adenosine receptors, CB_2R, matrix metalloproteinases 2 and 9, $P2X_7R$, $P2Y_7R$, and B-lymphocyte antigens 19 and 20 (Shukuri et al. 2016; Moldovan et al. 2017; Beaino et al. 2016; Ory et al. 2016; Han et al. 2017; Janssen et al. 2018). The MAO-B ligand **^{11}C-deuterium-L-deprenyl**, has already been extensively used for imaging AD patients, showing significantly increased tracer retention in the patients as compared to healthy controls (Santillo et al. 2011; Carter et al. 2012), a result confirmed in the **Tg2576** mouse model, which demonstrated an increased tracer uptake in the cortical region and hippocampus of young animals (Rodriguez-Vieitz e al. 2015).

2.5.3 Targeting cannabinoid receptor 1

Radioligand development procedures have to follow many guidelines before PET tracer can be successfully used for *in vivo* imaging. Desirable features of the ideal ligand include low lipophilicity, and high affinity and molar activity among many other characteristics. The developmental path in creating reliable PET ligands targeting cerebral CB_1Rs has attracted increasing interest because of the involvement of this receptor in neuropsychiatric and neurodegenerative diseases, but obstacles due to the undesirable molecular features of these compounds. CB_1Rs are one of the most abundant receptors in the brain, which means that the affinity of the radioligand has to be subtle for the receptors compared to low-expressing receptors in the brain. This requires careful data quantification to avoid non-specific and misinterpretations of the tracer binding. In addition, CB_1R radioligands tend to have a transmembrane domain binding site, which makes them more lipophilic than the other types of ligands, which in turn, might lead to non-specific lipid or protein binding in the brain (Terry 2009a). Not surprisingly, all of the first generation CB_1R radioligands, which were radiolabeled tetrahydrocannabinol (**(-)-5'-^{18}F-fluoro-Δ9-THC**, Charalambous et al. 1991) or rimonabant analogues (Gatley et al. 1998; Berding et al. 2004), suffered from extremely high lipophilicity, low affinity, high non-specific binding, and low brain uptake. However, a rimonabant analogue **^{18}F-SR-14485** has displayed good molar activity and excellent brain penetration in mice, but no further evaluation has been conducted (Mathews et al. 1999 and 2000). Finally, after 15 years since the description of the first CB_1R radioligand, a group of second generation radioligands was shown to possess more

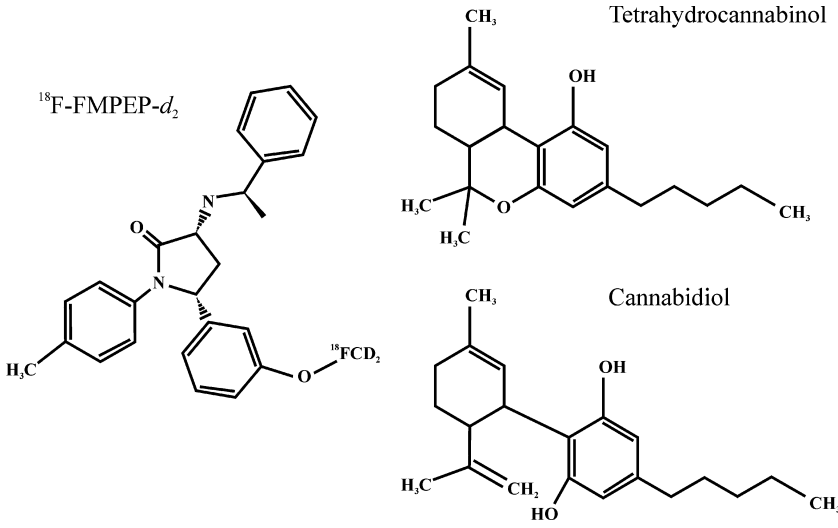

Figure 14. Molecular structures of type 1 cannabinoid receptor inverse agonist ^{18}F-FMPEP-d_2, a full agonist tetrahydrocannabinol, i.e. Cannabis Saliva, and the major compound of cannabis, cannabidiol.

feasible features for imaging purposes. A cyano-des-methyl derivative of a CB_1R antagonist (NIDA-41020) **^{11}C-OMAR** was developed in 2006 (Horti et al. 2006) demonstrating lower lipophilicity, greater binding affinity for CB_1Rs, and rapid kinetics as compared to the older compounds, but only moderate brain uptake in the baboon brain. In the human studies, healthy men exhibited greater cerebral ^{11}C-OMAR SUVs, but lower mean V_T values than females, revealing gender-related differences in CB_1R PET binding (Normandin et al. 2015). Similar findings were obtained with another second generation CB_1R PET ligand, **^{18}F-MK9470**, when healthy aging was examined in humans (Van Laere et al. 2008). In this study, males exhibited increased tracer uptake in the brain as compared to females, whereas age-dependent increases in ^{18}F-MK9470 binding were detected only in females. However, a comprehensively low cerebellar uptake was evident, which is in contrast to the histological distribution pattern since this area has high CB_1R density (Van Laere et al. 2008). A third reversible CB_1R tracer, **^{11}C-MePPEP**, has though demonstrated superior monkey brain uptake compared to the previous two new generation CB_1R radioligands with a moderate lipophilicity (Yasuno et al. 2008b), and a test-retest reproducibility of 15−16%, depending on the quantification method (Terry et al. 2009b; Riaño Barros et al. 2014). Unfortunately, ^{11}C-MePPEP has some limitations, including a low free fraction in plasma and unknown radiometabolite status in the brain (Terry 2009a; Terry et al. 2010). Hence, in an attempt to develop an analogue from ^{11}C-MePPEP with an extended half-life, a CB_1R inverse agonist **^{18}F-FMPEP-d_2**, was produced and evaluated in the monkey and human brain (Donohue 2008a and 2008b). ^{18}F-FMPEP-d_2 (*Figure 14*) has similar lipophilic properties, but better brain uptake and higher affinity than ^{11}C-MePPEP or other ^{18}F-labelled candidates. In addition, ^{18}F-FMPEP-d_2 showed approximately 90% specific binding to CB_1Rs and stable V_T already within 90 min after the injection, properties not seen with the previous

tracers. With this ligand, the plasma free fraction was found to be similarly low as with ^{11}C-MePPEP, however, the peak uptake was shown to reach SUV near 5 (Terry et al. 2010), which might be due to the reversible binding to plasma proteins.

At present, the role of CB_1R in the pathogenesis in AD is still controversial. Previous *post mortem* studies from AD brain tissue sampling have yielded heterogeneous results, which has been also the case in preclinical studies with AD mouse models. The conflicting results might originate from the discrepancies between the study protocols and the stage of the disease under investigation. Hence, monitoring CB_1R in a living brain could provide a noninvasive way to examine the possible changes within the receptor system and to monitor the effects of future disease modulatory interventions targeting CB_1Rs. However to date, the distribution of CB_1Rs in the AD human brain has been examined only once using ^{18}F-MK9470 (Ahmad et al. 2014). In that cross-sectional study, 11 AD patients and 7 healthy volunteers aged between 57–81 years were imaged with ^{18}F-MK9470 and ^{11}C-PiB to compare the CB_1R distribution with the amyloid burden. Unfortunately, no differences were detected between AD patients and healthy controls with regard to *in vivo* CB_1R availability. These results might suffer from the non-discrimination of the genders in the different cohorts, or from the broad age spectrum of the study subjects between 57 and 81 years that could have diminished to discriminate different AD disease stages. In terms of preclinical animal studies, before **III,** no AD model has been examined with CB_1R PET. In the future, however, since there are significant differences in the regional CB_1R distribution and signaling between human and mouse brain, extrapolating imaging results from preclinical experiments to clinical outcome will need to be done carefully (Herkenham et al. 1990).

As a summary of this review of the literature, PET offers a broad spectrum of applications that may help to improve the diagnostic accuracy of AD. Accurate and early detection of AD are crucial if one wishes to make an early diagnosis in differentiating healthy subjects from subjects suffering from neurodegenerative diseases. This could eventually lead to progress in intervention studies targeting AD progression. Hence, the present thesis work was initially generated based on the lack of ^{18}F-FDG PET imaging data on cerebral glucose metabolism in APP_{swe}-$PS1_{dE9}$ and Tg2576 mouse models, which nowadays are widely used and commercially available disease models for AD. Secondly, this thesis work aimed to evaluate for the first time changes in cerebral glucose metabolism in a novel AD mouse model, APP/PS1-21, because past imaging findings with different disease models had shown to be sparse and incomparable. In addition to validating disease models, this study also included experiments on evaluating modern PET radiotracers targeted for neuroinflammation and CB_1R for future preclinical imaging studies with mice.

3 AIMS OF THE STUDY

The overall aim of this thesis was to evaluate the translational applicability of disease models tailored for AD-related amyloidosis and PET tracers targeting cerebral glucose utilization, neuroinflammation, and CB_1R in preclinical *in vivo* imaging studies.

The following specific objectives were determined for this thesis:

I Evaluate differences in cerebral glucose metabolism in APP_{swe}-$PS1_{dE9}$ and Tg2576 mouse models of AD using an equivalent and cross-sectional *in vivo* ^{18}F-FGD PET study design and experimental protocols. The secondary objective was to examine the correlation between cerebral glucose metabolism and the stage of amyloidosis and microgliosis using *ex vivo* methods.

II Follow and quantify the relationship between temporal changes in cerebral glucose metabolism and glial activation in the APP/PS1-21 mouse model of AD using longitudinal *in vivo* ^{18}F-FDG and ^{18}F-DPA-714 PET imaging and *ex vivo* digital autoradiography.

III Evaluate the applicability of ^{18}F-FMPEP-d_2 for preclinical *in vivo* imaging studies (i.e. interventional studies and basic research) using pretreatment experiments and radiometabolite analysis in WT mice. Secondly, to follow and quantify temporal changes in cerebral CB_1R availability in the APP/PS1-21 mouse model of AD using longitudinal *in vivo* ^{18}F-FMPEP-d_2 PET imaging and *ex vivo* experiments, including digital autoradiography and Western blot.

4 MATERIALS AND METHODS

4.1 EXPERIMENTAL STUDY FLOW (I-III)

In Study **I**, brain glucose utilization was examined in two TG mouse models of AD using cross-sectional ^{18}F-FDG-PET imaging. Different animal models as well as TG and WT animals at different ages, which were exhibiting an early (6 months) and late (12 months or 17 months) stage of amyloidosis, were used as explanatory variables in the experimental units. The ^{18}F-FDG uptake was compared to underlying Aβ and microglial pathology determined with immunohistological quantification.

Study **II** was a continuation of Study **I**. Brain glucose utilization in accordance with the glial activation was examined with longitudinal PET imaging with ^{18}F-FDG and ^{18}F-DPA-714 in a novel mouse model of AD. Individual TG and WT mice were repeatedly imaged with both tracers at four different time points of 6, 9, 12, and 15 months. Animal groups allocated according to different ages were treated as experimental units in the analyses. The temporal change and in-between correlation of the tracer uptake in the brain regions were used as primary outcomes to measure the relationship of pathological events.

Study **III** was a continuation of Study **II** with regard to the animal model evaluation. The pharmacological profile and metabolism of ^{18}F-FMPEP-d_2 were evaluated in WT mice. Afterwards, temporal changes in the availability of CB_1Rs during amyloidosis in a mouse model of AD were examined using longitudinal ^{18}F-FMPEP-d_2 PET imaging. TG and WT mice were repeatedly examined at four different time points of 6, 9, 12, and 15 months, and the experimental units consist of animal groups at different ages. Changes in the ^{18}F-FMPEP-d_2 uptake were compared to the underlying CB_1R expression determined with Western blot and immunohistological examination.

4.2 EXPERIMENTAL ANIMALS (I-III)

All animal experiments of this thesis were approved by the State Provincial Office of Southern Finland (permission numbers ESAVI/3899/04.10.07/2013 and ESAVI/4499/04.10.07/2015). Animal wellbeing complied with the ethical guidelines of the International Council of Laboratory Animal Science (ICLAS). In addition, Studies **II** and **III** were performed in compliance with the Animal Research: Reporting of *In Vivo* Experiments guidelines with the principles of the 3Rs (Replacement, Reduction and Refinement) by using longitudinal PET imaging to examine the same animals repeatedly.

All animals were group-housed according to their sex in individual ventilated cages in the Central Animal Laboratory at University of Turku. Animals were living at a consistent temperature of 21 (1.2) °C and humidity of 55 (5) % with a diurnal rhythm of 12-hour light phase between 6 am

Table 3. Experimental animals with the descriptive statistics as arithmetic means (standard deviation) used for Studies **I-III**.

Study	**I**				**II**		**III**		
Strain	APP_{swe}-$PS1_{dE9}$	WT	Tg2576	WT	APP/PS1-21	WT	C57	APP/PS1-21	WT
n total	12	15	15	9	61	38	19	44	40
n dropouts	0	1	1	0	1	1	0	1	2
n failures	0	0	0	0	10	11	0	2	0
Sex	F	F	F	F	23 F, 38 M	21 F, 17 M	M	13 F, 31 M	13 F, 27 M
Age (months)	6, 12	6, 12	6, 17	6, 17	6, 9, 12, 15	6, 9, 12, 15	2-4	6, 9, 12, 15	6, 9, 12, 15
Weight (g)	26.1 (4.5)	27.6 (4.0)	25.0 (2.3)	26.2 (6.0)	31.9 (7.8)	39.8 (9.2)	31.9 (4.0)	34.6 (7.2)	44.4 (8.4)
PET tracer	^{18}F-FDG				^{18}F-FDG, ^{18}F-DPA-714		^{18}F-FMPEP-d_2		
Injected dose (MBq)	6.6 (1.4)	6.7 (1.0)	6.4 (1.2)	5.9 (0.9)	7.9 (0.6)*, 5.1 (1.4)**	8.0 (0.3)*, 5.8 (1.1)**	1.6 (1.0)	2.3 (0.9)	2.3 (0.8)
Experiment									
Cross PET	x	x	x	x			x		
Long PET					x	x		x	x
ARG	x	x	x	x	x	x	x	x	x
Pretreatment							x		
RadioTLC							x		
Western blot								x	x
Thio S					x	x		x	x
IHC	x	x	x	x	x	x		x	x

Note: *^{18}F-FDG; **^{18}F-DPA-714

Abbreviations: *ARG*, autoradiography; *C57*, C57Bl/6N mouse line; *Cross PET*, cross-sectional PET imaging; *F*, female; *IHC*, immunohistochemistry; *Long PET*, longitudinal PET imaging; *M*, male; *RadioTLC*, thin-layer chromatography on radioactive compounds; *Thio S*, Thioflavine S; *WT*, wild-type

and 6 pm. The mice had free access to tap water and certified standard laboratory soy-free chow (RM3 soya-free, 801710, Special Diets Service, Essex, UK). Animals were weighed at the beginning of each experimental session, and in studies **I** and **II**, their body temperature and fasting blood glucose were measured before and after every ^{18}F-FDG injection with a microprobe rectal thermometer (Physitemp Instruments, Inc., USA) and Accu-Chek Aviva Nano (Roche Diagnostics, USA), respectively. The number of experimental animals used in each study and in experiments with additional details are presented in *Table 3*.

4.2.1 Wild-type animals

C57BL/6N mice were bred in the Central Animal Facility of University of Turku and used for breeding with APP/PS1-21 mice (**II** and **III**), and were also used for the radiometabolite analysis and pretreatment experiments (**III**).

Table 4. The genetic and phenotype features of the transgenic mouse models used in Studies **I–III**. Data are collected from the Alzforum Research Model Database on November 2018.

Strain	**APP_{swe}-$PS1_{dE9}$**	**Tg2576**	**APP/PS1-21**
Transgenes	APP, PSEN1	APP	APP, PSEN1
Mutations	hu/mo$APP695_{swe}$, $PSEN1_{dE9}$	hu/mo$APP695_{swe}$,	huAPP_{swe}, $PSEN1_{L116P}$
Promoter	Murine prion	Hamster PrP	Murine Thy1
Known pathological features			
Amyloid deposits	4 months	11-13 months	6 weeks
Microgliosis	4 months	17 months	6 weeks
Astrocytosis	3 months	NA	6 weeks
Neurofibrillary tangles	No	No	No
Phosphorylated tau	Yes	Yes	Yes
Neuronal loss	No	No	17 months
Behavioral changes	12 months	6, 12 months	7-8, 12 months

4.2.2 Transgenic mouse models

APP_{swe}-$PS1_{dE9}$

APP_{swe}-$PS1_{dE9}$ (B6.Cg(APPswe, PSEN1d9E)85Dbo/Mmjax; The Jackson Lab., JAX MMRRC) and the corresponding WT mice were obtained from Jackson Laboratories Inc., for Study **I**. The investigated time points for this model were 6 and 12 months. The APP_{swe}-$PS1_{dE9}$ mouse model expresses mouse *APP* with humanized Aβ region and the *Swedish* mutation at amino acids 595/596, and human *PSEN1* with exon 9 deletion (Jankowsky et al. 2001). The mice exhibit $Aβ_{1-42}$-type peptide aggregations over $Aβ_{1-40}$ in the brain, which primarily accumulate into abundant plaques at 6 months of age in the cortical region and hippocampus, and eventually to other brain regions (Garcia-Alloza et al. 2006; Brendel et al. 2015; Sérrière et al. 2015). This model also expresses other characteristical AD features such as gliosis, but does not display any NFT changes (*Table 4*; Jackson et al. 2016; Alzforum).

Tg2576

Tg2576 (B6;SJL-Tg(APPswe)2476Kha; Taconic Inc.) and corresponding WT mice were obtained from Taconic Farms Inc. for Study **I**. The examined time points of this mouse model were 6 and 17 months. Tg2576 mice express the 695-amino acid isoform of human *APP* carrying the *Swedish* mutation KM670/671NL (Hsiao et al. 1996). This model exhibits a 5-fold increase in $Aβ_{1-40}$ and a 14-fold increase in $Aβ_{1-42}$ peptides in the brain, forming weak plaques by the age of 11-13 months in the cortical and limbic regions. In addition, Tg2576 mice show increased signs of microgliosis and astrocytosis around the Aβ plaques at a very old age (*Table 4*).

APP/PS1-21

APP/PS1-21 (B6.Cg-Tg(Thy1-APPswe, Thy1-PSEN1*L166P)21Jckr) mice were originally purchased from Koesler, Germany. The animals were further bred in the Central Animal Laboratory of University of Turku with C57BL/6N mice to enlarge the colony. Breeding produced heterozygote TG and the corresponding WT mice. The genotype of each newborn animal was tested and confirmed by Clinical Research Service Turku for Studies **II** and **III**. This model was examined at different time points of 1, 2, 3, 6, 9, 12, and 15 months. The APP/PS1-21 mice co-express human *APP* with the *Swedish* double mutation KM670/671NL and the L166P mutated human *PSEN1* under the control of a neuron-specific murine Thy-1 (Radde et al. 2006). These mutations initiate primarily $A\beta_{1-42}$-driven plaque formation in an aggressive manner in 6-week-old animals, which worsen as the mice age. The Aβ deposits appear first in the neocortex, and later in the hippocampus, striatum, thalamus, and brainstem by the age of 5 months. The plaques are accompanied by microglia proliferation, astrocytosis, and the presence of phosphorylated tau trajectory protein with a modest neuronal loss (*Table 4*; Rupp et al. 2011; Unpublished data).

4.3 RADIONUCLIDE AND TRACER PRODUCTION (I-III)

The radionuclide ^{18}F was produced via ^{18}O (p, n) ^{18}F in a nuclear reaction in the Accelerator Laboratory of Turku PET Centre by using CC-18/9 cyclotron (Efremov Scientific Institute of Electrophysical Apparatus, St. Petersburgh, Russia).

^{18}F-FDG, ^{18}F-DPA-714, and ^{18}F-FMPEP-d_2 were synthetized in the Radiopharmaceutical Chemistry Laboratory of Turku PET Centre as described previously (Hamacher et al. 1986; James et al. 2008; Donohue et al. 2008). The molar activities, batches, and radiochemical purities of the tracers used in Studies **I-III** are presented in *Table 5*.

4.4 *IN VIVO* PET IMAGING (I-III)

All *in vivo* PET/computed tomography (CT) scans were conducted with the Inveon Multimodality PET/CT device (Siemens Medical Solutions, Knoxville, TN, USA), which has a spatial resolution of 1.3 mm.

The CT modality preceded PET scan, and it was used as a transmission phase for primary anatomical reference and attenuation correction for PET imaging data. In Studies **I** and **II**, dynamic 60-min 3D PET list mode scans were conducted in tandem with the tracer injection, whereas in Study **III**, 3D PET list modes were recorded as 30-min static modalities at 90 min after the ^{18}F-FMPEP-d_2 injection. Afterwards, the PET list mode data were reconstructed as described previously (**I** and **II)** using Fourier-rebinning and 2D filtered back-projection

Table 5. Radioactive tracer and imaging quantification specifics used in Studies **I–III**.

Study	**I**	**II**		**III**
PET tracer	^{18}F-FDG	^{18}F-FDG	^{18}F-DPA-714	^{18}F-FMPEP-d_2
Am_{EOS} (GBq/µmol)	> 100	> 100	> 1000	> 500
Am_{Inj} (GBq/µmol)	NA	NA	541 (220)	359 (71)
Injected mass (ng)	NA	NA	4.5 (2.1)	3.2 (1.1)
Radiochemical purity (%)	> 98	> 98	> 99.5	> 95
Number of batches	37	27	16	34
PET imaging	dynamic	dynamic	dynamic	static
Duration (min)	60	60	60	30
Quantification ΔT (min p.i.)	20-35	30-60	30-50	90-120
Quantification unit	SUV, SUVglu	SUV	SUV, VOI/CB	SUV, VOI/THA
***Ex vivo* autoradiography**				
Quantification ΔT (min p.i.)	30	60	60	120
Quantification unit	ROI/WB	ROI/CB	ROI/CB	ROI/THA

Note: Mean molar activity and injected mass are presented with standard deviation. **Abbreviations:** *Am*, molar activity; *CB*, cerebellum; *EOS*, end of synthesis; *Inj*, injection; *NA*, not applicable; *p.i.*, post injection; *ROI*, region of interest; *SUV*, standardized uptake value; *THA*, thalamus; *VOI*, volume of interest; *WB*, whole brain

reconstruction algorithm, and divided into 51 time frames (30*10 s, 15*60 s, 4*300 s, and 2*600 s) in Studies **I** and **II** or 10 time frames (5*60s and 5*300s) in Study **III**. All PET scans and tracer injections were performed in animals anesthetized with an inhalation of 2.5% isoflurane/oxygen mixture on fasted (**I**, **II** with ^{18}F-FDG) or nonfasted (**II** with ^{18}F-DPA-714, **III**) mice. The tracer injections were delivered via IV cannula inserted in the mouse tail vein (left or right). The full *in vivo* PET imaging work flow is illustrated in *Figure 15* containing the details of fasting (**I**, **II**), anesthesia (**I-III**), and glucose and temperature measurements (**I**, **II**).

PET imaging data were analyzed as volumes of interest (VOIs) using Inveon Research Workplace Image Analysis software v. 4.1 and 4.2 (Siemens Medical Solutions). VOIs were first predefined, then uploaded and manually adjusted to an individual PET image after a coregistration of the corresponding anatomical CT image and a representative MRI mouse brain template (Mouse MRI brain template), which guided the anatomical 3D orientation of the following analyzed brain regions (*Figure 16*): the whole brain including the olfactory bulbs, cortex, frontal cortex, parietotemporal cortex, hippocampus, striata, thalamus, hypothalamus (**III**) and cerebellum. PET imaging data were semi-quantified as SUVs (**I-III**), which refers to a division of the regional radioactivity by the ratio of injected dose and mouse body weight. In Studies **I** and **II**, SUVs were also normalized with the individual blood glucose value measured before ^{18}F-FDG injection in order to obtain the SUV_{glu} (SUV*prescan blood glucose value). In addition, regional radioactivity concentration ratios relative to the reference region were also determined (**II** and **III**). Details of the study-specific quantification time period and units as well as the reference regions are presented in *Table 5*.

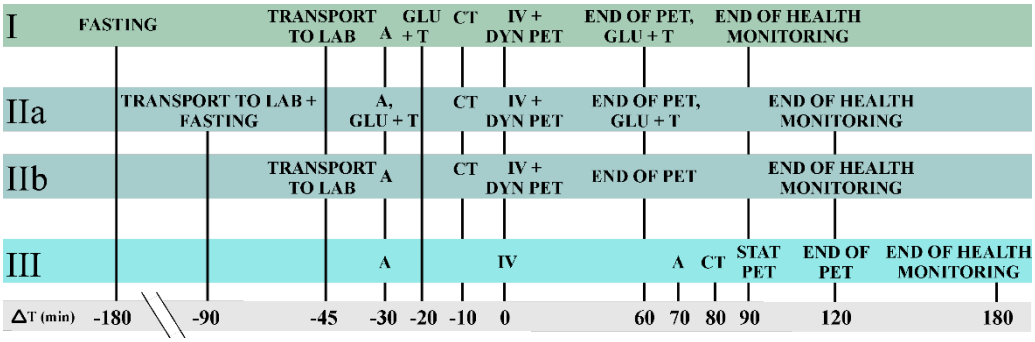

Figure 15. ***In vivo*** **PET imaging work flow for studies I-III in accordance to the tracer injection time at 0.** ^{18}F-FDG was used in studies **I** and **IIa**, whereas ^{18}F-DPA-714 was used in **IIb**. For Study **III**, ^{18}F-FMPEP-d_2 was utilized for PET imaging. *A*, anesthesia; *CT*, computed tomography; *dyn*, dynamic; *GLU*, glucose; *IV*, intravenous injection of the tracer; *PET*, positron emission tomography; *stat*, static; *T*, body temperature.

4.5 *EX VIVO* BRAIN AUTORADIOGRAPHY (I-III)

All tracer injections were administered to the fasted (**I**, **II** with ^{18}F-FDG) or non-fasted (**II** with ^{18}F-DPA-714, **III**) animals in anesthetized with 2.5 % isoflurane/air mixture via an IV cannulated mouse tail vein (left or right). The specific or non-specific regional ^{18}F-FDG uptake was measured in the brains of 6- to 17-month-old TG and WT mice with a distribution time of 30 (**I**) or 60 min (**II**) after the tracer injection. The ^{18}F-DPA-714 binding (**II**) was examined in the brains of 1- to 15-month-old TG and WT mice with a distribution time of 60 min after the tracer injection. The specific regional ^{18}F-FMPEP-d_2 binding (**III**) was evaluated in the brain of 6- to 15-month-old TG and WT mice with a distribution time of 120 min after the injection. After the distribution time (*Figure 17*), animals were anesthetized with 4.0% isoflurane/air mixture to perform cardiac puncture and transcardial perfusion with physiological saline. Brains were removed from the skull, weighed, and measured for the radioactivity using 2480 Wizard^2 automatic gamma counter (Perkin Elmer, Turku, Finland). *Ex vivo* tissue counting was also performed with cardiac blood sample, tail, and additional organs (**I**; *Unpublished data*). Brains were rapidly frozen in isopentane, which was chilled with solid carbon dioxide. Shortly, the brains were cut into coronal 20 µ-thick cryosections with a cryostat (Leica CM3050S, Leica Biosystems, Nußloch, Germany) at the bregma levels from -6.00 to +2.60. Cryosections on the microscope slides were air-dried and exposed to imaging plates (Fuji Imaging Plate BASTR2025, Fuji Photo Film Co., Japan) for two half-lives of ^{18}F. The ^{18}F-radioactivity distribution on the plate was digitized using the BAS5000 analyzer (Fujifilm Lifesciences, Japan). Digital autoradiography data were analyzed as regions of interest (ROI) using Aida Image Analysis software (Image Analyzer v. 4.22; Raytest Isotopenmeßgeräte GmbH, Straubenhardt, Germany). ROIs were manually drawn on the digitized autoradiographs over the following brain regions: frontal cortex, parietal cortex (**I**), temporal cortex (**I**), parietotemporal cortex, striatum, thalamus, hippocampus (**I**), anterior

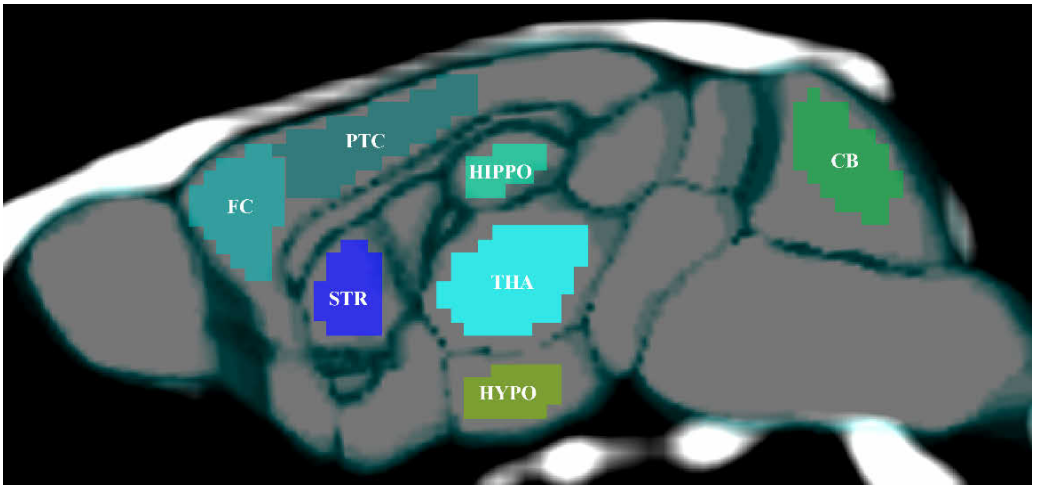

Figure 16. Mouse brain MRI template aligned with a representative mouse computed tomography with representative volumes of interest used for PET image quantification in I-III. *CB*, cerebellum; *FC*, frontal cortex; *HIPPO*, hippocampus; *HYPO*, hypothalamus; *PTC*, parietotemporal cortex; *STR*, striata; *THA*, thalamus.

hippocampus (**II**, **III**), posterior hippocampus (**II**, **III**), hypothalamus (**III**), cerebellum (**I**, **II**), cerebellar gray matter (**III**), and cerebellar white matter (**III**) (*Figure 18*). The digital autoradiograph ROIs were analyzed for count densities and expressed as background-erased photostimulated luminescence intensity per square millimeter (PSL/mm^2) ratios relative to the selected reference region (*Table 5*).

4.6 PRETREATMENT EXPERIMENT (III)

The specific binding of ^{18}F-FMPEP-d_2 in mouse brain was evaluated with a CB_1R inverse agonist, rimonabant (SR141716; No. 9000484, Cayman Chemical, MI, USA) to determine the preliminary usability of this tracer in murine imaging studies. C57BL/6N mice were first anesthetized with 2.5% isoflurane/air mixture 20 min prior to pretreatment. Mice were IV cannulated via a tail vein and pretreated with rimonabant (2 mg/kg) or with vehicle 10 min prior to ^{18}F-FMPEP-d_2 IV injection. ^{18}F-FMPEP-d_2 (3.4 (0.2) MBq) was administered and a dynamic 90-min 3D PET/CT list mode scan was initiated in tandem. After the scan, the mice were sacrificed as described in chapter 4.5. The *ex vivo* autoradiography experiment was used for the visual examination and *in vivo* PET for the quantification of the pretreatment experiment. The equivalent size of VOI was manually drawn over the whole brain, and the radioactivity of the VOI was semi-quantified as SUV. The *in vivo* data was verified with *ex vivo* tissue counting of the brain and quantified as %ID/g.

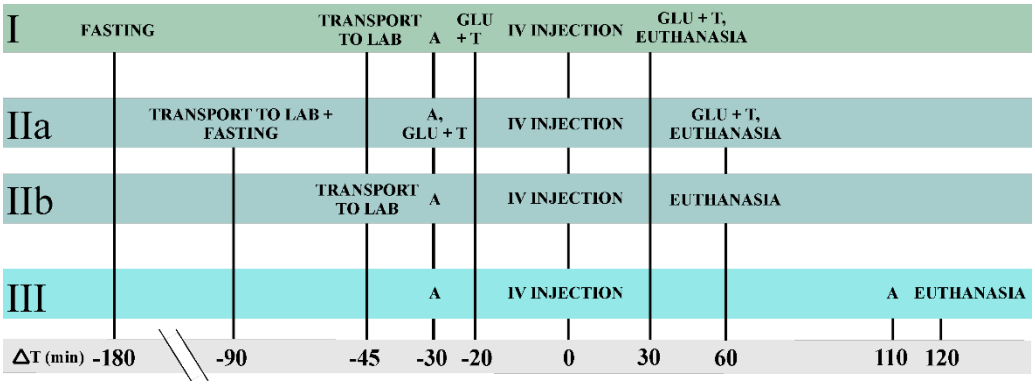

Figure 17. ***Ex vivo*** **autoradiography work flow for studies I-III in accordance to the tracer injection time at 0**. ^{18}F-FDG was used in studies **I** and **IIa**, whereas ^{18}F-DPA-714 was used in **IIb**. For Study **III**, ^{18}F-FMPEP-d_2 was utilized for autoradiography. *A*, anesthesia; *GLU*, glucose; *IV*, intravenous; *T*, temperature.

4.7 RADIOMETABOLITE ANALYSIS (III)

The amounts of unchanged ^{18}F-FMPEP-d_2 and its radiometabolites were examined in the mouse plasma and brain using thin-layer chromatography (TLC) and digital autoradiography with distribution time points between 5 and 240 min. Brains of the C57BL/N mice were dissected as described earlier in Chapter 4.5. Plasma samples were collected by centrifuging the cardiac puncture blood and separating the supernatant. Brain homogenates were prepared by manually homogenizing brain tissue samples from the parietotemporal cortical region into acetonitrile. After centrifugation, the supernatants of both brain and plasma samples were collected and pipetted on top of Silica Gel High-performance RP-18 TLC plates (Merck, Darmstadt, Germany). ^{18}F-FMPEP-d_2 from the same batch was used as a reference standard in the analyses. The TLC plates were developed in 1% trifluoroacetic acid/acetonitrile (40:60 v/v) mobile phase, after which the plates were dried and exposed to imaging plates for two half-lives of ^{18}F, and the radioactivity in the plates was digitized with the BAS5000 Analyzer. The proportions of unchanged and metabolized ^{18}F-FMPEP-d_2 in the plasma and brain total ^{18}F-radioactivity and their retention factors (R_f) were calculated from the autoradiograms using Aida Image Analysis software.

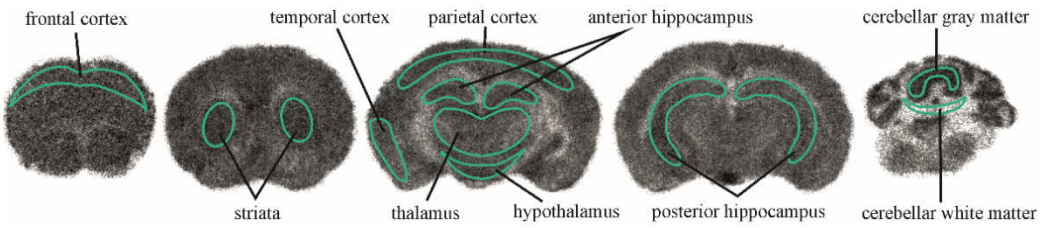

Figure 18. Regions of interest drawn over the digital autoradiographs in Studies I–III.

4.8 WESTERN BLOT (III)

The *in vivo* ^{18}F-FMPEP-d_2 binding was validated with *ex vivo* Western blot to examine whether the CB_1R expression is altered in APP/PS1-21 mouse model of AD in comparison to non-diseased WT mice. Following brain regions were examined: frontal cortex, parietotemporal cortex, hippocampus, and thalamus. Nine-month-old female and male APP/PS1-21 and WT mouse brain samples were assessed separately to quantify the gender difference within the CB_1R protein levels. Brain samples were dissected during the *ex vivo* digital autoradiography and tissue counting experiments, and immediately frozen in liquid nitrogen. Samples were mechanically homogenized on ice with an equal volume of lysis buffer as described in detail in **III**. In brief, the homogenates were boiled for 5 min at 95°C and centrifuged for 25 min in 12,000 rpm from which the supernatants were collected to determine the total protein concentration of the homogenates using the Pierce™ BCA protein assay kit (Thermo Scientific). The samples were denatured with a master buffer for 5 min at 95°C and equal amounts of protein were pipetted onto a 10% SDS-polyacrylamide gel lanes. Proteins were first separated according to their weight by electrophoresis and transferred onto nitrocellulose pure transfer membranes (UltraCruz®, Santa Cruz Biotechnology, Texas, US) using a Mini Trans-Blot cell electroblotter (BIO-RAD Life Science Group, CA). Membranes were blocked either in 3% (w/v) bovine serum albumin (BSA, Sigma Aldrich) diluted in 0.1% Tween Tris-buffered saline (TBS-T) at 4°C overnight or in 5% (w/v) dry skim milk diluted in TBS-T for 90 min at room temperature depending on the following primary antibody. Overnight incubation at 4°C was performed first with anti-CB_1R primary antibody (1:500 dilution in 3% BSA TBS-T) and secondly with a housekeeping primary anti-β-actin antibody (1:1000 dilution in 5% skim milk TBS-T). Membranes were washed with TBS-T and incubated with the secondary antibody (Donkey anti-Rabbit IgG H+L, 1:2000 dilution in TBS-T) for 1 h at room temperature. Membranes were washed again with TBS-T before detecting the fluorescent signal using LI-COR Odyssey® CLx Imaging System (LI-COR, Inc.). The fluorescent signals of the membranes were analyzed using Image Studio Software Lite software v. 5.2 (LI-COR, Inc.). The signal intensities of the CB_1R bands were normalized to a reference band of the β-actin housekeeping protein in each membrane, and membranes normalized to the protein marker before being compared with each other.

4.9 IMMUNOHISTOCHEMISTRY (I-III)

Immunohistochemical stainings were performed with fresh frozen mouse brain 20-µm thick coronal cryosections collected from the *ex vivo* digital autoradiography experiments in Studies **I–III**. The sections were stored at -20°C before proceeding to staining according to previously described protocols and employed reagents within Studies **I-III**. In Study **I**, APP_{swe}-$PS1_{dE9}$ and Tg2576 brain cryosections were stained with a monoclonal antibody against Aβ (*6E10*, 1:400)

and ionized calcium-binding adapter molecule 1 (*Iba1*, 1:1000), whereas in Study **II**, APP/PS1-21 brain cryosections were dyed with Thioflavine S (0.025%) and stained with antibodies against $A\beta_{1\text{-}42}$ and Iba1 (1:500 for both). In Study **III**, anti-CB_1R (1:500) and GFAP (1:500, unpublished) were used for staining the APP/PS1-21 mouse brain sections. Stained sections were imaged using the 3DHISTECH Midi Scanner (Thioflavine S) or Slide Scanner 250 (antibodies). In Study **I**, the amounts of regional Aβ and microgliosis were determined in different brain regions of APP_{swe}-$PS1_{dE9}$ and Tg2576 mice with primary evaluation procedures using CaseViewer software v. 1.3 (3DHISTECH, Budapest, Hungary) and quantified using Image J software (Wayne Rasband, National Institute of Health, MD, USA). In Studies **II** and **III**, no quantification procedures were conducted.

4.10 STATISTICAL ANALYSES (I-III)

Descriptive statistics, i.e. molar activity at the time of injection, injected dose, weight of the animals, glucose values, and *in vivo* PET imaging and *ex vivo* results from Studies **II** and **III** are presented as arithmetic means with standard deviation in brackets after the mean values. Due to the normal distribution of the numeric data in Study **I**, *in vivo* and *ex vivo* results are presented as medians and interquartile ranges.

In Study **I**, cross-sectional *in vivo* and *ex vivo* differences in regional glucose tracer uptake and microglial staining between TG and WT mice in various time points were examined with Kruskal-Wallis test, following Dunn's multiple comparison. The non-parametric Mann-Whitney U-test was used for exploring the differences in the formation of amyloid in TG mice in various ages. In Studies **II** and **III**, longitudinal PET data were examined using hierarchical mixed linear model with a compound symmetry covariance structure, including one within-factor (*time*), one between-factor (*genotype*), and an interaction term (*time* × *genotype*). Interactions were investigated by examining whether the mean change during the longitudinal study was different between the genotypes. When a significant interaction was encountered, contrasts were programmed to study when the interaction occurred between TG and WT animals. The normal distribution assumption was checked based on the studentized residuals. *Ex vivo* results in Studies **II** and **III** were examined using the non-parametric Mann-Whitney U-test or 2-way ANOVA based on the distribution parameters of the data set. Examinations of correlation conducted in Studies **I**–**III** were quantified with the Pearson test or with the Spearman's test based on the normal distribution of the data set. All statistical tests were performed as two-sided with the statistical significance level set at 0.05. The distribution of data and statistical analyses were performed using GraphPad Prism v. 5.01 and 6.00 (GraphPad Software, San Diego, CA, USA), SAS System v. 9.3 for Windows (SAS Institute Inc., Cary, NC, US), and SPSS Statistics v. 23 (IBM).

5 RESULTS

5.1 AMYLOIDOSIS IN THE TRANSGENIC MOUSE MODELS

At 6 months of age, both APP_{swe}-$PS1_{dE9}$ mice and APP/PS1-21 mice exhibited extensive 6E10- and $A\beta_{1-42}$-positive amyloid deposition, respectively, mainly in the cerebral cortex and hippocampus (*Figure 19*). Amyloidosis further expanded to the other brain regions, including thalamus, striata, and cerebellum with the highest burden observed when older animals at the age of 12 or 15 months were examined (**I**, **II**). In APP/PS-21, the number of $A\beta_{1-42}$-positive plaques seemed to grow as the mice aged, but the size of the plaques did not increase in a temporal manner, whereas in APP_{swe}-$PS1_{dE9}$ mice, 6E10-positive depositions formed dense Aβ-positive groups and/or accumulated more to create larger plaques.

When compared to the APP/PS1-based models, Tg2576 mice showed a much slower temporal course of amyloidosis: Sparsely located single Aβ deposits were found randomly in the brain of 6-month-old Tg2576 mice. Not until the age of 17 months, increases in the numbers of the Aβ-positive deposits in the cortical and hippocampal region were measurable in this AD mouse model.

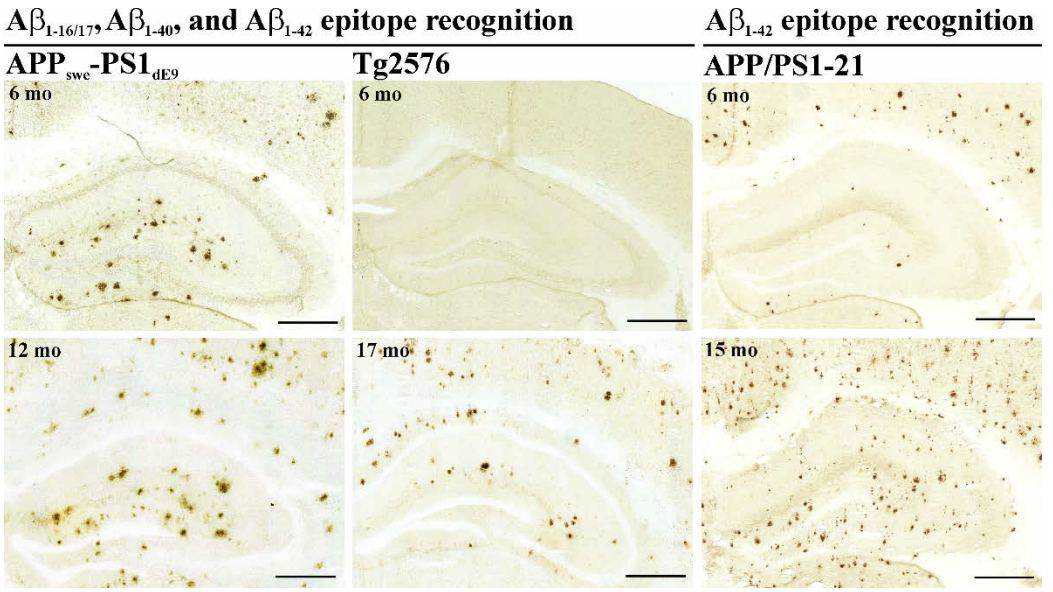

Figure 19. Temporal amyloidosis in the transgenic mouse models used in studies I-III. *mo*, months. Scale bar 200 μm.

5.2 CEREBRAL GLUCOSE METABOLISM DETECTED WITH ^{18}F-FDG

The three AD mouse models were examined to search if there were differences in their cerebral glucose metabolism compared to the corresponding WT mice by using dynamic ^{18}F-FDG PET imaging and *ex vivo* brain autoradiography.

^{18}F-FDG accumulated into the brain rapidly, having a peak uptake as assessed by the SUV between 1.5 and 2.0 approximately at 4 min after the IV injection, after which, a washout began slowly. In APP_{swe}-$PS1_{dE9}$ and APP/PS1-21 mice, the peak uptake plateaued more rapidly within the first 20 min of the dynamic scan, whereas in Tg2576 mice, the washout stage was more profound during the last 30 min of the modality without losing the plateau phase (*Figure 20*). ^{18}F-FDG mainly remained in the brain at 60 min, and was eventually eliminated by radioactive decay, and only partly eliminated through the renal system. In all models, ^{18}F-FDG accumulated predominantly into the midbrain region and cerebellum, concentrating in the vessel-enriched regions (*Figure 21*). In addition, the tracer underwent significant accumulation into the Harderian glands in all mice causing a partial volume effect in frontal brain.

The APP_{swe}-$PS1_{dE9}$ and APP/PS1-21 models showed significantly decreased ^{18}F-FDG SUVs ($p < 0.05$) at different ages in the brain compared to WT mice (*Fig. 2 and 3 in **I**; Table 2 in **I**; Fig. 1 in **II***). APP_{swe}-$PS1_{dE9}$ mice demonstrated a moderate hypometabolic pattern already at the age of 6 months, whereas in APP/PS1-21 mice, altered glucose utilization was significant at 12 months. In the late disease stage at 12 and 15 months, both APP_{swe}-$PS1_{dE9}$ and APP/PS1-21 mice exhibited further declines in the ^{18}F-FDG retention as compared to their WT littermates, the latter showing statistically significant ($p < 0.05$) changes in all analyzed brain regions. In detail, the most profound regional differences between the genotypes and age groups were examined in subcortical regions, hippocampus, striata, thalamus, and cerebellum in both models ($p < 0.05$). However in APP_{swe}-$PS1_{dE9}$ mice, when SUVs were normalized to the individual blood glucose values, the intragroup variation increased, which prevented the detection of a significant difference between the genotypes. On the contrary, 15-month-old, but not 6-month-old APP/PS1-21 mice showed significantly ($p < 0.005$) larger declines in the cerebral ^{18}F-FDG retention after the SUVs were normalized to the blood glucose values (*Figure 20*), even though the intragroup variation was parallely increased. Tg2576 did not demonstrate differences in the cerebral glucose metabolism when compared to WT mice (*Table 3 in **I***).

An increased trend in the temporal ^{18}F-FDG retention within the same strain was observed in studies **I** and **II**. APP_{swe}-$PS1_{dE9}$ and WT mice showed age-related glucose hypermetabolism from 6 to 12 months in different brain regions (*Table 2 in **I***), whereas the same APP/PS1-21 and WT mice demonstrated significant ($p < 0.05$) cerebral hypermetabolism, when they were examined from 6 to 15 months of age (Unpublished data for Study **II**).

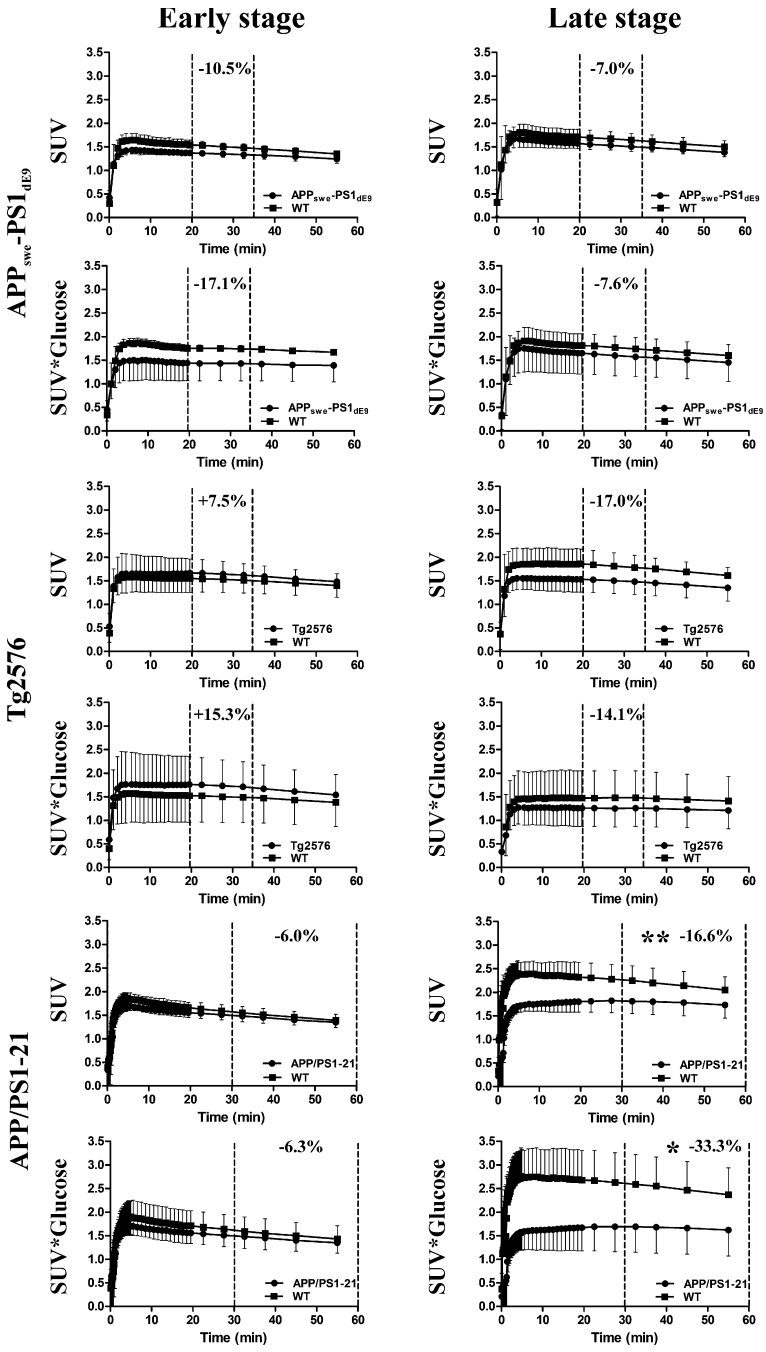

Figure 20. Mean cerebral time activity curves for ^{18}F-FDG retention in transgenic mouse models of Alzheimer's disease and the corresponding wild-type (WT) control mice. An early disease stage (6 months) and a late disease stage (12, 17, or 15 months respectively) as standard uptake values (SUV) and normalized SUVs against the individual blood glucose values 20 min before the IV injection were examined. Dashed lines represent the time frame used for quantification of the summed PET images post injection. Percentage of the mean ^{18}F-FDG uptake in transgenic mice compared to the mean tracer uptake of WT mice in presented above the quantified time frame.

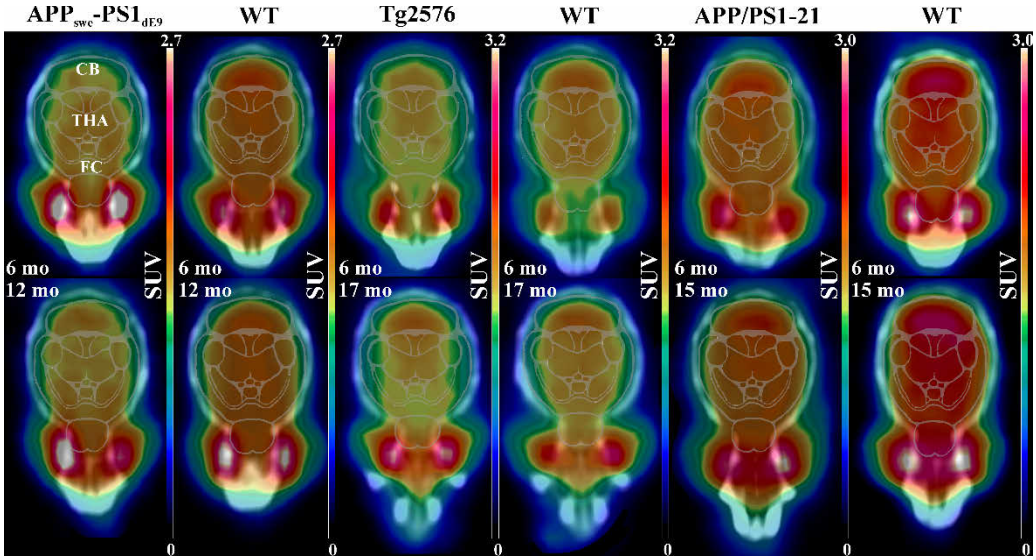

Figure 21. Cerebral ^{18}F-FDG retention in transgenic mouse models of Alzheimer's disease and the corresponding wild-type (WT) mice. An early (6 months) and late (12, 15, or 17 months) examination stages were investigated and represented as summed 60-min PET/CT images aligned with an illustrative MRI-template of an adult mouse brain with the colors adjusted according to the genotype-dependent standard uptake minimum and maximum values. *mo*, months; *SUV*, standardized uptake values.

The *ex vivo* ^{18}F-FDG uptake in the murine brain showed a similar pattern of the tracer distribution seen in the *in vivo* data under enhanced spatial resolution (*Figure 22*). However, the *ex vivo* quantification as ratios relative to the pseudo-reference region cerebellum (**II**) or the whole brain estimate (**I**) did not fully confirm the *in vivo* hypometabolism detected with PET imaging due to the obvious differences in the quantification method between PET and autoradiography. Instead, hypermetabolic cortical and hippocampal changes were detected in 12- to 15-month-old APP/PS1-21 and 6- and 12-month-old APP$_{swe}$-PS1$_{dE9}$ mice as compared to age-matched WT mice when relative measures were applied (*Table S1 in **I**; Fig. 3 in **II***).

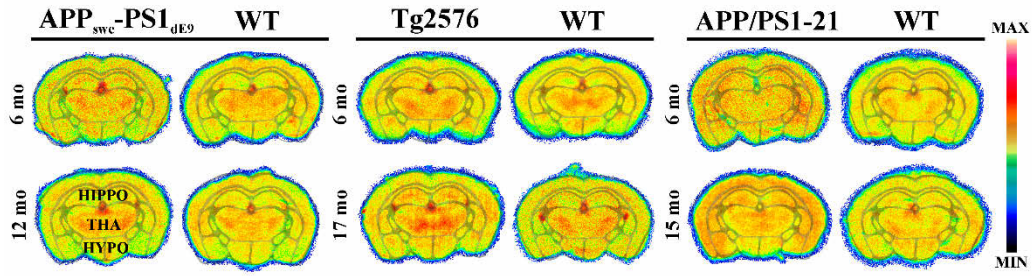

Figure 22. Representative coronal ^{18}F-FDG autoradiographs of young (6 months) and old (12, 15, or 17 months) transgenic mice of Alzheimer's disease and the corresponding wild-type (WT) mouse brain cryosections. *mo*, months; *HIPPO*, hippocampus; *HYPO*, hypothalamus; *THA*, thalamus.

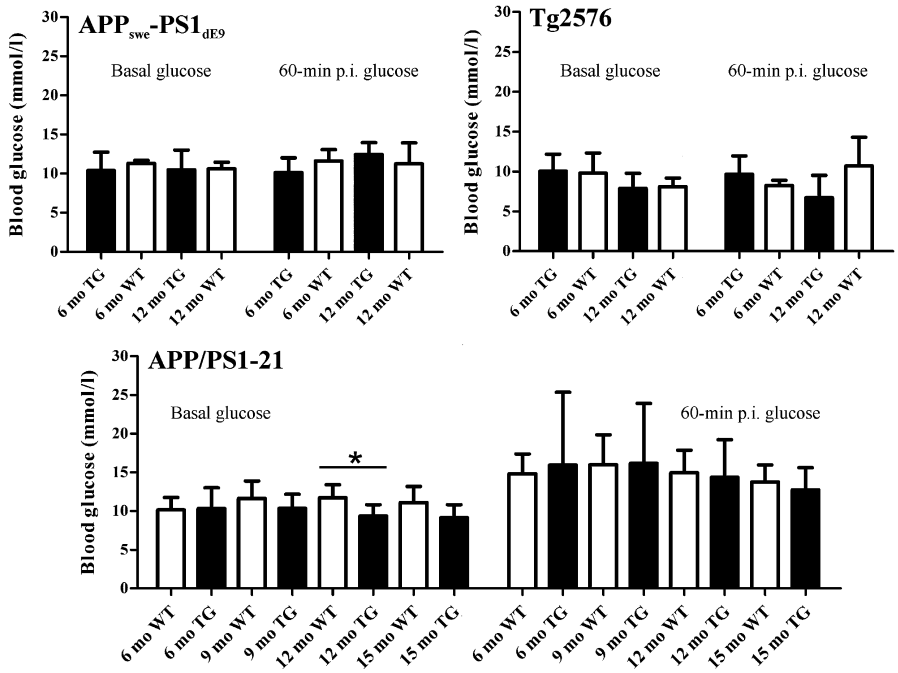

Figure 23. Basal and 60-min *in vivo* ^{18}F-FDG-PET post injection (p.i.) blood glucose values. The tail blood glucose of transgenic (TG) mice of Alzheimer's disease and the corresponding wild-type (WT) mice were measured before and after every *in vivo* experiment in studies **I** and **II.**

In vivo, cerebral glucose hypometabolism was shown to correlate negatively in a moderate manner with the Aβ depositions in 12-month-old APP$_{swe}$-PS1$_{dE9}$ mice, whereas no such correlation was detected in Tg2576 mice (*Fig. 4 in **I***). The amyloidosis in APP/PS1-21 mice was not quantified in this study, however, Aβ$_{1-42}$-positive deposits were localized abundantly already at the age of 6 months in cortical lobes and thalamus, which escalated in number and size to the other brain regions as the mice aged, at the same time as the regional hypometabolism detected with *in vivo* ^{18}F-FDG was developing.

Changes in the blood glucose values and temperatures during ^{18}F-FDG-PET

In studies **I** and **II**, the basal blood glucose values of any TG and WT mice i.e. 20 min before the *in vivo* ^{18}F-FDG-PET imaging did not differ compared to the post injection (p.i.) blood glucose values measured immediately after the 60-min dynamic PET scan. However, the basal blood glucose measurements between 12-month-old APP/PS1-21 and age-matched WT mice differed significantly (*Figure 23*). APP/PS1-21 showed further increased intragroup variations in their glucose values after the PET scan, which was not seen in either APP$_{swe}$-PS1$_{dE9}$ or Tg2576 mice. The body temperature of mice was measured before (basal) and immediately after the ^{18}F-FDG scan. Under basal circumstances, murine rectal temperatures did not differ between TG and WT mice nor between different models, whereas a significant decrease ($p < 0.01$) was detected after

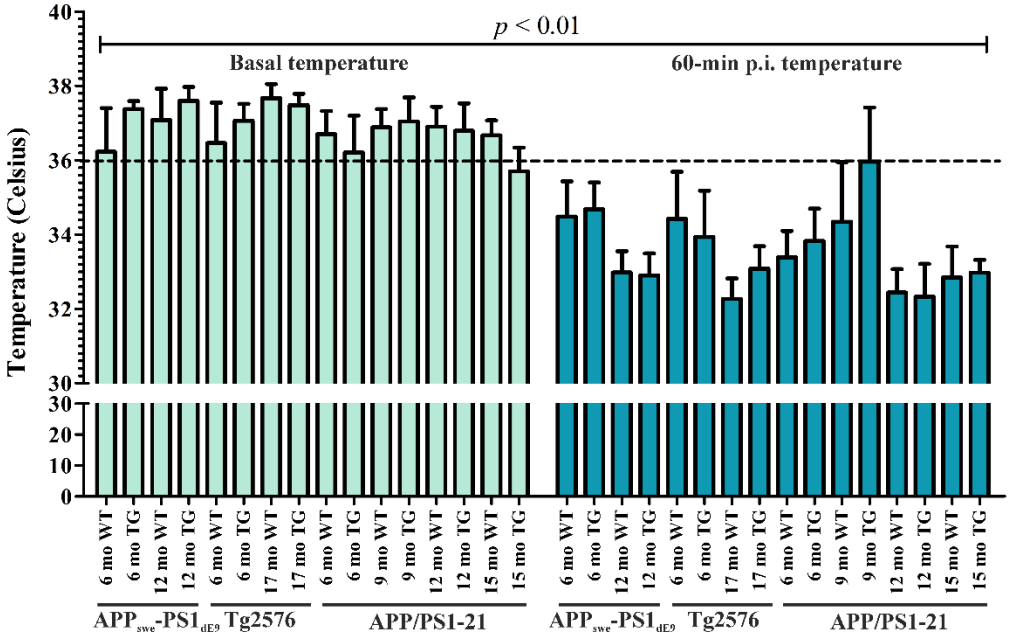

Figure 24. Mean basal and 60-min post injection (p.i.) temperature values with standard deviation for transgenic (TG) mouse models of Alzheimer's disease and the corresponding wild-type (WT) mice. Temperature was measured before and after *in vivo* ^{18}F-FDG-PET imaging in studies **I** and **II**.

the 60-min dynamic PET scan when all data from studies **I** and **II** were pooled together (*Figure 24*).

5.3 CEREBRAL GLIOSIS DETECTED WITH ^{18}F-DPA-714 AND GLIAL ANTIBODIES

Glial activation was utilized as a biomarker for AD-related neuroinflammation in Studies **I** and **II** by using specific glial antibodies targeting microgliosis and astrocytosis, and immunohistochemistry. Gliosis was also monitored *in vivo* with the TSPO radionuclide ^{18}F-DPA-714 in the APP/PS1-21 mouse model (**II**), and verified with *ex vivo* autoradiography with enhanced spatial resolution with the same tracer.

The brain uptake of ^{18}F-DPA-714 peaked between 2 and 4 min after the tracer injection, which was characterized by low brain radioactivity as the peak uptake reached approximately a SUV of 1 (*Figure 25*). The washout phase began immediately after the peak without reaching a stable plateau, and finally, ^{18}F-DPA-714 was excreted via the hepatobiliary pathway.

Although the brain uptake of ^{18}F-DPA-714 was low, it was concentrated into the cerebellar and thalamic regions. Enhanced uptake into the Harderian and pituitary glands was evident both in TG and WT mice, affecting the spillover into the frontal lobes and hypothalamus, respectively

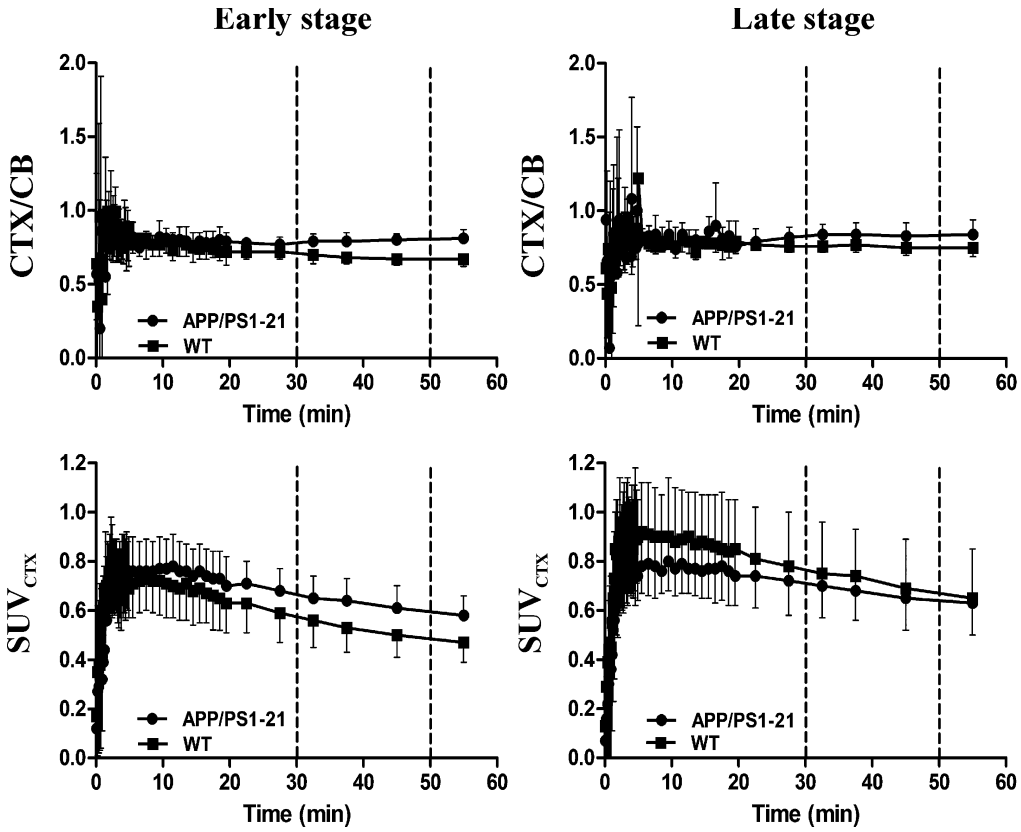

Figure 25. Cortical time activity curves for ^{18}F-DPA-714 retention in APP/PS1-21 mouse model of Alzheimer's disease and the corresponding wild-type (WT) control mice. An early (6 months) and late disease stage (15 months) as cortical (CTX) ratios relative to the cerebellum (CB) and standard uptake values (SUV) are represented. Dashed lines represents the time frame used for quantification of summed PET images 30-50 min post-injection.

(*Figure 26*). In APP/PS1-21 mice, TSPO PET showed elevated ($p < 0.05$) relative levels when assessed against cerebellum in the cerebral cortex and striata already at the age of 6 months as compared to the age-matched WT mice. The differences between TG and WT mice spread to the other brain regions, but not to the hypothalamus due to the spillover effect outside the brain, when mice aged. The temporal elevation of tracer binding from 6 to 9 months in the same TG mouse brain was statistically significant, a phenomenon not seen in WT mice (*Fig. 2 in **II**; Table 2 in **II***). When comparing the different quantification methods for ^{18}F-DPA-714 uptake in the brain, ratios relative to the cerebellum displayed lower variation within the groups than SUVs (*Figure 25*). The variation increased in 15-month-old animals in terms of SUV, which was not seen in the relative measures. *Ex vivo* studies confirmed the PET findings at 15 months, showing significantly ($p < 0.05$) increased ^{18}F-DPA-714 uptake ratios relative to the cerebellum in cerebral cortex and hippocampal region, and striata. Even in very young TG mice at 1 and 3 months, elevated TSPO tracer binding was evident in the same brain regions as seen in the older TG mice when compared to 2-month-old WT mice (*Fig. 3 in **II***).

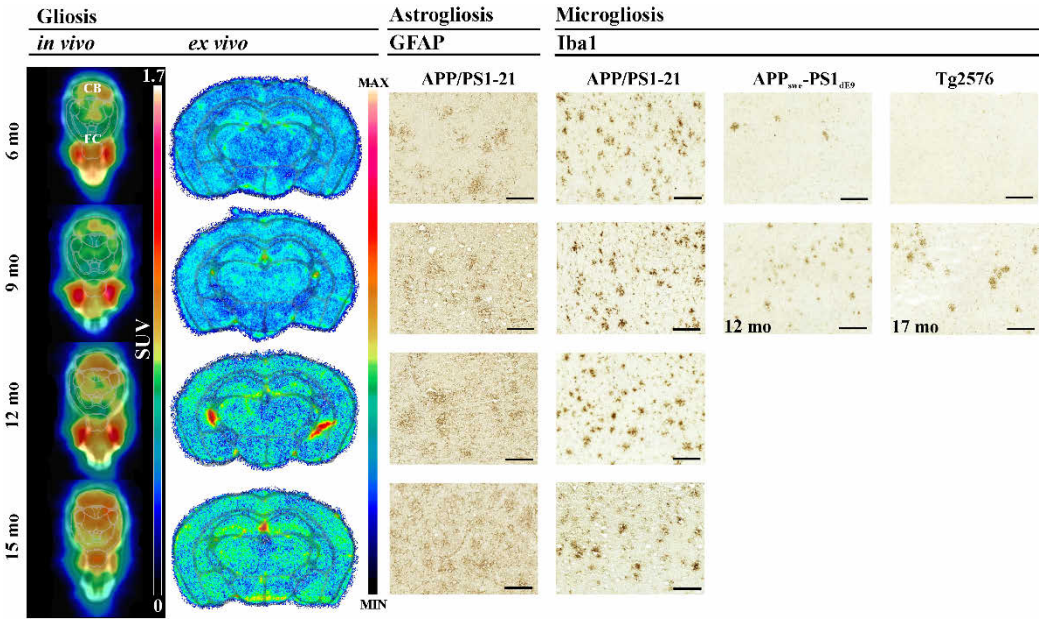

Figure 26. Gliosis in transgenic mouse models of Alzheimer's disease at ages between 6 and 17 months. Gliosis was assessed via an *in vivo* and *ex vivo* ^{18}F-DPA-714 tracer measurement in 6-, 9-, 12- and 15-month old APP/PS1-21 mice. Astrocytosis assessed as a GFAP-reactive immunostaining is visualized in the same-aged APP/PS1-21 mice. Microgliosis assessed as an Iba1-reactive immunostaining is visualized in all three mouse models. Scale bar 100 µm.

When investigating the age-related effect on tracer accumulation, ^{18}F-DPA-714 cerebellar ratios were significantly increased in frontal and parietotemporal cortices between 1-month-old and 15-month-old TG mice ($p < 0.05$) and in hypothalamus between 3- and 10-month-old TG mice ($p < 0.005$), demonstrating that even the 1-month-old TG mice can be discriminated from the 2-month-old WT mice with ^{18}F-DPA-714, and the TSPO-related pathology further worsens until the age of 15 months (*Fig. 3 in* ***II***; Unpublished statistics). When the employed quantification method for measuring the ^{18}F-DPA-714 uptake was evaluated from the pooled data from all analyzed brain regions of 15-month-old animals, there was a moderately strong positive correlation (r = 0.40, n = 48, two tailed $p = 0.005$) between *in vivo* and *ex vivo* relative measures to cerebellar uptake confirming the advantage of using cerebellum as a pseudo-reference region (*Figure 27A*). In addition, when *in vivo* quantification as relative measurement against cerebellar uptake and SUVs were examined in terms of interaction, a moderate correlation was found (r = 0.34, n = 64, two tailed $p = 0.0066$) (*Figure 27B*).

Reactive microgliosis as assessed as Iba1-positive staining was detected in all animal models. In the APP_{swe}-$PS1_{dE9}$ and Tg2576 models, the IHC quantification revealed significantly larger and abundant Iba1-driven microgliosis in the cortical lobes and hippocampus at 12 months of age compared to 6 month-old TG or 6- and 12-month-old WT mice (*Fig. 5 in* ***I***). In the APP/PS1-21

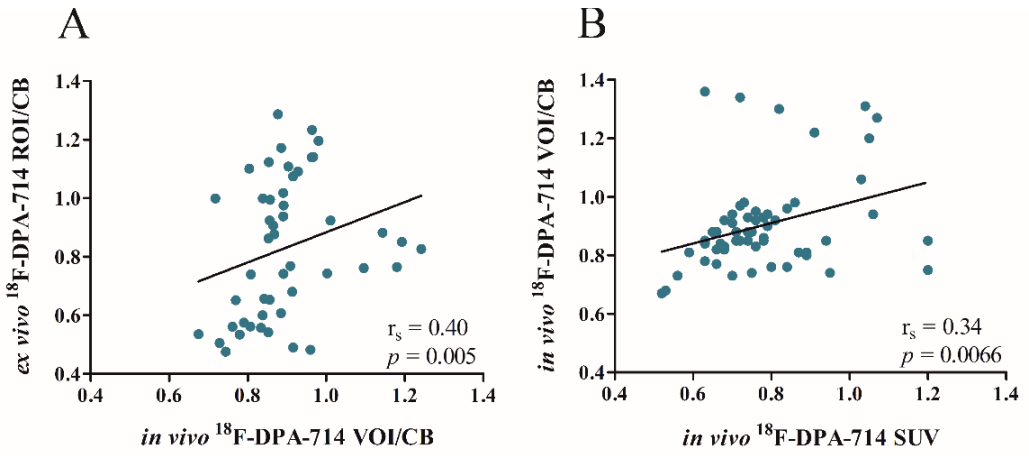

Figure 27. Correlation between different quantification methods used for the ^{18}F-DPA-714 analysis. Pooled data from 15-month-old APP/PS1-21 and wild-type group means of all analyzed brain regions were examined. Regions of interest (ROISs) from *ex vivo* digital autoradiography and volumes of interest (VOIs) from *in vivo* PET imaging data were inspected as relative measures against cerebellar radioactivity (A), and VOIs against cerebellar radioactivity and standardized uptake values (SUVs) (B) were used for the Spearman correlation examination.

mice, even though the Iba1 quantification was not performed in this study, the staining revealed a clear distinction between TG and WT mice already at the age of 6 months, with Iba1-immunoreactive staining further intensifying in the cerebral cortex, hippocampus, thalamus, and striata of TG mouse cryosections from 9 to 15 months. On the contrary in the WT mice, the Iba1-driven microgliosis was not detectable in any of the age groups (*Fig. 4 and supplemental data in **II***).

The GFAP-immunoreactive detection of astrocytosis displayed a similar enhanced pattern during aging in the APP/PS1-21 model. At 6 months, APP/PS1-21 mice already showed evidence of large GFAP-positive astrocytes in the cerebral cortex (*Figure 26*), thalamus, and hippocampus (*Data not shown*). By the age of 15 months, the size of the astrocytes was enlarged even further; they formed dense accumulation groups with a visibly increased number of reactive astrocytes.

5.4 Cerebral CB_1Rs detected with ^{18}F-FMPEP-d_2 and CB_1R antibody

Cerebral CB_1R occupancy was examined using ^{18}F-FMPEP-d_2 PET imaging and *ex vivo* methods utilizing ^{18}F-FMPEP-d_2 and CB_1R antibodies. Dynamic 120-min ^{18}F-FMPEP-d_2 scan showed that the tracer accumulated slowly in the murine brain, reaching a peak uptake approximately at 30 min after the tracer injection (*Unpublished data*). The washout phase of ^{18}F-FMPEP-d_2 progressed slowly, clearly and quickly plateauing, never reaching SUV below 1.5 (*Figure 28*). In the brain, the initial binding of ^{18}F-FMPEP-d_2 was located in the whole brain during the first 90 min, specifically in the central gray during the peak uptake (*Figure 28*). After 90 min, the tracer

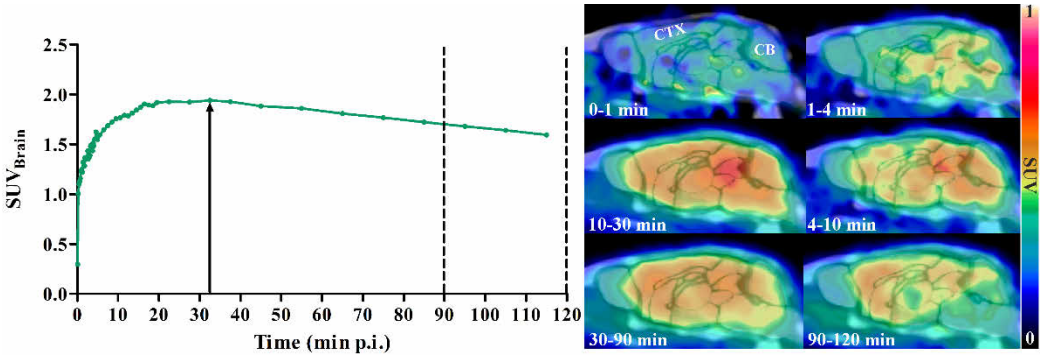

Figure 28. Cerebral time activity curve and the corresponding summed PET images for ^{18}F-FMPEP-d_2 retention in wild-type control mouse. In the time-activity curve (below), the arrow represents the peak uptake, and dashed lines represent the time frame mimicing for quantification of the summed PET images 90-120 min post injection used in the Study **III**.

became eliminated from the midbrain and thalamic region, lingering longer in the cortical and cerebellar area for up to 120 min. No significant exterior cranial uptake was observed, which hindered the interpretation of the possible partial volume effect nor was there any spillover effect in the regional quantification. While the tracer elimination was proceeding, ^{18}F-FMPEP-d_2 produced two radioactive metabolites in the plasma, which were detected with TLC examination time windows between 5 to 240 min. One of the radiometabolites also gained access into the brain (*Fig. 3 in* ***III***). Eventually, ^{18}F-FMPEP-d_2 was taken up into the gallbladder and thus, excreted via bile and also through the renal system.

Pretreatment *ex vivo* experiment showed that a 2 mg/kg dose of rimonabant blocked the ^{18}F-radioactivity of ^{18}F-FMPEP-d_2 in treated mice approximately 67% (2.5 (0.1) %ID/g, n = 2) compared to vehicle treated mice (7.5 (0.1) %ID/g, n = 2), when decay-corrected measurements with γ-counter were conducted and analyzed on dissected mouse brains (*Fig. 4 in* ***III***).

In the longitudinal Study **III**, static 30-min PET modalities, 90 min after the ^{18}F-FMPEP-d_2 injection, were quantified in the plateau phase. The longitudinal assessment revealed that in 6-month-old male APP/PS1-21 mice, the relative thalamic measures in hypothalamus were significantly lower ($p < 0.05$) than in age-matched male WT mice, which were then replaced by significantly lower tracer binding ratios in the other brain regions including frontal and parietotemporal cortices, hippocampus, and cerebellum by the age of 9 months. During the last examination at age 15 months, TG mice had approximately 10% lower thalamic ratios only in the cerebral cortex when compared to WT mice of the same age (*Table 2 in* ***III***). On the contrary, the assessment of the *in vivo* quantification as SUV could not discriminate TG mice from their WT counterparts, even though there was a very strong correlation (r = 0.84, n = 64, two tailed $p <$ 0.0001) between *in vivo* SUV and relative thalamus measurements when all analyzed brain regions of 6-, 9-, 12-, and 15-month-old TG and WT mice were pooled together and examined (*Figure 29A*).

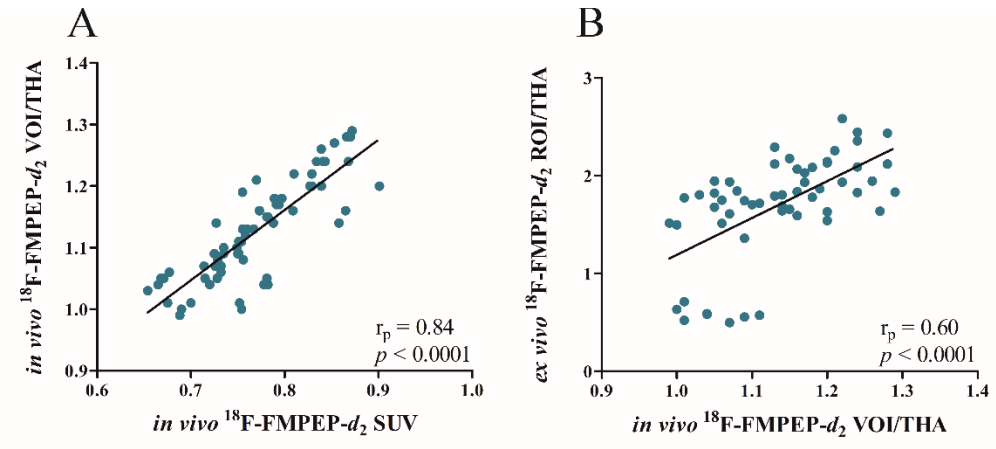

Figure 29. Correlation between *in vivo* and *ex vivo* ^{18}F-FMPEP-d_2 quantification methods used in Study III. Correlation between *in vivo* standard uptake values (SUVs) and *in vivo* radioactivity ratios relative to the thalamic radioactivity concentration (A) and the correlation between *ex vivo* and *in vivo* quantification as radioactivity ratios relative to the thalamic radioactivity concentration were examined in male APP/PS1-21 and WT mice, when all quantified brain regions and age groups were pooled together.

The decreasing trend in the ^{18}F-FMPEP-d_2 retention in male TG mice was also examined in the *ex vivo* autoradiographical experiments, however, striata were the only brain region to show a significant difference between 15-month-old TG and WT mice. On the contrary, female APP/PS1-21 mice demonstrated a higher degree of decreased tracer binding, showing significantly lower thalamic ratios in parietotemporal cortex, striata, and posterior hippocampus at 9 months when compared to the female WT mice (*Fig. 2 in* ***III***). While male and female mice displayed different ^{18}F-FMPEP-d_2 binding patterns in the brain between genotypes, distinguishing TG mice from WT mice significantly during aging, no such differences were observed in terms of CB_1R expression as assessed by Western blot. Instead, female mice exhibited significantly higher levels of CB_1R in cortical and thalamic samples when compared to their male counterparts, but no differences were detected between TG and WT mice of both sexes (*Fig. 5 in* ***III***).

The autoradiographical data confirmed that thalamus was virtually devoid of specific tracer binding at 120 min, underlining the justification of using thalamus as a pseudo-reference region for preclinical ^{18}F-FMPEP-d_2 quantification (*Figure 30*). This proposal was also confirmed by the strong correlation ($r = 0.60$, $n = 56$, two tailed $p < 0.0001$) between *in vivo* and *ex vivo* results as tracer binding ratios relative to thalamic radioactivity when all analyzed brain regions of 6-, 9-, 12-, and 15-month-old male TG and WT mice were pooled together and examined (*Figure 29B*). Similarly, the discrimination between cerebellar white and gray matter was detectable in the autoradiographs, and cerebellar gray matter showed nearly 4-fold higher thalamic ratios as compared to cerebellar white matter at 120 min after the ^{18}F-FMPEP-d_2 injection in both TG and WT mice at all ages (when all data were pooled together from **III**).

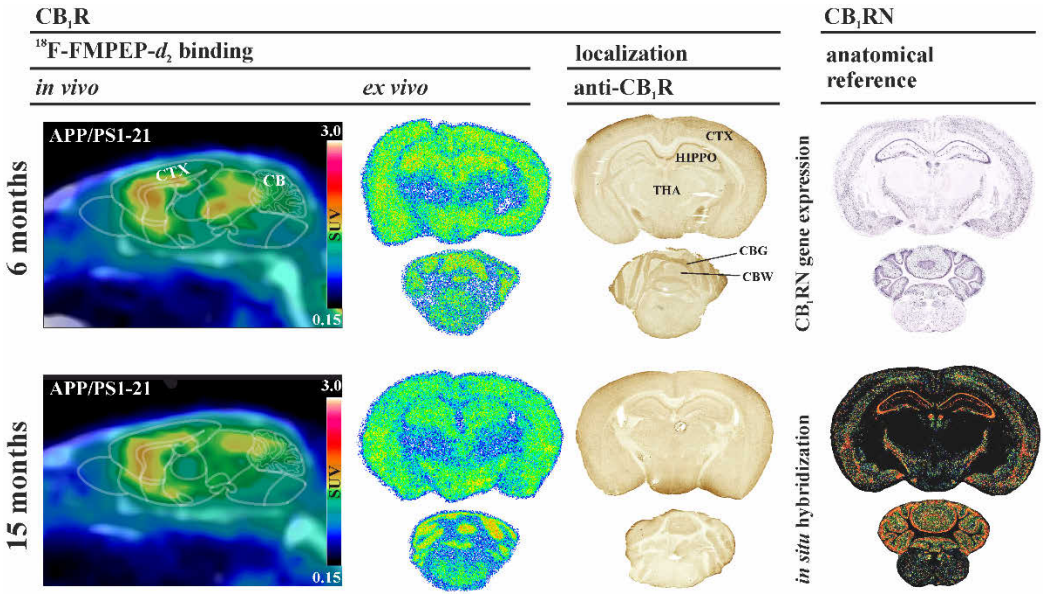

Figure 30. CB_1R availability and location detected with *in vivo* and *ex vivo* ^{18}F-FMPEP-d_2 experiments and CB_1R-reactive immunohistochemistry. An early (6 months) and late (15 months) examination stage in APP/PS1-21 mouse model are presented (*left column*). Classical anatomical references from Allen Brain Atlas (accessed 09/2013) were utilized to justify the use of thalamus (THA) as a pseudo-reference region for the ^{18}F-FMPEP-d_2 quantification in murine brain (*right column*). *CB*, cerebellum; *CBG*, cerebellar gray matter; *CBW*, cerebellar white matter; *CTX*, cortex; *HIPPO*, hippocampus.

5.5 PATHOLOGICAL CHANGES IN AGING APP/PS1-21 MICE

APP/PS1-21 mice were examined longitudinally to clarify if there were temporal changes in glucose metabolism, glial activation, and CB_1R availability in studies **II** and **III**. Even though the mice, which were followed and examined with repeated scans, were not the same as examined in studies **II** and **III**, the interconnection could be analyzed due to the relatively large group sizes and the longitudinal aspect of the experiments. Hence, when glucose hypometabolism as detected with ^{18}F-FDG and glial activation assessed with ^{18}F-DPA-714 were examined, APP/PS1-21 mice showed a moderate positive correlation ($r = 0.51$, $n = 24$, two tailed $p = 0.01$), when all ages and brain regions were pooled (*Figure 31*). When individual age groups were examined, 12-month ($r = 0.76$, $n = 8$, two tailed $p = 0.03$) and 15-month-old ($r = 0.74$, $n = 8$, two tailed $p = 0.04$) TG mice exhibited a strong positive correlation between ^{18}F-FDG and ^{18}F-DPA-714 uptake, when all brain regions were pooled together (*Data not shown*). When the correlation between the glial activation as assessed with *in vivo* ^{18}F-DPA-714 and CB_1R availability as assessed with *in vivo* ^{18}F-FMPEP-d_2 was examined, a moderate negative correlation ($r = -0.40$, $n = 24$, two tailed $p = 0.05$) was observed, when all age groups and quantified brain regions were pooled together (*Figure 31*).

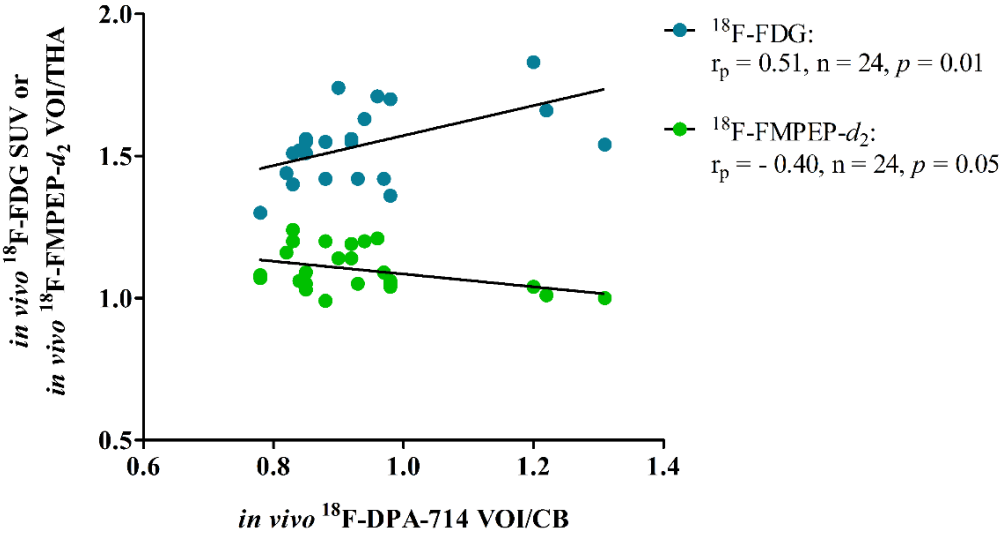

Figure 31. Correlation between *in vivo* hypometabolism, TSPO upregulation, and CB_1R availability in APP/PS1-21 mice detected with longitudinal PET imaging. *In vivo* ^{18}F-FMPEP-d_2 binding and ^{18}F-DPA-714 uptake in aging APP/PS1-21 male mice revealed a temporal negative relationship between CB_1R abnormalities and TSPO upregulation. *In vivo* ^{18}F-FDG and ^{18}F-DPA-714 uptake displayed a moderate correlation with each other, mirroring a significant relationship between brain glucose hypermetabolism and TSPO upregulation in the same TG mice.

6 DISCUSSION

6.1 CEREBRAL GLUCOSE METABOLISM

6.1.1 ^{18}F-FDG µPET findings in Alzheimer models

In this thesis work, all three TG mouse models of AD were examined with ^{18}F-FDG to discover the possible changes in the cerebral glucose metabolism in relation to normal changes during aging. At the time of the beginning of each study, no previous reports of the cerebral ^{18}F-FDG uptake profile of the employed mouse models were available. Thus, it was considered crucial to evaluate possible AD-related metabolic alterations in these models regarding future interventional imaging studies. Consequently, it was observed that the mouse models exhibited different regional metabolic patterns in the brain: Female **Tg2576** mice showed no abnormalities in the ^{18}F-FDG uptake as SUVs nor SUV_{glu}s compared to WT mice at either 6 or 17 months of age, although amyloidosis and microgliosis were detectable at the late stage of 17 months (*Fig. 2-5 in **I***). Similar findings have been obtained previously with 13-to-15-month-old male and female Tg2576 mice, after a prolonged 8-hour fasting and 30-min static PET modality, 60 min after the IV tracer injection, and the results quantified as %IDkg/g values and radioactivity ratios relative to the whole brain estimate (Kuntner et al. 2009). On the contrary, at the time when Study **I** was being performed, Luo et al. reported that female Tg2576 mice had greater SUVs in hippocampus, cortical region, and thalamus at 7 months of age, but lower SUVs in the same regions at 19 months compared to age-matched WT mice, when a 6-hour fasting and medetomidine/ketamine anesthesia were utilized prior to the dynamic 60 min modality (Luo et al. 2012). A recent report, however, failed to detect differences between 18-month-old Tg2576 mice and age-matched WT mice, when a 24-hour fasting and isoflurane anesthesia were used prior to the static 60 min scans (Coleman et al. 2017). In that study, ^{18}F-FDG results were reported as glucose-corrected SUVs, which decreased the intragroup variation, but did not differentiate TG from WT mice. On the contrary, the benefits of normalizing SUVs with the individual blood glucose values were not that evident in the results from **I** and **II;** there was increased intragroup variation in both APP_{swe}-PSI_{dE9} and APP/PS1-21 mouse models at all age groups (*Figure 20*). As a summary, the Tg2576 model has failed in the previous and present studies to mimic the hypometabolic pattern present in the AD patient brain, and therefore, does not seem to be a feasible disease model for examining glucose metabolism in preclinical AD studies. In the **APP_{swe}-$PS1_{dE9}$** model, however, regional hypometabolism exhibited in various brain structures, such as frontal cortex, striata, thalamus, hippocampus, and cerebellum (**I**). At the late examination age, APP_{swe}-$PS1_{dE9}$ mice had abundant Aβ plaques, which had spread into various brain regions accompanied by elevated Iba1-reactive microgliosis. The imaging results are in line with the human PET data obtained with ^{18}F-FDG, but not with the previous preclinical imaging studies. Until recently, female APP_{swe}-PSI_{dE9} mice had not displayed altered %ID/g values in their brains

at 9 months (Liu et al. 2017), but have shown increased SUV ratios, assessed relative to the cerebellar uptake, in the cortical region and hippocampus at 2−3.5 months, and in thalamus and striata at 3.5−8 months (Li et al. 2016), when conscious mice had received either an IP or an IV tracer injection, respectively. Both studies were conducted after prolonged fasting of 6 (Li et al. 2016) or 12 hours (Liu et al. 2017). As a result, the conflicting results from the past and the present studies with this model are not truly comparable due to the different quantification units as well as the different durations of fasting and tracer delivery. Therefore, the temporal glucose metabolism of APP_{swe}-$PS1_{dE9}$ remains unresolved.

In Study **II**, the **APP/PS1-21** model showed the most evident hypometabolism in the brain during the longitudinal follow-up period. Decreases in the ^{18}F-FDG uptake as SUVs were seen by the age of 12 months, with the most affected regions being cerebral cortex, hippocampus, striata, thalamus, and cerebellum (*Fig. 1 in **II***). When SUVs were normalized against the individual blood glucose values, intragroup variation as well as the mean group differences increased ($p <$ 0.005) in the whole brain (*Figure 20*). Our imaging results are in line with the human findings and a previous preclinical study, in which female APP/PS1-21 mice were examined at 12 months of age undergoing 8-to-12-hour fasting and a non-anesthetic IV injection protocol 20 min before being subjected to static 45-min scans (Waldron et al. 2015b). Significantly lower statistical tracer uptake were shown in thalamus and striata, whereas glucose-corrected %ID/g-values failed to reveal any differences between TG and WT mice. A more recent study confirmed this hypometabolic feature in thalamus and hippocampus of aging female APP/PS1-21 mice when the SUVs were normalized to the 10-to14-hour fasting blood glucose level (Deleye et al. 2017). Thus, when considering all of the animal models examined in these studies, the APP/PS1-21 model seems to be the most promising model to mimic the human PET findings. However, from a clinical point-of-view, the aggressive amyloidosis in this model might exaggerate temporal glucose dysfunction, which would not be comparable with the pathogenesis occurring in human AD.

APP_{swe}-$PS1_{dE9}$, APP/PS1-21, and their corresponding WT littermates revealed age-related increases in ^{18}F-FDG retention, which has also previously been observed in APP/PS1-21 mice between 1.5 and 12 months of age (Deleye et al. 2017), as well as in WT mice (Brendel et al. 2016 and 2017a). In the TG mice, the temporal changes in the hypermetabolism could originate from the elevated levels of amyloidosis and microgliosis in response to the genetic manipulation. However since the WT mice for APP_{swe}-$PS1_{dE9}$ in the present study as well as WT mice from the previous studies displayed similar increases in the ^{18}F-FDG uptake, the temporal changes might be a consequence of age-related increases in TSPO upregulation and microglial soma enlargement occurring during non-AD aging (Brendel et al. 2017). Another aspect to be considered is the obvious metabolic differences between humans and mice (Fueger et al. 2006).

6.1.2 Challenges in ^{18}F-FDG µPET

^{18}F-FDG imaging poses many challenges, although it is the most widely utilized PET radioligand with many clinical applications, e.g. in oncology and neurology. The tracer does not bind to any specific target, instead it mimics cellular glucose metabolism. For this reason, while stringent regulation of experimental procedures between individuals is extremely difficult, it is nonetheless crucial. In human brain studies, a period of 6-hour fasting is used to prevent competition reactions between any consumed food and ^{18}F-FDG. This also tends to decrease the endogenous glucose utilization in skeletal and cardiac muscle, and brown adipose tissue, which increases the cerebral ^{18}F-FDG uptake (Toyama et al. 2004; Fueger et al. 2006). In cardiac imaging, prolonged fasting periods of 10 to 12 hours are used in order to fine-tune the metabolic profile. Patients are also advised to avoid strenuous exercise and alcohol consumption 24 hours before the scan, since the muscular glucose uptake might be elevated, which could affect the interpretation of the PET imaging data due to spillover. A resting phase is initiated approximately 30-60 min before the ^{18}F-FDG injection to prevent the metabolic acceleration, and blood glucose levels are measured to ensure that they are suitable for PET/CT scan with a limiting value of 10 mmol/l (Surasi et al. 2014; VSSHP guidelines for PET/CT experiment). As a result, the PET imaging data is visualized and quantified as arterial input function.

On the contrary, animal ^{18}F-FDG studies differ from their human counterparts due to the species related differences in both metabolism and behavior (Deleye et al. 2017). Imaging TG mouse models introduces variables, including *genotype* and *genotype*age* related differences between the models. Previous ^{18}F-FDG studies using AD mouse models have yielded varying results that are most probably due to the differences in the models, age of the study subjects, and study protocols, such as fasting time, use of anesthesia, ^{18}F-FDG route, and quantification method. At a fundamental level, it is apparent that humans and mice are already discriminated by their metabolism: An average mouse has an almost 7-fold faster metabolic rate as compared to humans at the thermoneutral temperature of these animals, which is between 30 to 34 degrees. However at room temperature of 21 degrees, an additional 1.66-fold increase in the murine metabolic rate has been measured (Kleiber 1975; Schmidt-Nielsen 1984; Gordon 1993). **Fasting** has a major impact on the overall metabolism of mice, triggering changes in the hormone and fatty acid signaling, increasing stress, and if prolonged, even causing a substantial decrease in the body weights of the animals, all of which can lead to misinterpretation of the changes in the cerebral metabolic rate (Wingfield and Kitaysky 2002; Deleye et al. 2016). Fasting mice before the ^{18}F-FDG scan could offer similar benefits as seen in the human imaging studies. However in the previous ^{18}F-FDG-µPET studies with AD models, fasting was less frequently incorporated into the study protocol, and the mice were allowed to eat *ad libitum* (Poisnel et al. 2012; Rojas et al. 2013; Macdonald et al. 2014; DeBay et al. 2017). If fasted, duration of fasting between 8 to 12 hours has been applied more frequently (Kuntner et al. 2009; Waldron et al. 2015 and 2017;

Deleye et al. 2016; Liu et al. 2017) with the exception of overnight (Deleye et al. 2016; Coleman et al. 2017) or shorter fasting times (Luo et al. 2012; Li et al. 2016). In studies **I** and **II**, it was ensured that environmental factors were similar within the experimental groups. In both studies, short fasting periods of 3 (**I**) and 1.5 hours (**II**) were utilized to guarantee balancing the endogenous glucose levels while minimizing the stress reactions, which would occur if there were to be prolonged fasting. In general, mice have a nocturnal circadian rhythm, i.e. they consume two thirds of their daily food intake in the night time, thus short fasting times were used to sustain the normal rhythm and minimize stress by starting the fasting at sunrise, when the murine food intake would naturally decrease (Jensen et al. 2013). By restricting the food and water intake, and removing the bedding supplements from the cages, it was anticipated that fasting would decrease the **basal blood glucose values** of the mice while minimizing the intragroup variance. However in **I**, APP_{swe}-$PS1_{dE9}$ mice exhibited somewhat greater basal glucose values than Tg2576 mice with increased intragroup variation in comparison with the corresponding WT mice (*Figure 23; Table 1 in **I***). After the scan, glucose values were slightly, but not significantly, elevated in APP_{swe}-$PS1_{dE9}$ and WT mice, whereas in the Tg2576 mice, glucose levels remained at the basal level or lower with the exception of 17-month-old WT mice, which displayed elevated glucose levels. The APP/PS1-21 model and its corresponding WT mice differed from the other models, showing higher glucose values after the ^{18}F-FDG scan with relatively greater intragroup variation, especially in the TG mice (*Figure 23; Supplemental data in **II***). The increased variability between groups before and after the ^{18}F-FDG-PET scans might be a consequence of the isoflurane-based anesthesia and an inappropriate fasting duration for the TG model, which eventually affected the ^{18}F-FDG outcome.

Anesthetic compounds used in the Studies **I-III** were inhalation isoflurane/air or isoflurane/oxygen mixtures, which were intended to reduce the variation between the individual activity levels and to minimize stress. Isoflurane, as such, tends to increase endogenous glucose levels, especially in the heart, while decreasing the brain and brown adipose tissue uptake of glucose (Toyama et al. 2004; Fueger et al. 2006). Isoflurane has been the most popular inhalation anesthetic in previous preclinical ^{18}F-FDG studies with AD models, however, only a few of them (Kuntner et al. 2009; Poisnel et al. 2012; Luo et al. 2012; Rojas et al. 2013) have administered ^{18}F-FDG under anesthesia. In general, human ^{18}F-FDG PET studies are not conducted under anesthesia, instead the individuals are scanned awake. Hence in the preclinical studies, as isoflurane decreases the cerebral glucose utilization, it might reduce the spatial tracer uptake differences between different brain regions and underestimate the study outcome. However, handling awake mice might increase stress among animals and further alter the ^{18}F-FDG retention such that more goes to brown adipose tissue, Harderian glands, muscle, and heart (Fueger et al. 2006), which lessens the brain uptake. The extensive Harderian gland accumulation might further cause spillover into the brain, interfering with the results of the PET analysis. In addition, low body temperature can trigger similar changes as stress. Therefore in Studies **I-III**, a heating pad

was used for **the body temperature** maintenance, when mice were anesthetized. Unfortunately, the temperature measurements revealed that a significant decrease from the basal body temperature occurred after the PET scan when all imaging data were pooled together (*Figure 24*). However, no statistically significant intergroup differences were detected, except for the 9-month-old APP/PS1-21 and their corresponding WT mice, which showed significantly elevated body temperatures and cerebral ^{18}F-FDG uptake due to a malfunction of the heating pad inside the PET/CT scanner at the time of the experiment. Therefore, this age group was eliminated from the published quantification data, but was taken into the relevant *Results* section of this thesis.

The *ex vivo* findings in **I** and **II** on the cerebral glucose metabolism were not applicable to confirm the *in vivo* ^{18}F-FDG PET data due to the fact that ^{18}F-FDG lacks an appropriate **reference region**. Therefore, the use of a pseudo-reference region is also questionable in terms of preclinical imaging studies, although pons has been proposed to be reasonable reference region as it is part of the encephalon, but posses high number of axons crossing over one to another (Lowe et al. 2009; Scheltens et al. 2018). This means that the *ex vivo* autoradiography results obtained in Studies **I** and **II** must be viewed as descriptive features of the ^{18}F-FDG biodistribution in the murine brain, and not as a confirmative variable for the *in vivo* data. Previous studies with APP_{751SL}/$PS1_{M146L;\ PS1M146L}$ (Poisnel et al. 2012), 5×FAD (Rojas et al. 2013), PS2APP (Brendel et al. 2016), and APP_{swe}-$PS1_{dE9}$ (Li et al. 2016) mouse models of AD have used cerebellum as a reference region for quantifying ^{18}F-FDG data, but this has led to erroneously increased uptake ratios for TG mice as compared to WT mice. In addition to the relative measures, %ID/g has also been employed as a descriptive unit in preclinical ^{18}F-FDG studies with Tg2576 (Kuntner et al. 2009) and APP_{swe}-$PS1_{dE9}$ (Liu et al. 2017) models but this parameter was unable to discriminate TG from WT mice. However, when %ID/g values have been normalized with the individual blood glucose values of the fasted mice, decreased ^{18}F-FDG uptake has been observed in thalamus and midbrain of TASTPM mice at 13.5 months (Waldron et al. 2015a) and in thalamus and striata of APP/PS1-21 mice at 12 months (Waldron et al. 2015b). When taking into account the possible differences in the body weight of the animals, SUV has been demonstrated to be a valuable parameter in previous ^{18}F-FDG µPET studies, revealing decreased tracer retention not only in **II**, but already in 5- (DeBay et al. 2017) and 13-month-old 5×FAD mice (Macdonald et al. 2014) even without fasting. In the TASTPM mouse model, a hypometabolic pattern after 6 months of age is detectable only after correcting the SUVs with the blood glucose values (Deleye et al. 2016; Waldron et al. 2017), but in Tg2576 mice (Coleman et al. 2017), no single quantification unit has been able to demonstrate a hypometabolic pattern in the brains of these animals (Coleman et al. 2017; **I**).

When considering the results obtained from the present and previous ^{18}F-FDG studies with AD mouse models, it is evident that adjusting for environmental factors (i.e. temperature, handling,

fasting, and anesthesia) and monitoring blood glucose values at multiple time points before, during, and after the PET modality are crucial in order to produce reliable imaging results, which truly reflect cerebral glucose metabolism. This means that TG models might require individually adjusted fasting periods, suitable resting temperatures, and standardized anesthesia conditions, which will need to be further evaluated in future imaging studies. Hence, even though different mouse models have been used for exploring the pathogenesis behind the cerebral dysmetabolism, with the results being further extrapolated to the condition of the human AD brain, based on the current knowledge obtained from the present and previous studies, none of the models can be viewed as being reliable enough to be considered as a proper disease model for screening alterations in glucose metabolism in AD.

6.2 NEUROINFLAMMATION

6.2.1 Glial activation in Alzheimer models

The **APP/PS1-21** model was the only model to be examined with TSPO PET for measuring the overall extent of gliosis in the AD mouse brain. The longitudinal ^{18}F-DPA-714 imaging study revealed increased radioactivity concentration ratios relative to the cerebellum in the different cortical lobes, thalamic and striatal regions, and part of a limbic system, already at the beginning age of the experiment of 6 months in TG mice. Furthermore, from 6 to 15 months, the differences between TG and WT did not expand further because the mean radioactivity ratios between the genotypes had reached their limit. Hence, at 6 months, TSPO upregulation seemed to be already significantly discriminating the genotypes from each other, suggesting that the pathology has begun in much younger animals, reached its peak, and then plateaued as the mice aged. On the contrary, Iba1-reactive microglia were present at low levels at 6 months as compared to 15 month-old TG mice, whereas GFAP-positive astrocytes seemed to reach their peak number in the cerebral cortex already at 6 months, but did not seem to expand further during aging (*Figure 26*). These consumptions need to be verified in the future quantification experiments, although a previous ^{18}F-PBR111 PET study with the same APP/PS1-21 model demonstrated a low positive correlation between tracer uptake and Iba1-reactive microgliosis, but a trend towards a weak negative correlation between tracer uptake and GFAP-driven astrocytosis (Deleye et al. 2017). On the contrary, the brains of 2-month-old female APP/PS1-21 mice have displayed enhanced levels of GFAP-positive astrocytosis; this progressed until the age of 8-months throughout the entire neocortex, and was distinct from the amyloid plaques, but in parallel to microgliosis (Radde et al. 2006). Beyond, female APP/PS1-21 mice showed overall ^{18}F-PBR111 SUV increases in the cortex, thalamus, and hippocampus, when 6-to-7-week-old and 4-, 7-to-8-, and 12-to-13-month-old TG mice were compared to their age-matched WT counterparts (Deleye et al. 2017). It was recently shown *in vivo* using a novel TSPO tracer and analogue for ^{18}F-DPA-714, ^{18}F-FDPA, that 12-month-old APP/PS1-21 mice expressed increased SUVs in the whole brain, frontal cortex,

and hippocampus, whereas *ex vivo* autoradiography ratios relative to hypothalamus showed increases in the tracer uptake in the frontal cortex of much younger, 4.5-month-old TG mice. Similarly to the present study, Keller et al. observed age-related increases in the ^{18}F-FDPA uptake between 4.5- and 15-month-old APP/PS1-21 mice, but not in WT mice (Keller et al. 2018).

Even though female **APP$_{swe}$-PSI$_{dE9}$** mice were not examined with ^{18}F-DPA-714 in the present study, differences have been evaluated previously in two longitudinal follow-up studies, in which male TG mice demonstrated increased relative measurements against cerebellum in the cortical region and hippocampus at 18 months (Chaney et al. 2018), which was confirmed in older study with 19-month-old TG mice (Sérrière et al. 2015). These studies also evaluated the PET imaging results with the antibody-reactive microgliosis (Sérrière et al. 2015) and overall gliosis with astrocyte- and microglial-specific antibodies (Chaney et al. 2018) at the same experimental age. In study **I**, female APP$_{swe}$-PSI$_{dE9}$ mice showed microgliosis with Iba1-immunohistological experiments at 6 and 12 months of age, and a similar finding was noted in female Tg2576 mice at 17 months, which confirmed the previously published findings with the same animal models (*Figure 26*). In terms of neuroinflammation, **Tg2576** mice have previously been studied only with the MAO-B targeting radionuclide, ^{11}C-DED, in order to image the extent of astrocytosis in the brain (Rodriguez-Vieitez et al. 2015). Six-month-old Tg25786 mice showed increased binding potentials in several brain regions as compared to either 8- to 15-month-old or 18- to 24-month-old TG or WT mice; this finding was confirmed with GFAP-positive immunostaining only at the ages between 18-24 months. Progressive microgliosis in the Tg2576 brain, which was shown in **I** with Iba1 immunohistochemistry, has been demonstrated previously, indicative of an increase in microglial magnitude and density near to Aβ plaques at 10- and 16-month-old TG mice (Frautschy et al. 1998).

6.2.2 Challenges in TSPO µPET

TSPO has been the most widely investigated target for imaging neuroinflammation over the past decade. Even though upregulation of TSPO in the brain indicates possible pathological conditions related to glial activation and thus, neuroinflammation in several neurological disorders, it also suffers from many limitations in its ability to demonstrate applicable features, especially in terms of TSPO tracer specificity and its usefulness in preclinical imaging studies involving small rodent brains. Caution is needed in the attribution of cerebral TSPO binding exclusively to microglia, since it is not possible to determine whether the PET signal in the brain contributes from microglia or astrocytes. In addition, the disruption in the blood-brain barrier, which occurs in some pathological conditions, might cause an abnormal leakage of mononuclear-phagocytes from the periphery into the brain, expressing TSPO more as its own levels and affecting the interpretation of the radioactive signal detection (Anholt et al. 1986). However, according to the ^{11}C-PBR28 findings in a 5×FAD mouse model (Mirzaei et al. 2016) as well as the ^{18}F-PBR111 uptake results

in the APP/PS1-21 model (Deleye et al. 2017), microglia seem to be the predominant source of the tracer uptake rather than astrocytes; a proposal which was confirmed with immunohistochemical procedures. Thus, the contribution of the glial cell division in each animal model should be examined in parallel to TSPO PET imaging studies, which has been suggested previously (Venneti et al. 2013). TSPO PET imaging further lacks the ability to discriminate between the different subtypes of microglial cells, which are involved in temporal changes during inflammatory processes, and whose pro-, anti-inflammatory, or combination stage might be crucial for understanding the microglial functions during the neuroinflammation. Instead, TSPO PET might reflect the changes in the glial cell density, which is known to vary among different species (Owen et al. 2017). However, there are some benefits associated with utilizing small animal TSPO PET, including the lack of the functional polymorphism of TSPO gene in mice or rats, which limits the human TSPO PET sensitivity with most of the tracers. In order to increase the value of translational small animal PET in the clinic and serve as a reliable research tool for human healthcare purposes, other targets related to the complex neuroinflammatory pathway, such as COX, CB_2R, $P2X_7R$, are being evaluated as novel imaging agents targeting AD and other neurodegenerative disorders (Janssen et al. 2018).

Small animal ^{18}F-DPA-714 PET **data quantification** faces similar problems as ^{18}F-FDG as there is really no proper reference region in the brain for TSPO. Throughout the healthy brain, there is a constant low TSPO expression in gray and white matter, and blood vessel walls (Lyoo et al. 2015). In human PET studies, the quantitative analysis of ^{18}F-DPA-714 involves the determination of relative measurement against cerebellar uptake or an arterial input function in a two-compartment model, which is corrected for the presence of possible radioactive metabolites. The latter leads to a total V_T of the tracer, which is composed of specific and non-specific binding. Unfortunately, in preclinical imaging studies with mice, it is not feasible nor would it be ethical to conduct arterial sampling during the PET scan due to the small total blood volume of these species. Therefore, other quantification techniques has been applied, and in the previous TSPO μPET studies (*Table 2*), %ID/g from the ^{11}C-PK11195, ^{18}F-GE-180, and ^{18}F-PBR06 uptake (Venneti et al. 2009a; Liu et al. 2015; James et al. 2015), SUV from the ^{11}C-PK11195, ^{18}F-PBR111, and ^{18}F-FDPA uptake (Rapic et al. 2013; Deleye et al. 2017; Keller et al. 2018), and statistical parametric mapping (SPM) from the ^{18}F-GE-180 uptake (Brendel et al. 2017b) have been used as the main values extracted from the TSPO imaging data, since they are non-invasive ways of assessing the regional uptake of the tracer in a specific time frame. These experiments have demonstrated increased TSPO tracer uptake in the TG mouse brain compared to WT mice, except for APP/PS1 model examined at 13 months with ^{11}C-PK1195 (Rapic et al. 2013). Relative measures have also been applied in previous μPET studies, with cerebellum being the most attractive pseudo-reference region as was applied in Study **II**. Using this approach, ^{18}F-DPA-714 (Sérrière et al. 2015; Chaney et al. 2018) and ^{18}F-GE-180 (Brendel et al. 2016 and 2017) have discriminated APP_{swe}-$PS1_{dE9}$, PS2APP, and APP23, respectively, mice from their age-matched

WT littermates. In addition to cerebellum, relative measures to the whole brain (James et al. 2015), striatal (Maeda et al. 2011), thalamic (Liu et al. 2015), muscle (James et al. 2015), and heart (Mirzaei et al. 2016) estimates have been reported with other TSPO radioligands, which have demonstrated increases in the tracer uptake in favor of AD mice. In conclusion from the past studies, a pseudo-reference region inside the brain might be applicable if the chosen mouse model exhibits relatively low TSPO tracer uptake in the selected region, and the radioactivity concentration measured with SUV in that site does not differ between TG and WT mice, when equivalent radioactivity doses are delivered to equal-sized animals. Additional experiments, including immunohistochemical and protein extraction procedures, for detecting TSPO in the brain, however, are desirable due to the obvious limitations of TSPO imaging.

6.3 CANNABINOID RECEPTOR 1

6.3.1 ^{18}F-FMPEP-d_2 μPET findings in APP/PS1-21 mice

The longitudinal follow-up study **III** showed age- and genotype-dependent alterations in the relative measurements of ^{18}F-FMPEP-d_2 binding assessed against thalamic radioactivity concentrations in male APP/PS1-21 mice. The differences between TG and WT mice were more evident in the cortical and hippocampal region, striata, and cerebellum at 9 months, which then plateaued. The *in vivo* data was confirmed with the *ex vivo* measurements that revealed a significant reduction in the relative measurements for only striatum in 15-month-old male TG mice (*Supplemental data 3 in **III***). In female APP/PS1-21 mice, which were only examined using *ex vivo* ^{18}F-FMPEP-d_2 autoradiography, significantly lower thalamic ratios were measured in the parietotemporal cortex, striata, and posterior hippocampus of 9-month-old TG mice when the ratios were compared to the age-matched female WT mice. With regard to the above mentioned results, CB_1R expression was examined in 9-month-old mice to evaluate the ^{18}F-FMPEP-d_2 values in both male and female mice, when the genotype related differences started to appear. The total amount of CB_1R protein was determined using Western blot; these indicated that female mice had 2- to 4-fold higher levels of CB_1R protein in different brain regions, excluding hippocampus (*Fig. 5 in **III***) than male mice, whereas there were no differences between TG and WT mice. It is concluded that CB_1R PET imaging studies should be conducted as single-gender modalities or alternatively should examine female and male subjects as separate variables. According to Study **III**, there are either alterations in the ^{18}F-FMPEP-d_2 binding capability to the cell membrane and/or endogenous CB_1Rs in the APP/PS1-21 G-protein coupling system, or there are alterations in the CB_1R receptor conformation on the membrane or inside the cell. The contradictory results from the PET imaging and Western blot experiments in Study **III** might also be explained if the concentrations of the endogenous CB_1R ligands had changed due to the genetic mutation of TG mouse model or if intracellular CB_1Rs are affected by other lysosomal pathological factors. Indeed, there is no data to which part of the cell ^{18}F-FMPEP-d_2 actually

binds. Neuronal studies have previously shown that the major proportion, up to 85%, of the total CB_1Rs are located endogenously in the intracellular vesicles and constantly migrate between the membrane and endosomes (Leterrier et al. 2006). However, it has been claimed that some endogenous CB_1Rs do not reach to the cell surface, instead they might have a distinct, yet unrevealed, functions compared to the membrane receptors i.e. what was previously thought of as down-regulation may in fact be the receptors becoming involved in different physiological process (Grimsey et al. 2010). One of those actions has been shown to be related to the modulation of the neuronal energy production, since CB_1Rs have been detected in the neuronal mitochondria and they signal pathways, which target ATP production (Hebert-Chatelain et al. 2016). Since CB_1Rs are harnessed only on-demand, disruption of this signaling system might also affect the ^{18}F-FMPEP-d_2 binding to these receptors. Nonetheless, evidence to support these hypotheses is lacking and hence, further studies are urgently needed to clarify the binding properties of ^{18}F-FMPEP-d_2 and other CB_1R targeting radioligands, such as ^{18}F-MK9470 (Van Laere et al. 2008), for both animal and human brain CB_1Rs. The results from Study **III** showed that there was an undefined pathological event proceeding related to the CB_1R function in the APP/PS1-21 mouse brain, but this was not related to the total CB_1R levels with regard to the regional co-localization. These results join the line of controversial findings from the previously published non-PET data, in which fluctuating CB_1R properties have been reported in different AD mouse models: Male APP_{swe}-$PS1_{dE9}$ have shown decreased CB_1R-immunoreactivity in the neocortex at 6 months (Aso et al. 2012) or hippocampus at 10 and 12 months of age (Kalifa et al. 2011). Other groups have claimed, however, that male 14-month-old APP_{swe}-$PS1_{dE9}$ had elevated CB_1R levels in the cortex (Mulder et al. 2011), but no changes in the redox-dependent receptor function of female TG mice at the same age as evaluated with ^{35}S-GTPγS autoradiography (Kärkkäinen et al. 2012). A recent study detected increased G-protein coupling of CB_1Rs in frontal cortex and striata of male APP_{swe}-$PS1_{dE9}$ compared to age-matched WT animals (Maroof et al. 2014). Male 3 x Tg-AD mouse model, on the other hand, have demonstrated significantly higher CB_1R mRNA expression in the prefrontal cortex, dorsal hippocampus, and basolateral amygdala complex at 6 and 12 months, but decreased protein immunoreactivity in the basolateral amygdala complex and dorsal hippocampus when the animals were aged 12 months (Bedse et al. 2014). Furthermore, the CB_1R activity as a ^{35}S-GTPγS measurement was examined in young (4 months) and old (15 months) male 3 x Tg-AD mice; there was evidence of upregulated thalamic activity at 4 months, but downregulated receptor activity in the nucleus basalis of Meynert (Manuel et al. 2016). In 4-month-old Tg2576 mouse model, hippocampal CB_1R membrane distribution and functional activity were restricted, which did not affect the expression levels of CB_1Rs (Maccarrone et al. 2018). When comparing between the AD mouse model and a CB_1R-knockout model, APP23/$CB1^{-/-}$ mice have demonstrated reductions in mutated APP levels and Aβ levels (Stumm et al. 2013), and 5-fold lower plaque formation abilities than in the APP23 mice, whereas APP_{swe}-

$PS1_{dE9}/CB1^{+/-}$ mice showed no differences in amyloid pathology when compared to non-knockout animals (Aso et al. 2018).

Study **III** revealed additional information with regard to age-related increases in the CB_1R *in vivo* PET tracer binding in WT male mouse brain, which has also been demonstrated in human PET ^{18}F-MK9470 studies with healthy female gender (Van Laere et al. 2008). Further increases in the CB_1R total levels have been observed in aging male rat dentate gyrus (Berrendero et al. 1998) and cortical region (Liu et al. 2003). The region-dependent CB_1R upregulation might be related to the compensatory reaction against endocannabinoid dysfunction based on normal aging (Maccarone et al. 2001). In contrast, other studies suggest that CB_1R gene expression either declines with aging in both the rodent and human brain (Berrendero et al. 1998, Westlake et al. 1994) or is preserved (Belue et al. 1995; Wang et al 2003). On the contrary, age-dependent changes in receptor function have been less frequently studied in female subjects, even though significant differences have been observed between the CB_1R abundances in male and female human (Van Laere et al. 2008) and rodent (Burston et al. 2010; Castelli et al. 2014; Gonzalez et al. 2005) brain, which might originate from the hormonal lipid differences among sexes. The female sex hormone, estrogen, regulates the expression of CB_1R in the brain via cerebral activation of GABA, dopaminergic, and glutamate pathways (Mani et al. 2001; Riebe et al. 2010; Wilson and Nicoll 2001). Hence, the CB_1R profile needs to be well characterized in both genders before one can determine whether an ECS-related pathogenic pathway is involved in the prognosis of AD. Should this prove to be the case, then it might lead to the establishment of novel diagnostic AD biomarkers, which can be subsequently monitored using functional PET imaging agents targeting ECS. Preferably, to combine different modalities, such as novel PET radioligands targeting GABA-A, dopamine, and opioid receptors, which are closely associated with the function of the CB_1R and endocannabinoid release, would provide an important tool for expanding the *in vivo* AD imaging research to the next level (Horti and Van Laere 2008).

6.3.2 Considerations for CB_1R µPET

Even though the current CB_1R targeting radioligands possess high receptor affinity, they are highly lipophilic compounds with logD7.4 values above 4, which is considered as an undesired feature of a ligand. Hence, the applicability of CB_1R PET tracers remain limited with regard to non-specific tracer binding or a tendency to bind plasma proteins. High plasma protein binding tends to lower the availability to target radioactivity concentration and to cause weaker first pass extraction, which was seen with the previous ^{11}C-OMAR imaging study (Normandin et al. 2015). In humans, by applying a threshold value, quantification procedures can be modified to take into account the estimates of compartment modelling, but in small animal brain quantification, this approach faces many challenges. In Study **III**, relative measures were applied to compare the ^{18}F-FMPEP-d_2 binding between APP/PS1-21 and WT mice. Thalamus was chosen as the pseudo-

reference region because of the extremely low murine CB_1R expression in that region (*Figure 30*). The *ex vivo* data further revealed another candidate, cerebellar white matter, that could be used as a reference region. However, the poor spatial resolution of the PET imaging device makes it impossible to discriminate between the cerebellar white and gray matters. Therefore, in order to analyze the tracer data equivalently in every *in vivo* and *ex vivo* experiment, thalamus was chosen instead of the white matter. In contrast, previous ^{18}F-MK-9470 PET imaging studies with in rodents have normalized target brain region values to an estimate of the whole brain instead of choosing a pseudo-reference region (Casteels et al. 2010 and 2011; Miederer et al. 2013; Vandeputte et al. 2012). Nevertheless, the fast clearance of ^{18}F-FMPEP-d_2 from the thalamus confirmed the benefits of this brain region as a feasible reference, since the PET quantification showed approximately 20% lower tracer levels as confirmed by autoradiography data (40% lower tracer radioactivity concentration) in that region when compared to CB_1R-rich brain regions, such as cortex and cerebellum (*Data not shown*). Furthermore, SUVs detected with PET and CB_1R expression as assayed with Western blot did not differ between the genotypes. Similar features were observed in a previous CB_1R PET study, in which the clearance rate of ^{11}C-JHU75528 was much higher in thalamus and brain stem than in the other brain regions (Horti et al. 2006). Therefore, based on the findings from Study **III**, thalamus is a suitable pseudo-reference region for murine ^{18}F-FMPEP-d_2 PET studies. However, with regard to the future PET studies with humans, PET images cannot be analyzed similarly, because there are differences in the CB_1R distributions pattern between mouse and human brain, which means that the quantification method has to be based on a function derived from the arterial input.

6.4 RESEARCH MATERIAL AND METHODS

6.4.1 Animal models

The commercially available **Tg2576** model showed the most modest pathological profile with regard to slow amyloidosis and microgliosis accompanied by the lack of hypometabolic features, which makes this model an unattractive research tool for future preclinical studies targeting longitudinal assessment of the disease course or drug discovery in AD. **APP_{swe}-$PS1_{dE9}$**, on the other hand, exhibited fast and aggressive amyloidosis, accompanied in parallel with microgliosis and cerebral hypometabolism, which mirrors the pathological features seen in AD patients. Similarly, the other double mutated mouse model, **APP/PS1-21**, featured equivalent pathological changes in the brain, but in a much more aggressive manner.

In Studies **II** and **III**, monitoring cerebral glucose consumption, TSPO upregulation, and CB_1Rs should have started in much younger APP/PS1-21 mice in order to observe the initiation of the pathology related to these conditions. An ideal disease model should demonstrate similar aspects as the human disease, which none of the AD models currently have. On the other hand, an

exaggerated disease onset in mouse models could overestimate the temporal course of the pathological events in the brain, which might lead to misinterpreted results in future studies. The involvement of tau should be incorporated into the pathological profile of a good disease model of AD, because it is one of the hallmarks of the disease and the primary cause of the neurodegeneration. Preferably, the genetic factors involved in LOAD accompanied with pro-inflammatory phenotype could offer an interesting way to study the sporadic form of AD, and models targeting LOAD should be further developed and evaluated, distinct from EO-FAD disease models. With regard to small animal imaging studies, the small size of the mouse brain and the poor spatial resolution of PET imaging devices pose challenges for reliable investigation of the pathological events in tiny brain regions, such as hippocampus. Hence, imaging AD rat models could be more feasible, because of the larger body size and their pathological profiles, which are more comparable to human disease, as has been shown in the TgF344-AD rat model of AD (Cohen et al. 2013).

6.4.2 Quantification of the µPET data

In Studies **I-III**, a MRI mouse brain template was used for the spatial guidance to localize the smallest brain regions in the murine brain. However, the spatial resolution of the PET/CT device is only 1.3 mm, which leads to the *partial volume effect* due to the relatively large pixel size. The *spillover* effect from the adjacent brain structures with high radioactivity uptake is also manifested in small regions, including hippocampus and hypothalamus, leading to some overestimation of radioactivity concentrations in these regions. In addition, high uptake from the tissues outside the brain, such as the Harderian gland and pituitary gland, might have increased the extrapolation of the frontotemporal and hypothalamic activities in ^{18}F-FDG and ^{18}F-DPA-714 PET studies, respectively.

Small animal PET has traditionally been validated with *ex vivo* autoradiography experiments to obtain more precise information about the spatial biodistribution of the tracer of interest. Aforementioned experiments should share similarities within the quantification, i.e. same reference region should be utilized in order to compare the ligand retention results. Unfortunately, this type of comparison could not be conducted in Studies **I** and **II** due to the lack of a reference region for ^{18}F-FDG. In the experiments with ^{18}F-DPA-714 and ^{18}F-FMPEP-d_2, the use of a pseudo-reference region was justified and *ex vivo* experiments were able to confirm the *in vivo* trend. As a result to summarize the usefulness of preclinical PET imaging studies conducted in this thesis work, APP_{swe}-$PS1_{dE9}$ and APP/PS1-21 are suitable for future longitudinal studies to unravel both the temporal aspects and causal features of AD-like pathogenesis during Aβ pathogenesis. This also means that these models can be disease mimicking tools in interventional drug discovery research with some limitations. Hence, in future studies similar to this thesis work, the following recommendations are provided:

1. The pathogenetic profile of AD animal model must be monitored in temporal manner before the initiation of any pathological events, if a PET method is being applied.
2. Longitudinal PET imaging studies should be evaluated with antibody-based *ex vivo* experiments with appropriate agents and age-matched replicates related to the PET radioligand target.
3. Justification of using ^{18}F-FDG in small animal PET should be thoroughly considered.
4. Small animal studies harnessing ^{18}F-FDG should be conducted with careful considerations regarding the chosen animal model and the appropriate environmental factors influencing the model (i.e. fasting, anesthesia, quantification technique).
5. Imaging small animals with TSPO targeting PET radioligand should include antibody-based *ex vivo* experiments for the detection of microglial, astroglial, and TSPO expression, and these experiments should be compared retrospectively.
6. Monitoring CB_1R system with targeting PET radioligands should include the discrimination of female and male test subjects due to the differences in receptor expression and functional properties between the genders.
7. The exploitation of ^{18}F-FMPEP-d_2 for monitoring cerebral CB_1Rs must be evaluated with concomitant experiments regarding the receptor expression (ELISA, Western blot) and function (^{35}S-GTPγS) to validate the meaning of the tracer binding in the brain.

6.5 STUDY LIMITATIONS

Specific limitations of the studies:

I The small number of animals limited the possibility to conduct longitudinal investigations and hence, to detect the earlier pathological phase prior to Aβ pathology, which would have been rather informative. Larger number of animals would have provided the opportunity to investigate different fasting durations and thus, tolerance for food deprivations and effects on blood glucose. Blood glucose should have been measured more frequently, i.e. before the fasting and ^{18}F-FDG injection. However, such procedures might increase the stress imposed on the mice, which should be avoided in ^{18}F-FDG imaging studies. Additional immunoreactive staining on neuronal and synaptic markers could have provided a secondary marker to be compared to the imaging data.

II One obvious limitation was the *ex vivo* quantification in ^{18}F-FDG studies, in which an inappropriate reference region was utilized that could not be mirrored with the longitudinal *in vivo* PET data. The longitudinal assessment should have been initiated in much younger animals, because *ex vivo* ^{18}F-DPA-714 revealed that TSPO upregulation had already occurred in 1-month-

old APP/PS1-21 mice. Furthermore, immunoreactive TSPO staining, and Iba1 and GFAP quantification would have given more information about the PET ligand specificity and possibly revealed differences in the activation of different glial cell types between TG and WT mice. Correlation between Aβ pathology and temporal changes in glucose metabolism and glial activation detected with PET should have been examined in order to reliably investigate the pathological profile of APP/PS1-21 model.

III The limited animal availability in *ex vivo* experiments prevented the investigation of gender-related differences in the CB_1R expression and availability at various ages. As described in Study **II**, the amyloidosis of APP/PS1-21 mouse model should have been quantified in order to correlate these changes to ^{18}F-FMPEP-d_2 binding detected with longitudinal PET. Additional immunohistochemical and immunoblotting experiments with antibodies targeting other ECS agents would have added value to the imaging results. The greatest limitations of ^{18}F-FMPEP-d_2 was the radioactive metabolite in the murine brain, which represented part of the total ^{18}F-radioactivity detected with PET.

6.6 FUTURE PROSPECTS

The basis of AD has been the vicious cycle of the production of Aβ molecules, which aggregate into toxic oligomers, and then proceed into aggressive accumulation of neuritic plaques within the neurons. *Post mortem* findings of this recognized proteinopathy have been summarized via the amyloid cascade hypothesis, which has been a dogma directing research and subsequently drug discovery programs. As a consequence of technological improvements and intensive scientific efforts, other theories have been postulated to explain the metabolic and inflammatory changes in AD beyond the amyloid pathology. At present, many hypotheses, which have been generated from the *post mortem*, *ex vivo*, and *in vitro* based evidence, need further evaluation through novel *in vivo* biomarkers targeting these theoretical culprits. One of the main theories, i.e. that the pathogenetic course involves heavily on immunoreactive tau aggregates and NFT accumulation, cannot yet be assessed by PET as there are no reliable radioligands, which would reveal the presence of tauopathy in young individuals as well as in asymptomatic AD patients. Current AD PET imaging has focused on targeting dense amyloid plaques for confirming the diagnosis of the disease or for re-evaluating the treatment efficacy in clinical trials. Even though such studies have yielded some promising results, which do mirror *post mortem* findings with proteinopathy markers, strategies toward detecting the soluble, more neurodestructive Aβ oligomers have gained more interest both in imaging ligand development and drug discovery (Jack et al. 2013; Sehlin et al. 2016).

The perfect timing to examine AD disease stage sets great challenges. Biases may be encountered whether known or novel disease biomarkers are monitored at the “wrong” disease stage during the temporal course of AD. The expression tone and timing of the different proteins and receptors

involved in the disease pathway may fluctuate from the initiation of AD as well as during its progression, and hence, the onset of different biomarkers must be investigated in prospective longitudinal assessments, which cannot be captured in cross-sectional settings. In clinical point-of-view, early disease detection targeting amyloid and non-amyloid pathology in non-symptomatic patients would be valuable for the initiation of disease modifying intervention, if ever applicable. Interest toward new interventional targets should include neuroinflammation and the ECS, especially the novel subtargets such as $P2X_7R$, TREM2, interleukins, and CB_2R (Holland et al. 2014; Janssen et al. 2018), which are also captivating targets for the further PET radioligand development. Imaging *in vivo* of amyloid protofibrils has also suggested to be valuable target for in-depth recognition of amyloid formation (Syvänen et al. 2017). In the end, new imaging agents could, in addition to monitoring drug efficacy in follow-up trials, ease on patient selection and characterization in a multidimensional way. Multitracer PET studies within the same subject could also provide in-depth information about the disease onset on an individual level, which could potentially offer a biomarker-based diagnosis for tailored combination treatment strategy in patient care. However, even though the development of new PET tracers targeting AD has been accelerated during the past decade, strong efforts must be conducted in terms of establishing effective drugs against the disease progression both against amyloid and other targets. These sort of investigations require reliable preclinical disease models and longitudinal assessments to gather the temporal and causal events in the AD-like brain. Current mouse and rat models need further evaluation to be able to be utilized for nonclinical drug discovery, and preferably, to be combined with LOAD models or EO-FAD models with additional LOAD phenotype. The validity of amyloid murine models in drug development must be carefully considered, and the selected disease model must be thoroughly evaluated as a feasible model for interventional studies. Nevertheless, despite the obvious limitations surrounding the applicability of the amyloid mouse models, these models have allowed researchers to investigate the AD brain at the cellular level, which is not feasible in AD patients. As an example, the pathogenesis affecting synaptic plasticity could previously only be evaluated via *ex vivo* examinations, but at present, it is possible to administer imaging ligands targeting synaptic proteins to visualize the condition of synapses *in vivo* both in AD models and patients (Nabulsi et al. 2016; Rabiner 2018). In my point of view, PET offers a unique way to track changes in a living brain that can be considered as the most important measurement in AD. However, imaging of AD is still in its infancy, and finding of reliable radioligands and imaging methods need further development and evaluation both in patients and disease models. The metabolic and proinflammatory changes in AD involve complex signaling pathways, which are independent, yet interacting with each other and are affected by the production of Aβ. However, the precise mechanisms and relationships between oxidative stress, neuroinflammation, glial cell abnormalities, and proteinopathies are still not clear, underlining the urgent desire for narrowing the gap between the underlying disease onset, the development of possible disease-modifying

therapeutics, and imaging modalities for studying these pathways *in vivo* (Heneka et al. 2015).

In regard to imaging cerebral glucose utilization, ^{18}F-FDG is a well-established feature in patients, however in rodent models, the full applicability is yet to be confirmed. Hence, other targets in energy metabolism should be established, and the potential feasibility to monitor their role during the disease progression in living subjects should be investigated. Evidence from past decades have shown that mitochondria and oxidative stress possess a greater role in AD than was earlier thought, and they share an additional impact on proinflammatory processes in the brain. Thus, novel imaging ligands targeting ROS and mitochondrial complex I have been established, and the feasibility of these new tracers are awaiting utilization in AD (Zhang et al. 2016; Tsukada et al. 2014). Neuroinflammation, on the other hand, as a potential target for drug discovery and tracer development, has encountered more interest and developmental leaps than energy metabolism. While TSPO has been dominating the overall PET imaging of neuroinflammation ever since the introduction of ^{11}C-PK11195 in 1986 (Charbonneau et al. 1986), but producing more questions than answers regarding the complexity of the pro-inflammatory signaling pathway, the establishment of other ligands targeting purinergic receptors, astrocytes, or interleukins, have been a welcome breath of fresh air in the inflammation research (Janssen et al. 2018). However, it is still wise to think that the temporal and causal role of microglial function is one of the most important events in AD progression, which is, unfortunately, impossible to examine using PET alone. Other research methods, including immunohistochemical staining, are needed to establish the phenotype status and the corresponding activations stage of these cells. In the meantime, PET has been acting as a prize-winning working horse in clinical drug trials by adjusting the patient selection criteria, monitoring the treatments effectiveness and study outcomes, and proofing the target engagement. Currently, major phase I-III studies on antibody-based anti-amyloid as well agents targeting metabolism, inflammation and cannabinoid-based treatment strategies are ongoing, and the first long-awaited results are not estimated to arrive earlier than 2020 (Cummings et al. 2018). The hope for the positive results from these trials has not diminished, even though there has been no success in the past clinical drug discoveries targeting the AD progression. Failures have, however, increased the interest in finding other drug targets. One of these exotic candidates has been the ECS, which offers a variation of potential, but challenging and controversial routes and molecules. Cannabinoid treatment strategies are suggested to ease on symptomatic features of AD while decreasing the amyloid burden. By far, findings from cannabinoid-based treatments in AD mouse models have demonstrated decreased Aβ levels and reduced gliosis and proinflammatory markers in Tg2576 and APP/PS1 models (Martín-Moreno et al. 2012; Aso et al. 2015). A non-psychoactive phytocannabinoid, cannabidiol, has further shown to downregulate proinflammatory responses and glial activation both *in vitro* and *in vivo* (summarized in Watt and Karl 2017). These novel findings, however, need further confirmation since the general guidelines for using these controversial compounds are stricter compared to other drug targets. Imaging of safety and efficacy of potential

cannabinoids with longitudinal ^{18}F-FMPEP-d_2 or other CB_1R PET modalities might lighten the fear of these intervention strategies. Furthermore, *in vivo* imaging might adjust the possible treatment planning, accuracy, and whether to use receptor agonist or antagonists in a case manner.

Despite all the effort made so far, AD is still an unknown disease, which affects millions of people in later life. However, our knowledge on the diseased brain has enhanced, which brings light to the possibility of finding effective medical treatment. This long journey might be relieved by utilizing longitudinal studies with a multitracer PET approach. These imaging tools could perhaps elucidate the independent and synergistic processes behind the neuropathological cascade regarding different signaling pathways in AD progression. The most complex, yet crucial cascades are related to energy metabolism, neuroinflammation, and the ECS that also serve as new insights into the disease as well as a broad platform of potential targets for disease-modifying therapies to be combined with the upcoming anti-amyloid treatment plan. The one thing left to do is to work hard, and never give up.

"You gain strength, courage, and confidence by every experience in which you really stop to look fear in the face. You are able to say to yourself,
'I lived through this horror. I can take the next thing that comes along'."
- Eleanor Roosevelt

7 CONCLUSIONS

Studies **I–III** of this thesis work demonstrated that, not only do TG mouse models of AD differ in terms of the extent of amyloidosis, but they also exhibit different patterns of cerebral glucose metabolism in the early and late disease stages. The exploitation of ^{18}F-FDG μPET is limited with regard to standardized environmental factors and examination of the characteristic features of the chosen AD model. The APP_{swe}-$PS1_{dE9}$ and APP/PS1-21 models demonstrated hypometabolic features in the brain and are more suitable than the Tg2576 model for longitudinal ^{18}F-FDG imaging studies intended to evaluate interventions targeting AD pathology and their effect on cerebral glucose metabolism, and thus neuronal function. ^{18}F-DPA-714 successfully showed elevated glial activation in the brains of the APP/PS1-21 model at a very young age. This model further demonstrated the most aggressive pathology regarding amyloidosis and the decreased CB_1R availability detected with PET. ^{18}F-FMPEP-d_2 demonstrated feasible features for future imaging studies in mice if gender- and tracer-related limitations are carefully taken into consideration.

Specific conclusions of the studies:

I The APP_{swe}-$PS1_{dE9}$ and Tg2576 mouse models differed with regard to Aβ pathology, microgliosis, and glucose metabolism when equivalent experimental protocols and quantification methods were applied. The amyloidosis correlated moderately with glucose hypometabolism in old APP_{swe}-$PS1_{dE9}$ mice, whereas with microgliosis, it correlated weakly in old APP_{swe}-$PS1_{dE9}$ and Tg2576 mice. This study underlines the need for standardized ^{18}F-FDG μPET protocols, individually adjusted for each strain.

II The APP/PS1-21 model had temporal changes in the Aβ-driven glucose hypometabolism and glial activation in the brain when longitudinal ^{18}F-FDG and ^{18}F-DPA-714 PET modalities were utilized. These changes were accompanied by progressive amyloidosis and microgliosis. The PET results are comparable to clinical AD findings, which makes this model an attractive research tool for future interventional studies targeting AD pathology.

III Age- and genotype-dependent alterations in ^{18}F-FMPEP-d_2 binding were demonstrated in male APP/PS1-21 mice with unchanged total CB_1R expression. ^{18}F-FMPEP-d_2 presented encouraging evidence of its applicability for monitoring cerebral CB_1Rs in preclinical studies with other disease models, as well as AD patients. However, evaluation of the binding differences between the genders and confirmation of the benefits of ^{18}F-FMPEP-d_2 as a PET tracer for imaging CB_1Rs in AD or other neurodegenerative diseases requires further research.

ACKNOWLEDGEMENTS

This study was performed between 2011 and 2019 in Turku PET Centre, Institute of Clinical Medicine, Department of Clinical Physiology and Nuclear Medicine, Turku University Hospital and in MediCity Research Laboratory at University of Turku, Turku, Finland. I want to express my deepest appreciation to Professor Juhani Knuuti, the Director of Turku PET Centre, Professor Jaakko Hartiala and Adjunct Professor Jukka Kemppainen, the former and present Head of Department of Clinical Physiology and Nuclear Medicine, and Professor Sirpa Jalkanen, the Head of MediCity Research Laboratory, for providing excellent research facilities for conducting the thesis work.

I wish to express my humblest gratitude to the supervisors of this thesis work - Adjunct Professor Merja Haaparanta-Solin, Professor Olof Solin, and Professor Juha Rinne. I feel that I have been privileged to have you as my mentors during this rough journey. Merja, to you I feel the most thankful. Your indisputable expertise on PET imaging, radiochemistry, and small animal research has given me the most admirable guidelines for becoming a better scientist. In addition to being an encouraging and supportive mentor, you have been like a second mom to me, always supporting me and making me feel like being at home, even though I have not be an easy kid. Olof, you are the most brilliant scientist I have ever met. Your critical expertise on radiochemistry and the overall study design has guided me through these years, and educated me to inspect things more deeply. Since the beginning, I have not respected anyone like I respect you. Juha, I want to express my deepest gratitude for introducing me to the world of PET and letting me take part in the preclinical Alzheimer research. I would not have achieved this without you.

I wish to express my sincerest gratitude to the preliminary examiners of the thesis, Professor Heikki Tanila and Associate Professor Andrea Varrone. Your comments and suggestions significantly improved the thesis. I also want to acknowledge my follow-up committee members – Adjunct Professor Francisco López-Picón, Adjunct Professor Sarita Forsback, and Professor Markku Koulu – for the valuable support and professional guidance during these years. Francisco, I value your in-depth knowledge on neuroscience and never-ending enthusiasm in doing research. I greatly appreciate your constant support and help with this thesis work as well as other projects. Sarita, your contribution to this thesis work is indisputable; your expertise on radiopharmaceuticals and chemistry has shown me the way to understanding PET more thoroughly. Markku, the Father of Terbio, King in the North. You were the one who helped me through the difficult times and the one without whom my master's, nor this doctoral work, would have been possible. I highly appreciate of all the discussions we have had, and I will remember them with great warmth in my heart. I also wish to warmly acknowledge the Doctoral Programme in Clinical Research and Professor Pirjo Nuutila and Doctor Antti Saraste, as its former and present director, for the excellent educational opportunities and financial support for this thesis work. In addition, I wish to acknowledge the coordinator of the Doctoral Programme in Clinical

Research, Kristiina Nuutila, and the educational manager, Outi Irjala, for being key persons in solving and helping with the doctoral studies.

My dear co-authors and colleagues, I wish to express my gratitude to you for the constant co-operation and guidance during these years. Together we have succeeded to produce excellent research. I want to especially acknowledge Anniina Snellman, whose admirable expertise on Alzheimer's disease, β-amyloid pathology, and small animal imaging, and impressive passion for science has worked as a role model for me to become a better person and scientist. In addition, I also wish to acknowledge Rea Pihlaja and Tamiko Ishizu for their comprehensive teaching and contribution to molecular biology experiments, all of which improved my thesis and knowledge significantly. Successful radiotracer production played a key role in this thesis work, for which I owe immense gratitude to the excellent radiochemists of Turku PET Centre, Anna Krzyczmonik, Anna Kirjavainen, Olli Eskola, and Tomas Keller. Thank you for making everything possible. Eliisa Löyttyniemi is warmly acknowledged for her statistical expertise on the longitudinal data, and Olof Eriksson is acknowledged for his valuable assistance in Study III.

I owe my deepest gratitude to Elisa Riuttala, Aake Honkaniemi, and Marko Vehmanen for their valuable assistance regarding the animal laboratory work and PET imaging studies. Elisa, you taught me everything I needed to know about the strict and agile working style that has helped me to become a professional and efficient scientist. Aake, I wish to thank you for perfectly scheduling my scans and tracer deliveries, especially regarding the longitudinal studies with three different tracers, which required exact timing in 2014 and 2015. Marko, thank you for being such great company and support during these years. I warmly cherish the long lunch breaks and conversations with you. Furthermore, I wish to acknowledge the staff at the Central Animal Laboratory, University of Turku. Anitta Niittymäki (in memoriam) and Terhi Hiltula-Maisala especially deserve my sincere gratitude for taking care of my mice and teaching me animal handling. I also wish to warmly acknowledge Professor Mathias Jucker for providing the animal model for Studies II and III. In addition to the colleagues mentioned earlier, I warmly thank all present and former co-workers at Turku PET Centre and MediCity Research Laboratory, who have made this journey pleasant and empowering. It has been a pleasure to have such excellent colleagues - Tove Grönroos, Susanne Vainio, Kirsi Mikkola, Jonna Sinkkonen, Obada Alzghool, Joni Merisaari, Katharina Grafinger, Riina Solja, Rana Almajidi, Justyna Zdrojewska, Saara Laine, Päivi Kotitalo, Richard Aarnio, Johanna Tuomela, and Tiina Saanijoki, to name a few. Mirja Jyrkinen and Lenita Saloranta are warmly acknowledged for their expertise on administrative matters, and Rami Mikkola and Marko Tättäläinen are acknowledged for their valuable assistance in all IT-related issues.

2006 was the most remarkable year in my life; my journey to becoming a true scientist began in Terbio and, at the same time, I started working in legendary Börs. All of the people from the Tbio2k6 group and colleagues from Börs and Amarillo (in memoriam), thank you for those years

filled with the best moments and memories of my life, which I will cherish until my last day. I feel blessed, Noora, for being able to share this journey with you from the very beginning. I reckon that the group assignment in 2007 – *human memory, memory disorders, Homer Simpson* – might have triggered us to become neuroscientists in the same field. I am forever grateful for every year in Terbio and beyond spent with you. Reija, it has been an overwhelming joy to have such a wonderful friend both at school and work. I reckon you have understood the most of this tricky life style ☺ In addition to the friends in science, I am thankful to have such wonderful friends outside the academy: The Rillo girls - Jessica, Riikka, Sanna, Laura, and Simona - as well as my dear Ticket Queens – Anni, Tiina, Tuuli, and Mari - thank you for the valuable friendship and priceless moments we have shared. Your support means the most.

Finally, I owe my deepest appreciation to my family. My sisters from at different blood line - Riikka and Ninnu - thank you for the past three decades and your endless support and praise, which I have needed during this journey. Minna, Jon, Jack, and Troy, my Australian family, thank you for the endless love and support. I miss you so much, and cannot wait to see you again. Marjo, haluan kiittää sinua kaikesta tuesta ja rakkaudesta, ja erityisesti pojastasi, josta olet kasvattanut aivan helvetin hyvän ihmisen. Rakkaalle isälleni, Asmolle, joka olet aina tukenut minua, myös niinä hetkinä, kun en ole sitä itsepäisyyttäni pyytänyt. Kiitos kaikesta. My brother, Juha, thank you for everything you have done, especially in the past 12 months. I hope that I have made you and mom proud. Teemu, my love, I would not have been able to do this without you. Thank you for taking care of our fluffies and our home, and prioritizing my journey above your own.

This thesis work has received funding from the European Community's 7th framework programme under grant agreement no. HEALTH-F2-2011-278850 (INMiND), the Academy of Finland (no. 266891), the Doctoral Programme in Clinical Research at the University of Turku, the Alfred Kordelin Foundation, the Instrumentarium Science Foundation, state research funding from the Hospital District of Southern Finland (ERVA), the Finnish Brain Foundation sr, the Paulo Foundation, and Orion Research Foundation.

Turku, March 2019

Jatta Takkinen

REFERENCES

Acosta C, Anderson HD, and Anderson CM (2017) Astrocyte dysfunction in Alzheimer disease. J Neurosci Res, 95:2430-47

Agca C, Klakotskaia D, Schachtman TR, et al. (2016) Presenilin 1 transgene addition to amyloid precursor protein overexpressing transgenic rats increases amyloid beta 42 levels and results in loss of memory retention. BMC Neurosci, 17(1):46

Ahmad R, Goffin K, Van den Stock J, et al. (2014) *In vivo* type 1 cannabinoid receptor availability in Alzheimer's disease. European Neuropsychopharmacology, 24:242-50

Aizenstein HJ, Nebes, Saxton JA, et al. (2008) Frequent amyloid deposition without significant cignitive impairment among the elderly. Arch Neurol, 65(11):1509-17

Alsop DC, Detre JA, and Grossman M (2000) Assessment of cerebral blood flow in Alzheimer's disease by spin-labeled magnetic resonance imaging. Ann Neurol, 47(1):93-100

Alzforum. Rodent models for Alzheimer's disease. https://www.alzforum.org/research-models/; accessed on 24.9.2018

Amtul Z (2016) Why therapies for Alzheimer's disease do not work: Do we have consensus over the path to follow? Ageing Research Reviews, 25:70-84

Anandatheerthavarada H and Devi L (2007) Amyloid Precursor Protein and Mitochondrial Dysfunction in Alzheimer's Disease. Neuroscientist, 13(6):626-38

Anholt RR, Aebi U, Pederson PL, et al. (1986) Solubilization and reassembly of the mitochondrial benzodiazepine receptor. Biochemistry, 25:2120-2125.

Arlicot N, Vercouillie J, Ribeiro MJ, et al. (2012) Initial evaluation in healthy humans of ^{18}F-DPA-714, a potential PET biomarker for neuroinflammation. Nucl Med Biol, 39:570–8

Aso E, Palomer E, Juvés S, et al. (2012) CB1 agonist ACEA protects neurons and reduces the cognitive impairment of AβPP/PS1 mice. J Alzheimers Dis, 30(2):439-59

Aso E and Ferrer I (2014) Cannabinoids for treatment of Alzheimer's disease: Moving toward the clinic. Front Pharmacol, 5:37

Aso E, Sánchez-Pla A, Vegamuistisais-Lozano E, et al. (2015) Cannabis-based Medicine reduces multiple pathological processes in AβPP/PS1. J Alzheimer Dis, 43:977-91

Aso E, Andrés-Benito P, and Ferrer I (2018) Genetic deletion of CB1 cannabinoid receptors exacerbates the Alzheimer-like symptoms in a transgenic animal model. Biochem Pharmacol, pii: S0006-2952(18)30327-7

Bachmeier C, Beaulieu-Abdelahad D, Mullan M, et al. (2013) Role of the cannabinoid system in the transit of betaamyloid across the blood-brain barrier. Mol Cell Neurosci, 56:255-62

Bali MJ (1977) Neuronal loss, neurofi brillary tangles and granulovacuolar degeneration in the hippocampus with ageing and dementia. Acta Neuropathol, 37(2):111-8

Banati RB, Cagnin A, Brooks DJ, et al. (2001) Long-term transsynaptic glial responses in the human thalamus after peripheral nerve injury. Neuroreport, 12:3439-42

Bartus RT, Dean RL, Beer B, et al. (1982) The cholinergic hypothesis of geriatric memory dysfunction. Science, 217:408-17

Beaino W, Janssen B, Kooij G, et al. (2017) Purinergic receptors P2Y12R and P2X7R: potential targets for PET imaging of microglia phenotypes in multiple sclerosis. J Neuroinflammation, 14:259

Bedse G, Romano A, Cianci S, et al. (2014) Altered expression of the CB1 cannabinoid receptor in the triple transgenic mouse model of Alzheimer's disease. J Alzheimers Dis, 40:701-12

Bedse G, Romano A, Lavecchia AM, et al. (2015) The role of endocannabinoid signaling in the molecular mechanisms of neurodegeneration in Alzheimer's disease. J Alzheimer Dis, 43(4):1115-36

Belue RC, Howlett AC, Westlake TM, et al. (1995) The ontogeny of cannabinoid receptors in the brain of postnatal and aging rats. Neurotoxicol Teratol, 17:25-30.

Benard G, Massa F, Puente N, et al. (2012) Mitochondrial CB(1) receptors regulate neuronal energy metabolism. Nat Neurosci, 15:558-64

Benito C, Nunez E, Tolon RM, et al. (2003) Cannabinoid CB2 receptors and fatty acid amide hydrolase are selectively overexpressed in neuritic plaque-associated glia in Alzheimer's disease brains. J Neurosci, 23:11136-41

Benito C, Tolon RM, Castillo AI, et al. (2012) beta-Amyloid exacerbates inflammation in astrocytes lacking fatty acid amide hydrolase through a mechanism involving PPAR-alpha, PPAR-gamma and TRPV1, but not CB1 or CB2 receptors. Br J Pharmacol, 166:1474-89

Bennett DA, Schneider JA, Wilson, RS, et al. (2004) Neurofibrillary tangles mediate the association of

amyloid load with clinical Alzheimer disease and level of cognitive function. Arch Neurol, 61:378-84

Berchtold NC and Cotman CW (1998) Evolution in the Conceptualization of Dementia and Alzheimer's Disease: Greco-Roman Period to the 1960s. Neurobiol Aging, 19(3):173-89

Berding G, Müller-Vahl K, Schneider U, et al. (2004) ^{123}I-AM281 single-photon emission computed tomography imaging of central cannabinoid CB1 receptors before and after Delta9-tetrahydrocannabinol therapy and whole-body scanning for assessment of radiation dose in tourette patients. Biol Psychiatry, 55(9):904-15

Berrendero F, Romero J, Garcia-Gil L, et al. (1998) Changes in cannabinoid receptor binding and mRNA levels in several brain regions of aged rats. Biochim Biophys Acta, 1407:205-14

Bharadwaj P, Wijesekara N, Liyanapathirana M, et al. (2017) The link between type 2 diabetes and neurodegeneration: Roles for amyloid-, amylin, and tau proteins. J Alzheimers Dis, 59:421-32

Bianca VD, Dusi S, Bianchini E, et al. (1999) Beta-amyloid activates the O-2 forming NADPH oxidase in microglia, monocytes, and neutrophils. A possible inflammatory mechanism of neuronal damage in Alzheimer's disease. J Biol Chem, 274(22):15493-9

Binder LI, Frankfurter A, and Rebhun KI (1985) The distribution of tau in the mammalian central nervous system. J Cell Biol, 101:1371-8

Blass JP, Baker AC, Ko L, et al. (1990) Induction of Alzheimer antigens by an uncoupler of oxidative phosphorylation. Arch Neurol, 47:864-69

Blennow K and Zetterberg H (2018) The past and the future of Alzheimer' disease fluid biomarkers. J Alzheimers Dis, 62:1125-40

Bohnen NI, Djang DS, Herholz K, et al. (2012) Effectiveness and safety of ^{18}F-FDG PET in the evaluation of dementia: a review of the recent literature. J Nucl Med, 53:59-71

Bonfirm TR, Forny-Germano L, Sathler LB, et al. (2012) An anti-diabetes agent protects the mouse brain from defective insulin signaling caused by Alzheimer's disease-associated Aβ oligomers. J Clin Invest, 122:1339-53

Bourdiol F, Toulmond S, Serrano A, et al. (1991) Increase in omega 3 (peripheral type benzodiazepine) binding sites in the rat cortex and striatum after local injection of interleukin-1, tumour necrosis factor-alpha, and lipopolysaccharide. Brain Res, 543:194-200

Braak H, Alafuzoff I, Arzberger T, et al. (2006) Stating of Alzheimer's disease-associated neurofibrillary pathology using paraffin sections and immunocytochemistry. Acta Neuropathologica, 112(4):389-404

Braak H, Braak E, Grundke-Iqbal I, et al. (1986) Occurence of neuropil threads in the senile human brain and in alzheimer's disease: a third location of paired helical filaments outside of neurofibrillary tangles and neuritic plaques. Neuroscience letters, 65:351-5

Braak H and Braak E (1997) Frequency of stages of Alzheimer-related lesions in different age categories. Neurobiol Aging, 18:351-7

Braak H and Del Tredici K (2011) The pathological process underlying Alzheimer's disease in individuals under thirty. Acta Neuropathol, 121:171-81

Braak H and Del Tredici K (2014). Are cases with tau pathology occurring in the absence of Abeta deposits part of the AD-related pathological process? Acta Neuropathol, 128:767-2

Brailoiu GC, Oprea TI, Zhao P, et al. (2011) Intracellular cannabinoid type 1 (CB1) receptors are activated by anandamide. J Biol Chem, 286:29166-74

Brendel M, Jaworska A, GrieBinger E, et al. (2015) Cross-sectional comparison of small animal ^{18}F-Florbetaben amyloi-PET between transgenic AD mouse models. Plos One, 10:e0116678

Brendel M, Probst F, Jaworska A, et al. (2016) Glial Activation and Glucose Metabolism in a Transgenic Amyloid Mouse Model: A Triple-Tracer PET Study. J Nucl Med, 57(6):954-60

Brendel M, Focke C, Blume T, et al. (2017a) Time courses of cortical glucose metabolism and microglial activity across the life span of wild-type mice: a PET study. J Nucl Med, 58:1984-90

Brendel M, Kleinberger G, Probst F, et al. (2017b) Increase of TREM2 during Aging of an Alzheimer's Disease Mouse Model Is Paralleled by Microglial Activation and Amyloidosis. Front Aging Neurosci, 31(9):8

Briard E, Shah J, and Musachio J (2005) Synthesis and evaluation of a new ^{18}F-labeled ligand for PET imaging of brain peripheral benzodiazepine receptors [abstract]. J Labeled Compd Radiopharm, 48

Brier MR, Gordon B, Friedrichsen K, et al. (2016) Tau and Aβ imaging, CSF measures, and cognition in Alzheimer's disease. Sci Transl Med, 8:338ra66

Brinkmalm A, Brinkmalm G, Honer WG, et al. (2014) SNAP-25 is a promising novel cerebrospinal fluid biomarker for synapse degeneration an Alzheimer's disease. Mol Neurodeneger, 9:53

Brown AK, Fujita M, Fujimura Y, et al. (2007) Radiation dosimetry and biodistribution in monkey and man of ^{11}C-

PBR28: a PET radioligand to image inflammation. J Nucl Med, 48:2072-79

Bush AI (2008) Drug development based on the metals hypothesis of Alzheimer's disease. J Alzheimers Dis, 15:223-40

Burston JJ, Wiley JL, Craig AA, et al. (2010) Regional enhancement of cannabinoid CB1 receptor desensitization in female adolescent rats following repeated Delta-tetrahydrocannabinol exposure. Br J Pharmacol, 161:103-12

Burte F, Carelli V, Chinnery PF, et al. (2015) Disturbed mitochondrial dynamics and neurodegenerative disorders. Nat Rev Neurol, 11:11-24

Cagnin A, Brooks DJ, Kennedy AM, et al. (2001) *In-vivo* measurement of activated microglia in dementia. Lancet, 358:461-7

Cai Q and Tammineni P (2016) Alterations in mitochondrial quality control in Alzheimer's disease. Front Cell Neurosci, 10:24

Cai Z, Hussain MD, and Yan LJ (2014) Microglia, neuroinflammation, and beta-amyloid protein in Alzheimer's disease. Int J Neurosci, 124(5):307-21

Cairns NJ, Ikonomovic MD, Benzinger T, et al. (2009) Absence of Pittsburgh Compound B Detection of Cerebral Amyloid Beta in a Patient With Clinical, Cognitive, and Cerebrospinal Fluid Markers of Alzheimer Disease. Arch Neurol 66(12): 1557-62

Callahan LM, Vaules WA, and Coleman PD (1999) Quantitative decrease in synaptop,hysin message expression and increase in cathepsin D message expression in Alzheimer disease neurons containing neurofibrillary tangles. J Neuropathol Exp Neurol, 58:275-87

Carter SF, Scholl M, Almkvist O, et al. (2012) Evidence for astrocytosis in prodromal Alzheimer disease provided by ^{11}C-deuterium-L-deprenyl: a multitracer PET paradigm combining ^{11}C-Pittsburgh compound B and ^{18}F-FDG. J Nucl Med, 53:37-46

Casteels C, Bormans G, and Van Laere K (2010) The effect of anaesthesia on ^{18}F-MK-9470 binding to the type 1 cannabinoid receptor in the rat brain. Eur J Nucl Med Mol Imaging, 37:1164-73

Casteels C, Vandeputte C, Rangarajan JR, et al. (2011) Metabolic and type 1 cannabinoid receptor imaging of a transgenic rat model in the early phase of Huntington disease. Exp Neurol, 229:440-9

Castelli MP, Fadda P, Casu A, et al. (2014) Male and female rats differ in brain cannabinoid CB1 receptor density and function and in behavioural traits predisposing to drug addiction: effect of ovarian hormones. Curr Pharm Des, 20:2100-13

Chan DC (2006) Mitochondrial fusion and fission in mammals. Ann Rev Cell Dev Biol, 22:79-99

Chaney A, Bauer M, Bochicchio D, et al. (2018) Longitudinal investigation of neuroinflammation and metabolic profiles in the APP_{swe}-PSI_{dE9} transgenic mouse model of Alzheimer's disease. J Neurochem, 144:318-35

Charalambous A, Marciniak G, Shiue CY, et al. (1991) PET studies in the primate brain and biodistribution in mice using (-)-5'-^{18}F-delta 8-THC. Pharmacol Biochem Behav, 40(3):503-7

Charbonneau P, Syrota A, Crouzel C, et al. (1986) Peripheral type benzodiazepine receptors in the living heart characterised by positron emission tomography. Circukztion, 73:476483

Chauveau F, Van Camp N, Dolle F, et al. (2009) Comparative evaluation of the translocator protein radioligands ^{11}C-DPA-713, ^{18}F-DPA-714, and ^{11}C-PK11195 in a rat model of acute neuroinflammation. J Nucl Med, 50:468-76

Chen MK and Guilarte TR (2008) Translocator protein 18 kDa (TSPO): molecular sensor of brain injury and repair. Pharmacol Ther, 118(1):1-17

Chen H, Chomyn A, and Chan D (2005) Disruption of fusion results in mitochondrial heterogeneity and dysfunction. J Biol Chem, 280:26185-92

Chen X, Zhang J, and Chen C (2011) Endocannabinoid 2-arachidonoylglycerol protects neurons against β-amyloid insults. Neuroscience, 178:159-68

Cheng-Hathaway PJ, Reed-Geaghan EG, Jay TR, et al. (2018) The Trem2 R47H variant confers loss-of-function-like phenotypes in Alzheimer's disease. Mol Neurodegener, 13(1):29

Cherry S and Dahlblom M (2004) PET: Physics, instrumentation and scanners. In PET Molecular Imaging and Its Biological Applications, M Phelps, ed (New York, NY, 10010 USA: Springer)

Chételat G, Desgranges B, Landeau B, et al. (2008) Direct voxel-based comparison between grey matter hypometabolism and atrophy in Alzheimer's disease. Brain, 131:60-71

Chien DT, Bahri S, Szardenings AK, et al. (2013) Early clinical PET imaging results with the novel PHF-tau radioligand ^{18}F-T807. J Alzheimers Dis, 34(2):457-68

Chiotis K, Saint-Aubert L, Rodriguez-Vieitez E, et al. (2018) Longitudinal changes of tau PET imaging in relation to hypometabolism in prodromal and

Alzheimer's disease dementia. Mol Psychiatry, 23(7):1666-73

Choi HB, Khoo C, Ryu JK, et al. (2002) Inhibition of lipopolysaccharide-induced cyclooxygenase-2, tumor necrosis factor-alpha and [Ca2+]i responses in human microglia by the peripheral benzodiazepine receptor ligand PK11195. J Neurochem, 83:546-55

Clark CM, Pontecorvo MJ, Beach TG, et al. (2012) Cerebral PET with florbetapir compared with neuropathology at autopsy for detection of neuritic amyloid-β plaques: a prospective cohort study. Lancet Neurol, 11:669-78

Clarke JR, Ribeiro FC, Frozza RL, et al. (2018) Metabolic Dysfunction in Alzheimer's Disease: From Basic Neurobiology to Clinical Approaches. J Alzheimers Dis, 64(s1):S405-26

Cohen RM, Rezai-Zadeh K, Weitz TM, et al. (2013) A transgenic Alzheimer rat with plaques, tau pathology, behavioral impairment, oligomeric aβ, and frank neuronal loss. J Neurosci, 33(15):6245-56

Coleman PD and Flood DG (1987) Neuron numbers and dendritic extent in normal aging and Alzheimer's disease. Neurobiol Aging, 8(6):521-45

Coleman RA, Liang C, Patel R, et al. (2017) Brain and Brown Adipose Tissue Metabolism in Transgenic Tg2576 Mice Models of Alzheimer Disease Assessed Using ^{18}F-FDG PET Imaging. Mol Imaging, 16:1536012117704557

Cosenza-Nashat M, Zhao ML, Suh HS, et al. (2009) Expression of the translocator protein of 18 kDa by microglia, macrophages and astrocytes based on immunohistochemical localization in abnormal human brain. Neuropathol Appl Neurobiol, 35:306-28

Cumming P, Burgher B, Patkar O, et al. (2018) Sifting through the surfeit of neuroinflammation tracers. J Cereb Blood Flow Metab, 38(2):204-24

Cummings J, Lee G, Mortsdorf T, et al. (2018) Alzheimer's disease drug development pipeline: 2018. Alzheimer's & Dementia: Translational Research & Clinical Intervention, 4:195-214

Dawkins E and Small DH (2014) Insights into the physiological function of the β-amyloid precursor protein: beyond Alzheimer's disease. J Neurochem, 129(5):756-69

De Felice FG (2013) Alzheimer's disease and insulin resistance: Translating basic science into clinical applications. J Clin Invest, 123(2):531-9

De Felice FG and Ferreira ST (2014) Inflammation, defective insulin signaling, and mitochondrial dysfunction as common molecular denominators connecting type 2 diabetes to Alzheimer disease. Diabetes, 63(7):2262-72.

De la Monte SM and Wands JR (2005) Review of insulin and insulin-like growth factor expression, signaling, and malfunction in the central nervous system: relevance to Alzheimer's disease. J Alzheimers Dis, 7:45-61

De la Torre JC (2009) Cerebrovascular and cardiovascular pathology in Alzheimer's disease. Int Rev Neurobiol, 84:35-48

De Vos F, Santens P, Vermeirsch H, et al. (2000) Pharmacological evaluation of ^{11}C-donepezil as a tracer for visualization of acetylcholinesterase by PET. Nucl Med Biol, 27(8):745-7

DeBay DR, Reid GA, Macdonald IR, et al. (2017) Butyrylcholinesterase-knockout reduces fibrillar β-amyloid and conserves ^{18}FDG retention in 5XFAD mouse model of Alzheimer's disease. Brain Res, 1671:102-10

Deleye S, Waldron AM, Richardson JC, et al. (2016) The Effects of Physiological and Methodological Determinants on ^{18}F-FDG Mouse Brain Imaging Exemplified in a Double Transgenic Alzheimer Model. Mol Imaging, 11:15

Deleye S, Waldron AM, Verhaghe J, et al. (2017) Evaluation of Small-Animal PET Outcome Measures to Detect Disease Modification Induced by BACE Inhibition in a Transgenic Mouse Model of Alzheimer Disease. J Nucl Med, 58:1977-83

Devane WA, Hanus L, Breuer A, et al. (1992) Isolation and structure of a brain constituent that binds to the cannabinoid receptor. Science, 258:1946-9

Devi L, Prabhu BM, Galati DF, et al. (2006) Accumulation of amyloid precursor protein in the mitochondrial import channels of human Alzheimer's disease brain is associated with mitochondrial dysfunction. J Neurosci, 30:9057-68

Donohue SR (2008a) Development of cannabinoid subtype-1 (CB1) receptor ligands for PET. In: Thesis for Doctoral degree Department of Clinical Neuroscience, Stockholm; Karolinska Institutet.

Donohue SR, Krushinski JH, Pike VW, et al. (2008b) Synthesis, *ex vivo* evaluation, nd radiolabelling of potent 1,5-diphenylpyrrolidin-2-one cannabinoid subtype-1 receptor ligands as candidates for *in vivo* imaging. J Med Chem, 51: 5833-42

Du H, Guo L, Yan S, et al. (2010) Early deficits in synaptic mitochondria in an Alzheimer's disease mouse model. Proc Natl Acad Sci USA, 107:18670-5

Duarte AI, Santos MS, Oliveira CR, et al. (2018) Brain insulin signalling, glucose metabolism and females'

reproductive aging: A dangerous triad in Alzheimer's disease. Neuropharmacology, 136:223-42

Dubois B, Feldman HH, Jacova C, et al. (2014) Advancing research diagnostic criteria for Alzheimer's disease: the IWG-2 criteria. Lancet Neurol, 13:614-29

Dubois B, Epelbaum S, Nyasse F, et al. (2018) Cognitive and neuroimaging features and brain β-amyloidosis in individuals at risk of Alzheimer's disease (INSIGHT-preAD): a longitudinal observational study. Lancet Neurol, 17: 335-46

Duff K, Eckman C, Zehr C et al. (1996) Increased amyloid-beta42(43) in brains of mice expressing mutant presenilin 1. Nature, 383(6602):710-3

Duyckaerts C (2011) Tau pathology in children and young adults: can you still be unconditionally baptist? Acta Neuropathol, 121:145-7

Edison P, Archer HA, Gerhard A, et al. (2008) Microglia, amyloid and cognition in Alzheimer's disease: an ^{11}C-R-PK11195-PET and ^{11}C-PIB-PET study. Neurobiol Dis, 32:412-9

Edison P, Donat CK, and Sastre M (2018) *In vivo* Imaging of Glial Activation in Alzheimer's Disease. Front Neurol, 9:625

Ehrhart J, Obregon D, Mori T, et al. (2005) Stimulation of cannabinoid receptor 2 (CB2) suppresses microglial activation. J Neuroinflammation, 2:29

Eljaschewitsch E, Witting A, Mawrin C, et al. (2006) The Endocannabinoid Anandamide Protects Neurons during CNS Inflammation by Induction of MKP-1 in Microglial Cells. Neuron, 49:67-79

Engler H, Forsberg A, Almkvist O, et al. (2006) Two-year follow-up of amyloid deposition in patients with Alzheimer's disease. Brain 129(Pt11):2856-66

Epis R, Gardoni F, Marcello E, et al. (2010) Searching for new animal models of Alzheimer's disease. European Journal of Pharmacology 626:57-63

Esposito G, Iuvone T, Savani C, et al. (2007) Opposing control of cannabinoid receptor stimulation on amyloid-beta-induced reactive gliosis: *In vitro* and *in vivo* evidence. J Pharmacol Exp Ther, 322:1144-52

Fan Z, Okello AA, Brooks DJ, et al. (2015) Longitudinal influence of microglial activation and amyloid on neuronal function in Alzheimer's disease. Brain, 138(Pt 12):3685-98

Fan Z, Calsolaro V, Atkinson RA, et al. (2016) Flutriciclamide (^{18}F-GE180) PET: First-in-Human PET Study of Novel Third-Generation *In Vivo* Marker of Human Translocator Protein. J Nucl Med, 57(11):1753-9

Farkas S, Nagy K, Palkovits M, et al. (2012) ^{125}I-SD-7015 reveals fine modalities of CB1 cannabinoid receptor density in the prefrontal cortex during progression of Alzheimer's disease. Neurochem Int, 60:286-91

Feeney C, Scott G, Raffel J, et al. (2016) Kinetic analysis of the translocator protein positron emission tomography ligand ^{18}F-GE-180 in the human brain. Eur J Nucl Med Mol Imaging, 43:2201-10

Fleminger S, Oliver D, Lovestone, et al. (2003) Head injury as a risk factor for Alzheimer's disease: the evidence 10 years on; a partial replication. J Neurol Neurosurg Psychiatry, 74:857-62

Fowler JS and Ido T (2003) Design and synthesis of 2-Deoxy-2-^{18}F-Fluoro-D-glucose. In: Hankbook of radiopharmaceuticals. Welch MJ and Redvanly CS, ed. Whiley, Chichester, England.

Forstl H and Howard R (1991) Recent studies on dementia senilis and brain disorders caused by atheromatous vascular disease: by A. Alzheimer, 1898. Alz Dis Assoc Dis, 5:257-64

Foster N, Heidebrink JL, Clark CM, et al. (2007) FDG-PET improves accuracy in distinguishing frontotemporal dementia and Alzheimer's disease. Brain, 130(Pt 10):2616-35

Franz G, Beer R, Kampfl A, et al. (2003) Amyloid β 1–42 and tau in cerebrospinal fluid after severe traumatic brain injury. Neurology, 60:1457-61

Frautschy SA, Yang F, Irrizarry M, et al. (1998) Microglial response to amyloid plaques in APPsw transgenic mice. Am J Pathol, 152(1):307-17

Freund TF, Katona I, and Piomelli D (2003) Role of endogenous cannabinoids in synaptic signaling. Physiol Rev, 83:1017-66

Frisoni GB, Bocchetta M, Chételat G, et al. (2013) Imaging markers for Alzheimer disease: which vs how. Neurology, 81(5):487-500

Fueger BJ, Czernin J, Hildebrandt I, et al. (2006) Impact of animal handling on the results of ^{18}F-FDG PET studies in mice. J Nucl Med, 47:999-1006

Förster S, Grimmer T, Miederer I, et al. (2012) Regional expansion of hypometabolism in Alzheimer's disease follows amyloid deposition with temporal delay. Biol Psychiatry, 71:792-7

Games D, Adams D, Alessandrini R, et al. (1995) Alzheimer-type neuropathology in transgenic mice overexpressing V717F beta-amyloid precursor protein. Nature, 373(6514):523-7

Garcia-Alloza M, Robbins EM, Zhang-Nunes SX, et al. (2006) Characterization of amyloid deposition in the

$APP_{swe}/PS1_{dE9}$ mouse model of Alzheimer disease. Neurobiol Dis, (3):516-24

Garibotto V, Herholz K, Boccardi M, et al. (2017) Clinical validity of brain flurododeoxyglucose positron emission tomography as a biomarker for Alzheimer's disease in the context of a structured 5-phase development framework. Neurobiol Aging, 52:183-95

Gatley SJ, Lan R, Volkow ND, et al. (1998) Imaging the brain marijuana receptor: development of a radioligand that binds to cannabinoid CB1 receptors *in vivo*. J Neurochem, 70(1):417-23

Gobbi LC, Knust H, Körner M, et al. (2017) Identification of three novel radiotracers for imaging aggregated tau in Alzheimer's disease with positron emission tomography. J Med Chem, 60:7350-70

Goedert M, Spillantini MG, Jakes R, et al. (1989) Multiple isoforms of human microtubule-associated protein tau: sequences and localization in neurofibrillary tangles of Alzheimer's disease. Neuron 3, (4):519-26

Golla SS, Boellaard R, Oikonen V, et al. (2015) Quantification of ^{18}F-DPA-714 binding in the human brain: initial studies in healthy controls and Alzheimer's disease patients. J Cereb Blood Flow Metab, 35:766-72

Gómez-Isla T, Price JL, McKeel, Jr. DW, et al. (1996) Profound loss of layer II entorhinal cortex neurons occurs in very mild Alzheimer's disease. J Neurosci, 16(14):4491-500

Gonzalez S, Mena MA, Lastres-Becker I, et al. (2005) Cannabinoid CB1 receptors in the basal ganglia and motor response to activation or blockade of these receptors in parkin-null mice. Brain Res, 1046:195-206

Gonthier MP, Hoareau L, Festy F, et al. (2007) Identification of endocannabinoids and related compounds in human fat cells. Obesity (Silver Spring), 15:837-45

Gordon JC (1993) Temperature Regulation in Laboratory Rodents. New York, USA. Cambridge University Press. Online ISBN:9780511565595

Goverman J (2009) Autoimmune T cell responses in the central nervous system. Nat Rev Immunol, 9:393-407

Grillo CA, Piroli GG, Lawrence RC, et al. (2015) Hippocampal insulin resistance impairs spatial learning and synaptic plasticity. Diabetes, 64:3927-36

Grimsey NL, Graham ES, Dragunow M, et al. (2010) Cannabinoid Receptor 1 trafficking and the role of the intracellular pool: implications for therapeutics. Biochem Pharmacol, 80(7):1050-62

Grueninger F, Bohrmann B, Czech C, et al. (2010) Phosphorylation of Tau at S422 is enhanced by Abeta in TauPS2APP triple transgenic mice. Neurobiol Dis, 37(2):294-306

Goate A, Chartier-Harlin MC, Mullan M, et al. (1991) Segregation of amissensemutation in the amyloid precursor protein genewith familial Alzheimer′s disease. Nature, 349:704-6

Guerreiro R, Wojtas A, Bras J, et al. (2013) TREM2 variants in Alzheimer's disease. N Engl J Med, 368:117–27

Gulyaeva NV, Bobkova NV, Kolosova NG, et al. (2017) Molecular and Cellular Mechanisms of Sporadic Alzheimer's Disease: Studies on Rodent Models *in vivo*. Biochemistry (Moscow), 82(10):1088-102

Gulyás B, Pavlova E, Kása P, et al. (2011) Activated MAO-B in the brain of Alzheimer patients, demonstrated by [^{11}C]-L-deprenyl using whole hemisphere autoradiography. Neurochem Int, 58(1):60-8

Gulyás B, Makkai B, Kása P, et al. (2009) A comparative autoradiography study in post mortem whole hemisphere human brain slices taken from Alzheimer patients and age-matched controls using two radiolabelled DAA1106 analogues with high affinity to the peripheral benzodiazepine receptor (PBR) system. Neurochem Int, 54(1):28-36

Gylys KH, Fein JA, Yang F, et al. (2004) Synaptic changes in Alzheimer's disease: increased Amyloid–β and gliosis in surviving terminals is accompanied by decreased PSD-95 fluorescence. Am J Pathol, 165:1809-17

Haass C, Schlossmacher MG, Hung AY, et al. (1992) Amyloid beta-peptide is produced by cultured cells during normal metabolism. Nature, 359(6393):322-5

Haltia Matti (2003) Vanhenevat aivot. Presentation at the Science Day on 8th January 2003

Hamacher K, Coenen HH, and Stöcklin G (1986) Efficient stereospecific synthesis of no-carrier-added 2-^{18}F-fluoro-2-deoxy-D-glucose using aminopolyether supported nucleophilic substitution. J Nucl Med, 27:235-8

Hamelin L, Lagarde J, Dorothee G, et al. (2016) Early and protective microglial activation in Alzheimer's disease: a prospective study using ^{18}F-DPA-714 PET imaging. Brain, 139:1252-64

Han J, Liu H, Liu C, et al. (2017) Pharmacologic characterizations of a P2X7 receptor-specific radioligand, ^{11}C-GSK1482160 for neuroinflammatory response. Nucl Med Commun, 38:372–82

Hanger DP, Anderton BH, and Noble W (2009) Tau phosphorylation: The therapeutic challenge for neurodegenerative disease. Trends Mol Med, 15:112-9

Hansen DV, Hanson JE, and Sheng M (2018) Microglia in Alzheimer's disease. J Cell Biol, 217(2):459-72

Hardy J and Selkoe DJ (2002) The amyloid hyptohesis of Alzheimer's disease: progress and problems on the road to therapeutics. Science, 297:353-6

Hardy JA and Higgins GA (1992) Alzheimer's disease: The amyloid cascade hypothesis. Science, 256:184-5

Harold D, Abraham R, Hollingworth P, et al. (2009) Genome-wide association study identifies variants at CLU and PICALM associated with Alzheimer's disease. Nat Genet, 41:1088-93

Hartman RE, Laurer H, Longhi L, et al. (2002) Apolipoprotein E4 influences amyloid deposition but not cell loss after traumatic brain injury in a mouse model of Alzheimer's disease. J Neurosci, 22:10083-7

Haruyama N, Cho A, and Kulkami AB (2009) Overview: Engineering transgenic constructs and mice. Curr Protoc Cell Biol, Chapter19 : Unit–19.10.

Harwood DG, Kalechstein A, Barker WW, et al. (2010) The effect of alcohol and tobacco consumption, and apolipoprotein E genotype, on the age of onset in Alzheimer's disease. Int J Geriatr Psychiatry, 25(5):511-8

Hauss-Wegrzyniak B, Dobrzanski P, Stoehr JD, et al. (1998) Chronic neuroinflammation in rats reproduces components of the neurobiology of Alzheimer's disease. Brain Res, 780(2):294-303

Hebert-Chatelain E, Desprez T, Serrat R, et al. (2016) A cannabinoid link between mitochondria and memory. Nature, 539(7630):555-9

Heneka MT, Carson MJ, El Khoury J, et al. (2015) Neuroinflammation in Alzheimer's disease. Lancet Neurol, 14(4):388-405

Herkenham M, Lynn AB, Little MD, et al. (1990) Cannabinoid receptor localization in brain. Proc Natl Acad Sci USA, 87:1932-36

Hide I, Tanaka M, Inoue A, et al. (2000) Extracellular ATP triggers tumor necrosis factor-alpha release from rat microglia. J Neurochem, 75(3):965-72

Holland JP, Liang SH, Rotstein BH, et al. (2014) Alternative approaches for PET radiotracer development in Alzheimer's disease: imaging beyond plaque. J Label Compd Radiopharm, 57:323–31

Hooijmans CR, Graven C, Dederen PJ, et al. (2007) Amyloid beta deposition is related to decreased glucose transporter-1 levels and hippocampal atrophy in brains of aged APP/PS1 mice. Brain Res, 1181:93-103

Horti AG, Fan H, Kuwabara H, et al. (2006) ^{11}C-JHU75528: a radiotracer for PET imaging of CB1 cannabinoid receptors. J Nucl Med, 47:1689-96

Horti A and Van Laere K (2008) Development of Radioligands for In Vivo Imaging of Type 1 Cannabinoid Receptors (CB1) in Human Brain. Current Pharmaceutical Design, 14:3363-83

Horti AG, Gao Y, Ravert HT, et al. (2010) Synthesis and biodistribution of ^{11}C-A-836339, a new potential radioligand for PET imaging of cannabinoid type 2 receptors (CB2). Bioorg Med Chem, 18:5202-7

Howlett DR, Richardson JC, Austin A, et al. (2004) Cognitive correlates of Abeta deposition in male and female mice bearing amyloid precursor protein and presenilin-1 mutant transgenes. Brain Res, 1017(1-2):130-6

Hsiao K, Chapman P, Nilsen S, et al. (1996) Correlative memory deficits, Abeta elevation, and amyloid plaques in transgenic mice. Science, 274(5284):99-102

Hutton M, Lendon CL, Rizzu P, et al. (1998) Association of missense and 5´-splice-site mutations in tau with the inherited dementia FTDP-17. Nature, 393:702-5

Hwang J, Adamson C, Butler D, et al. (2010) Enhancement of endocannabinoid signaling by fatty acid amide hydrolase inhibition: A neuroprotective therapeutic modality. Life Sci, 86:615-23

Hyman BT, Phelps CH, Beach TG, et al. (2012) National Institute on Aging-Alzheimer's Association guidelines for the neuropathologic assessment of Alzheimer's disease. Alzheimers Dement, 8:1-13

Ikawa M, Lohith TG, Shrestha S, et al. (2017) ^{11}C-ER176, a Radioligand for 18-kDa Translocator Protein, Has Adequate Sensitivity to Robustly Image All Three Affinity Genotypes in Human Brain. J Nucl Med, 58(2):320-5

Ito K, Fukuyama H, Senda M, et al. (2015) Prediction of Outcomes in Mild Cognitive Impairment by Using ^{18}F-FDG-PET: A Multicenter Study. J Alzheimers Dis, 45:543-52

Iyo M, Namba H, Fukushi K, et al. (1997) Measurement of acetylcholinesterase by positron emission tomography in the brains of healthy controls and patients with Alzheimer's disease. Lancet, 349(9068):1805-9

Jack CR Jr, Knopman DS, Jagust WJ, et al. (2010) Hypothetical model of dynamic biomarkers of the Alzheimer's pathological cascade. Lancet Neurol, 9(1):119-28

Jack CR Jr, Knopman DS, Jagust WJ, et al. (2013) Tracking pathophysiological processes in Alzheimer's

disease: an updated hypothetical model of dynamic biomarkers. Lancet Neurol, 12:207-16

Jack CR Jr, Bennett DA, Blennov K, et al. (2018) NIA-AA Research Framework: Toward a biological definition of Alzheimer's disease. Alzheimers Dement, 14(4):535-62

Jackson RJ, Rudinskiy N, Herrmann AG, et al. (2016) Human tau increases amyloid β plaque size but not amyloid β-mediated synapse loss in a novel mouse model of Alzheimer's disease. Eur J Neurosci, (12):3056-66

James ML, Fulton RR, Henderson DJ, et al. (2005) Synthesis and *in vivo* evaluation of a novel peripheral benzodiazepine receptor PET radioligand. Bioorg Med Chem, 13(22):6188-94

James ML, Fulton RR, Vercoullie J, et al. (2008) DPA-714, a new translocator protein-specific ligand: synthesis, radiofluorination, and pharmacologic characterization. J Nucl Med, 49:814-22

James ML, Belichenko NP, Nguyen TV, et al. (2015) PET imaging of translocator protein (18 kDa) in a mouse model of Alzheimer's disease using N-(2,5-dimethoxybenzyl)-2-^{18}F-fluoro-N-(2-phenoxyphenyl)acetamide. J Nucl Med, 56:311-16

Janssen B, Vugts D, Windhorst AD, et al. (2018) PET Imaging of Microglial Activation—Beyond Targeting TSPO. Molecules, 23:607

Jankowsky JL, Slunt HH, Ratovitski T, et al. (2001) Co-expression of multiple transgenes in mouse CNS: a comparison of strategies. Biomol Eng, 17(6):157-65

Jensen TL, Kiersgaard MK, Sorensen DB, et al. (2013) Fasting of mice: a review. Lab Anim 47: 225-40

Jonsson T, Atwal JK, Steinberg S, et al. (2012) A mutation in APP protects against Alzheimer's disease and age-related cognitive decline. Nature, 488(7409):96-9

Jonsson T, Stefansson H, Steinberg S, et al. (2013) Variant of TREM2 associated with the risk of Alzheimer's disease. N Engl J Med, 368:107-16

Junck L, Olson JM, Ciliax BJ, et al. (1989) PET imaging of human gliomas with ligands for the peripheral benzodiazepine binding site. Ann Neurol, 26:752-58

Jung KM, Astarita G, Yasar S, et al. (2012) An amyloid beta42-dependent deficit in anandamide mobilization is associated with cognitive dysfunction in Alzheimer's disease. Neurobiol Aging, 33:1522-32

Kalifa S, Polston EK, Allard JS, et al. (2011) Distribution patterns of cannabinoid CB1 receptors in the hippocampus of $APP_{swe}/PS1_{DeltaE9}$ double transgenic mice. Brain Res, 1376:94-100

Kametani F and Hasegawa M (2018) Reconsideration of Amyloid Hypothesis and Tau Hypothesis in Alzheimer's Disease. Front Neurosci, 12:25

Kano M, Ohno-Shosaku T, Hashimotodani Y, et al. (2009) Endocannabinoid-mediated control of synaptic transmission. Physiol Rev, 89:309-80

Keller T, Krzyczmonik A, Forsback S, et al. (2017) Radiosynthesis and Preclinical Evaluation of ^{18}F-F-DPA, A Novel Pyrazolo[1,5a]pyrimidine Acetamide TSPO Radioligand, in Healthy Sprague Dawley Rats. Mol Imaging Biol, 19(5):736-45

Keller T, López-Picón FR, Krzyczmonik A, et al. (2018) ^{18}F-F-DPA for the Detection of Activated Microglia in a Mouse Model of Alzheimer's Disease. Nuc Med Biol, 26;67:1-9

Keren-Shaul H, Spinrad A, Weiner A, et al. (2017) A Unique Microglia Type Associated with Restricting Development of Alzheimer's Disease. Cell, 169(7):1276-90.e17

Kitazawa M, Medeiros, Ro, and LaFerla FM (2012) Transgenic Mouse Models of Alzheimer Disease: Developing a Better Model as a Tool for Therapeutic Interventions. Curr Pharm, 18(8):1131-47

Kivipelto M, Helkala EL, Hänninen T, et al. (2001) Midlife vascular risk factors and late-life mild cognitive impairment: a population-based study. Neurology, 56:1683-89

KleiberM (1975) Body size and metabolic rate. In: The fire of life. Robert E. Krieger Publishing Company, Huntington, New York:179–222

Klein C, Kramer E.M, Cardine AM, et al. (2002) Process outgrowth of oligodendrocytes is promoted by interaction of fyn kinase with the cytoskeletal protein tau. J Neurosci, 22:698–707

Klunk W, Wang Y, Huang GF, et al. (2001) Uncharged thioflavin-T derivates bind to amyloid-beta protein with high affinity and readily enter the brain. Life Sci, 69(13):1471-84

Klunk WE, Engler H, Nordberg A, et al. (2004) Imaging brain amyloid in Alzheimer's disease with Pittsburgh Compound-B. Ann Neurol, 55(3):306-19

Knopman DS and Petersen RC (2014) Mild cognitive impairment and mild dementia: a clinical perspective. Mayo Clin Proc, 89(10):1452-9

Kreisl WC, Lyoo CH, McGwier M, Snow J, et al. (2013) *In vivo* radioligand binding to translocator protein correlates with severity of Alzheimer's disease. Brain, 136:2228-38

Kreisl WC, Lyoo CH, Liow JS, et al. (2017) Distinct patterns of increased translocator protein in posterior

cortical atrophy and amnestic Alzheimer's disease. Neurobiol Aging, 51:132-40

Krstic D, Madhusudan A, Doehner J, et al. (2012) Systemic immune challenges trigger and drive Alzheimer-like neuropathology in mice. J Neuroinflammation, 9:151

Koistinaho M, Lin S, Wu X, et al. (2004) Apolipoprotein E promotes astrocyte colocalization and degradation of deposited amyloid-beta peptides. Nat Med, 10(7):719-26

Kuntner C, Kesner AL, Bauer M, et al. (2009) Limitations of small animal PET imaging with ^{18}F-FDDNP and FDG for quantitative studies in a transgenic mouse model of Alzheimer's disease. Mol Imaging Biol, 11(4):236-40

Kärkkäinen E, Tanila H, and Laitinen JT (2012) Functional autoradiography shows unaltered cannabinoid CB1 receptor signalling in hippocampus and cortex of APP/PS1 transgenic mice. CNS Neurol Disord Drug Targets, 11:1038-44

Käypä Hoito A. Alzheimerin taudin diagnostiset kriteerit vuodelta 2007. Tarkistanut 8.6.2016 Juha Rinne. http://www.kaypahoito.fi/web/kh/suositukset/suositus?id=nix01590. Accessed 9.11.2018

Käypä Hoito B. Ohje potilaille ja läheisille: Alzheimerin tauti. 22.9.2016. http://www.kaypahoito.fi/web/kh/suositukset/suositus?id=nix01595. Accessed 9.11.2018

Lambert JC, Heath S, Even G, et al. (2009) Genome-wide association study identifies variants at CLU and CR1 associated with Alzheimer's disease. Nat Genet, 41:1094-9

Landau SM, Mintun MA, Joshi AD, et al. (2012) Amyloid deposition, hypometabolism, and longitudinal cognitive decline. Ann Neurol, 72:578-86

Largeau B, Dupont AC, Guilloteau D, et al. (2017) TSPO PET Imaging: From Microglial Activation to Peripheral Sterile Inflammatory Diseases? Contrast Media Mol Imaging, 6592139

Lee JH, Agacinski G, Williams JH, et al. (2010) Intact cannabinoid CB1 receptors in the Alzheimer's disease cortex. Neurochem Int, 57:985-89

Leibson CL, Rocca WA, Hanson VA, et al. (1997) The risk of dementia among persons with diabetes mellitus: a population-based cohort study. Ann NY Acad Sci, 826:422-7

Leinonen V, Alafuzoff I, Aalto S, et al. (2008) Assessment of beta-amyloid in a frontal cortical brain biopsy specimen and by positron emission tomography with carbon 11-labelled Pittsburgh Compound B. Arch Neurol, 65(10):1304-9

Lewczuk P, Matzen A, Blennow K, et al. (2017) Cerebrospinal fluid Aβ42/40 corresponds better than Aβ42 to amyloid PET in Alzheimer's disease. J Alzheimers Dis, 55:813-22

Lewis J, McGowan E, Rockwood J, et al. (2000) Neurofibrillary tangles,amyotrophy and progressive motor disturbance in mice expressing mutant (P301L) tau protein. Nat Genet, 25:402-5

Leon WC, Canneva F, Partidge V, et al. (2010) A novel transgenic rat model with a full Alzheimer's-like amyloid pathology displays pre-plaque intracellular amyloid-beta-associated cognitive impairment. J Alzheimers Dis, 20(1):113-26

Leterrier C, Laine J, Darmon M, et al. (2006) Constitutive activation drives compartment-selective endocytosis and axonal targeting of type 1 cannabinoid receptors. J Neurosci 26:3141-53

Levy-Lahad E, Wasco W, Poorkaj P, et al (1995) Candidate gene for the chromosome 1 familial Alzheimer's disease locus. Science, 269:973-7

Li J, Yang JY, Yao XC, et al. (2013) Oligomeric Aβ-induced microglial activation is possibly mediated by NADPH oxidase. Neurochem Res, 38(2):443-52

Li XY, Men WW, Zhu H, et al. (2016) Age- and Brain Region-Specific Changes of Glucose Metabolic Disorder, Learning, and Memory Dysfunction in Early Alzheimer's Disease Assessed in APP/PS1 Transgenic Mice Using ^{18}F-FDG-PET. Int J Mol Sci, 18;17(10)

Liu P, Bilkey DK, Darlington CL, et al. (2003) Cannabinoid CB1 receptor protein expression in the rat hippocampus and entorhinal, perirhinal, postrhinal and temporal cortices: regional variations and age-related changes. Brain Res, 979:235-9

Liu B, Le KX, Park MA, et al. (2015) *In Vivo* Detection of Age- and Disease-Related Increases in Neuroinflammation by ^{18}F-GE180 TSPO MicroPET Imaging in Wild-Type and Alzheimer's Transgenic Mice. J Neuroscience, 35(47):15716-30

Liu Y, Liu F, Iqbal K, et al. (2008) Decreased glucose transporters correlate to abnormal hyperphosphorylation of tau in Alzheimer disease. FEBS Lett, 582:359-64

Liu Y, Liu F, Grundke-Iqbal I, et al. (2011) Deficient brain insulin signalling pathway in Alzheimer's disease and diabetes. J Pathol 225:54-62

Liu W, Zhuo P, Long Li, et al. (2017) Activation of brain glucose metabolism ameliorating cognitive impairment in APP/PS1 transgenic mice by electroacupuncture. Free Radic Biol Med, 112:174-90

Lo RY, Hubbard AE, Shaw LM, et al. (2011) Longitudinal change of biomarkers in cognitive decline. Arch Neurol, 68:1257-66

López-Picón F, Snellman A, Eskola O, et al. (2018) Neuroinflammation Appears Early on PET Imaging and Then Plateaus in a Mouse Model of Alzheimer Disease. J Nucl Med, 59:509-15

Lowe VJ, Kemp BJ, Jack jr. CR, et al. (2009) Comparison of ^{18}F-FDG and PiB PET in Cognitive Impairment. J Nucl Med, 50(6):878-86

Lowe VJ, Curran G, Fang P, et al. (2016) An autoradiographic evaluation of AV-1451 tau PET in dementia. Acta Neuropathol Commun, 4:58

Luckhaus C, Flüß MO, Wittsack HJ, et al. (2008) Detection of changed regional cerebral blood flow in mild cognitive impairment and early Alzheimer's dementia by perfusion-weighted magnetic resonance imaging. Neuroimage, 40(2):495-503

Luo C, Rustay NR, Ebert U, et al. (2012) Characterization of 7- and 19-month-old Tg2576 mice using multimodal *in vivo* imaging: limitations as a translatable model of Alzheimer's disease. Neurobiol Aging, 33(5):933-44

Lyoo CH, Ikawa M, Liow JS, et al. (2015) Cerebellum can serve as a pseudo-reference region in Alzheimer disease to detect neuroinflammation measured with PET radioligand binding to translocator protein. J Nucl Med, 56:701-6

Maccarrone M, Attina M, Bari M, et al. (2001) Anandamide degradation and N-acylethanolamines level in wild-type and CB1 cannabinoid receptor knockout mice of different ages. J Neurochem, 78:339-48

Maccarrone M, Totaro A, Leuti A, et al. (2018) Early alteration of distribution and activity of hippocampal type-1cannabinoid receptor in Alzheimer's disease-like mice overexpressingthe human mutant amyloid precursor protein. Pharmacological Research, 130:366-73

Macdonalds IR, DeBay DR, Reid GA, et al. (2014) Early detection of cerebral glucose uptake changes in the 5XFAD mouse. Curr Alzheimer Res, 11(5):450-60

Mackie K (2005) Distribution of cannabinoid receptors in the central and peripheral nervous system. Handb Exp Pharmacol, 168:299-325

Maeda J, Suhara T, Zhang MR, et al. (2004) Novel peripheral benzodiazepine receptor ligand ^{11}C-DAA1106 for PET: an imaging tool for glial cells in the brain. Synapse, 52:283-91

Maeda J, Zhang MR, Okauchi T, et al. (2011) *In vivo* positron emission tomographic imaging of glial responses to amyloid-β and tau pathologies in mouse models of Alzheimer's disease and related disorders. J Neurosci, 31(12):4720-30

Magistretti PJ and Pellerin L (1999) Astrocytes couple synaptic activity to glucose utilization in the brain. News Physiol Sci, 14:177-82

Mani SK, Mitchell A, and O'Malley BW (2001) Progesterone receptor and dopamine receptors are required in Delta 9-tetrahydrocannabinol modulation of sexual receptivity in female rats. Proc Natl Acad Sci USA, 98:1249-54

Manuel I, Gonzalez de San Roman E, Giralt MT, et al. (2014) Type-1 cannabinoid receptor activity during Alzheimer's disease progression. J Alzheimers Dis, 42:761-66

Manuel I, Lombarddero L, Larefla FM, et al. (2016) Activity of muscarinic, galanin and cannabinoid receptors in the prodromal and advanced stages in the triple transgenic mice model of Alzheimer's disease. Neuroscience, 329:284-93

Maroof N, Ravipati S, Pardon MC, et al. (2014) Reductions in endocannabinoid levels and enhanced coupling of cannabinoid receptors in the striatum are accompanied by cognitive impairments in the $APP_{swe}/PS1_{E9}$ mouse model of Alzheimer's disease. J Alzheimers Dis, 42:227-45

Marquié M, Normandin MD, Vanderburg CR, et al. (2015) Validating novel tau positron emission tomography tracer ^{18}F-AV-1451 (T807) on *postmortem* brain tissue. Ann Neurol, 78:787-800

Marquié M, Normandin MD, Meltzer AC, et al. (2017a) Pathological correlations of ^{18}F-AV-1451 imaging in non-Alzheimer tauopathies. Ann Neurol, 81:117-28

Marquié M, Siao Tick Chong M, Antón-Fernández A, et al. (2017b) ^{18}F-AV-1451 binding correlates with *postmortem* neurofibrillary tangle Braak staging. Acta Neuropathol, 134:619-28

Marsicano G, Wotjak CT, Azad SC, et al. (2002) The endogenous cannabinoid system controls extinction of aversive memories. Nature, 418:530-4

Martin M, Ledent C, Parmentier M, et al. (2002) Involvement of CB1 cannabinoid receptors in emotional behaviour. Psychopharmacology (Berl.) 159:379-87

Martín-Moreno AM, Brera B, Spuch C, et al. (2012) Prolonged oral cannabinoid administration prevents neuroinflammation, lowers β-amyloid leveles and improves cognitive performance in Tg APP 2576 mice. J Neuroinflammation, 9:8

Mathews WB, Ravert HT, Musachio JL, et al. (1999) Synthesis of ^{18}F-SR144385: A selective radioligand for positron emission tomographic studies of brain cannabinoid receptors. J Labelled Compd Rad, 42:589-96

Mathews WB, Scheffel U, Finley P, et al. (2000) Biodistribution of ^{18}F-SR144385 and ^{18}F-SR147963: Selective radioligands for positron emission tomographic studies of brain cannabinoid receptors. Nucl Med Biol, 27:757-62

Mathis CA, Lopresti BJ, Ikonomovic MD, et al. (2017) Small-molecule PET Tracers for Imaging Proteinopathies. Semin Nucl Med, 47(5):553-75

Maurer I, Zierz S, and Möller H (2000) A selective defect of cytochrome c oxidase is present in brain of Alzheimer disease patients. Neurobiol Aging, 21:455-62

McBride HM, Neuspiel M, and Wasiak S (2006) Mitochondria: more than just a powerhouse Curr Biol, 16:R551-R560

McGeer EG and McGeer PL (2010) Neuroinflammation in Alzheimer's disease and mild cognitive impairment: a field in its infancy. J Alzheimers Dis, 19(1):355-61

McGrew RE (1985) Encyclopedia of Medical History. USA: Roderick E. McGrew.

McKhann G, Drachman D, Folstein M, et al. (1984) Clinical diagnosis of Alzheimer's disease: report of the NINCDS-ADRDA Work Group under the auspices of Department of Health and Human Services Task Force on Alzheimer's Disease. Neurology, 34(7):939-44

McKhann G, Knopman DS, Chertkow H, et al. (2011) The diagnosis of dementia due to Alzheimer's disease: recommendations from the National Institute on Aging-Alzheimer's Association workgroups on diagnostic guidelines for Alzheimer's disease. Alzheimers Dement, 7(3):263-9

McLarnon JG, Ryu JK, Walker DG et al. (2006) Upregulated expression of purinergic P2X7 receptor in Alzheimer disease and amyloid-beta peptide treated microglia and in peptide-injected rat hippocampus. J Neuropathol Exp Neurol, 65(11):1090-7

Mechoulam R, Ben-Shabat S, Hanus L, et al. (1995) Identification of an endogenous 2-monoglyceride, present in canine gut, that binds to cannabinoid receptors. Biochem Pharmacol, 50:83-90

Mehla J, Chauhan BC, and Chauhan NB (2014) Experimental induction of type 2 diabetes in aging-accelerated mice triggered Alzheimer-like pathology and memory deficits. J Alzheimers Dis, 39:145-62

Miederer I, Maus S, Zwiener I, et al. (2013) Evaluation of cannabinoid type 1 receptor expression in the rat brain using ^{18}F-MK-9470 microPET. Eur J Nucl Med Mol Imaging, 40:1739-47

Milton NG (2002) Anandamide and noladin ether prevent neurotoxicity of the human amyloid-beta peptide. Neurosci Lett, 332:127-30

Minoshima S, Foster NL, Sima AA, et al. (2001) Alzheimer's disease versus dementia with Lewy bodies: cerebral metabolic distinction with autopsy confirmation. Ann Neurol, 50(3):358-65

Mintun MA, Larossa GN, Sheline YI, et al. (2006) ^{11}C-PIB in a nondemented population Potential antecedent marker of Alzheimer disease. Neurology, 67:446–52

Mirzaei N, Tang SP, Ashworth S, et al. (2016) *In vivo* imaging of microglial activation by positron emission tomography with [^{11}C]PBR28 in the 5XFAD model of Alzheimer's disease. Glia, 64:993–1006

Mochida I, Shimosegawa E, Kanai Y, et al. (2017) Whole-Body Distribution of Donepezil as an Acetylcholinesterase Inhibitor after Oral Administration in Normal Human Subjects: A ^{11}C-donepezil PET Study. Asia Ocean J Nucl Med Biol, Winter 5(1):3-9

Moechars D, Dewachter I, Lorent K, et al. (1999) Early phenotypic changes in transgenic mice that overexpress different mutants of amyloid precursor protein in brain. J Biol Chem, 274(10):6483-92

Moldovan RP, Hausmann K, Deuther-Conrad W, et al. (2017) Development of highly affine and selective fluorinated cannabinoid type 2 receptor ligands. ACSMed ChemLett 8:566-71

Montine TJ, Phelps CH, Beach TG, et al. (2012) National Institute on Aging-Alzheimer's Association guidelines for the neuropathologic assessment of Alzheimer's disease: a practical approach. Acta Neuropathol 123:1-11

Moreira PI, Santos MS, Moreno A, et al. (2001) Amyloid-peptide promotes permeability transition pore in brain mitochondria. Biosci Rep, 21:789-800

Moreira PI, Santos MS, Moreno A, et al. (2002) Effect of amyloid-peptide on permeability transition pore: A comparative study. J Neurosci Res, 69:257-67

Morgello S, Uson RR, Schwartz E.J, et al. (1995) The human blood-brain barrier glucose transporter (GLUT1) is a glucose transporter of gray matter astrocytes. Glia, 14:43-54

Morovic S, Jurasić MJ, Martinić Popović, et al. (2009) Vascular characteristics of patients with dementia. Journal of the Neurological Sciences, 283(1–2):41-3

Moses W (2011) Fundamental Limits of Spatial Resolution in PET. Nucl Instrum Methods Phys Res A 648 Supplement 1: S236–S40

Mouse MRI brain template (2005) MRM NAt Mouse Brain Database, McKnight Brain Institute, http://brainatlas.mbi.ufl.edu/Database/ Accessed 17.5.2013

Mulder J, Zilberter M, Pasquare SJ, et al. (2011) Molecular reorganization of endocannabinoid signalling in Alzheimer's disease. Brain, 134:1041-60

Mullan M, Crawford F, Axelman K, et al. (1992) A pathogenic mutation for probable Alzheimer′s disease in the APP gene at the N-terminus of beta-amyloid. Nat Genet, 1:345-7

Munoz L and Ammit AJ (2010) Targeting p38 MAPK pathway for the treatment of Alzheimer's disease. Neuropharmacology, 58:561-8

Murrell J, Farlow M, Ghetti B, et al. (1991) A mutation in the amyloid precursor protein associated with hereditary Alzheimer′s disease. Science, 254:97-9

Myers RH, Schaefer EJ, Wilson PW, et al. (1996) Apoliporotein E e4 association with dementia in a population-based study: the Framingham study. Neurology, 46:673-7

Nabulsi NB, Mercier J, Holden D, et al. (2016) Synthesis and Preclinical Evaluation of ^{11}C-UCB-J as a PET Tracer for Imaging the Synaptic Vesicle Glycoprotein 2A in the Brain. J Nucl Med, 57(5):777-84

Ngandu T, Lehtisalo J, Solomon A, et al. (2015) A 2 year multidomain intervention of diet, exercise, cognitive training, and vascular risk monitoring versus control to prevent cognitive decline in at-risk elderly people (FINGER): a randomised controlled trial. Lancet, 385(9984):2255-63

Nikolaev A, McLaughlin T, O'Leary DD, et al. (2009) APP binds DR6 to trigger axon pruning and neuron death via distinct caspases. Nature, 457(7232):981-9

Nilsberth C, Westlind-Danielsson A, Eckman CB, et al. (2001) The 'Arctic' APP mutation (E693G) causes Alzheimer′s disease by enhanced Abeta protofibril formation. Nat Neurosci, 4:887-93

Normandin MD, Zheng MQ, Lin KS, et al. (2014) Imaging the cannabinoid CB1 receptor in humans with ^{11}C-OMAR: assessment of kinetic analysis methods, test-retest reproducibility, and gender differences. J Cereb Blood Flow Metab, 35(8):1313-22

Norton S, Matthews FE, Barnes DB, et al. (2014) Potential for primary prevention of Alzheimer's disease: an analysis of population-based data. Lancet, 13(8):788-94

Nunez E, Benito C, Tolon RM, et al. (2008) Glial expression of cannabinoid CB2 receptors and fatty acid amide hydrolase are beta amyloid linked events in Down's syndrome. Neuroscience, 151:104-10

Oakley H, Cole SL, Logan S, et al. (2006) Intraneuronal beta-amyloid aggregates, neurodegeneration, and neuron loss in transgenic mice with five familial Alzheimer's disease mutations: potential factors in amyloid plaque formation. J Neurosci, 26(40):10129-40

Oddo S, Caccamo A, Shepherd JD, et al. (2003) Triple-transgenic model of Alzheimer's disease with plaques and tangles: intracellular Abeta and synaptic dysfunction. Neuron, 39(3):409-21

Oh YJ, Francis JW, Markelonis GJ, et al. (1992) Interleukin-1-beta and tumor necrosis factor-alpha increase peripheral-type benzodiazepine binding sites in cultured polygonal astrocytes. J Neurochem, 58:2131-38

Onaivi ES, Ishiguro H, Gong JP, et al. (2006) Discovery of the presence and functional expression of cannabinoid CB2 receptors in brain. Ann NY Acad Sci, 1074:514-36

Onaivi ES, Ishiguro H, Gu S, et al. (2012) CNS effects of CB2 cannabinoid receptors: beyond neuro-immuno cannabinoid activity. J Psychopharmacol, 26(1):92-103

Onyango IG, Lu J, Rodova M, et al. (2010) Regulation of neuron mitochondrial biogenesis and relevance to brain health. Biochim Biophys Acta, 1802:228-34

Onyango IG (2018) Modulation of mitochondrial bioenergetics as a therapeutic strategy in Alzheimer's disease. Neural Regen Res, 13(1):19-25

Ory D, Celen S, Gijsbers R, et al. (2016) Preclinical Evaluation of a P2X7 Receptor-Selective Radiotracer: PET Studies in a Rat Model with Local Overexpression of the Human P2X7 Receptor and in Nonhuman Primates. J Nucl Med, 57(9):1436-41

Ostojic J, Elfgren C, Passant U, et al. (2004) The tau R406W mutation causes progressive presenile dementia with bitemporal atrophy. Dement Geriatr Cogn Disord, 17:298-301

Ott V, Benedict C, Schultes B, et al. (2011) Intranasal administration of insulin to the brain impacts cognitive function and peripheral metabolism. Diabetes Obes Metabol, 14:214-21

Owen DR, Narayan N, Wells L, et al. (2017) Pro-inflammatory activation of primary microglia and macrophages increases 18 kDa translocator protein expression in rodents but not humans. J Cereb Blood Flow Metab, 37(8):2679-90

Ozmen L, Albientz A, Czech C, et al. (2009). Expression of transgenic APP mRNA is the key determinant for beta-amyloid deposition in PS2APP transgenic mice. Neurodegener Dis, 6(1-2):29-36

Papadopoulos V, Baraldi M, Guilarte TR, et al. (2006) Translocator protein (18 kDa): new nomenclature for the peripheral-type benzodiazepine receptor based on its structure and molecular function. Trends Pharmacol Sci, 27: 402-9

Parbo P, Ismail R, Hansen KV, et al. (2017) Brain inflammation accompanies amyloid in the majority of mild cognitive impairment cases due to Alzheimer's disease. Brain, 140:2002-11

Parbo P, Ismail R, Sommerauer M, et al. (2018) Does inflammation precede tau aggregation in early Alzheimer's disease? A PET study. Neurobiol Dis, 117:211-6

Parvathetani KL, Tertyshnikova S, Greco CR, et al. (2003) P2X7 mediates superoxide production in primary microglia and is upregulated in a transgenic mouse model of Alzheimer's disease. J Biol Chem, 278(15):12209-17

Passamonti L, Rodriguez PV, Hong YT, et al. (2018) ^{11}C-PK11195 binding in Alzheimer disease and progressive supranuclear palsy. Neurology, 90:e1989-96

Pathak D, Shields LY, Mendelsohn BA, et al. (2015) The role of mitochondrially derived ATP in synaptic vesicle recycling. J Biol Chem, 290:22325-36

Patterson C (2018) World Alzheimer Report 2018. The state of the art of dementai research. New frontiers. Alzheimer's Disease International. Londres, 46 p

Perry VH and Teeling J (2013) Microglia and macrophages of the central nervous system: the contribution of microglia priming and systemic inflammation to chronic neurodegeneration. Semin Immunopathol, 35:601-12

Peyronneau MA, Saba W, Goutal S, et al. (2013) Metabolism and quantification of ^{18}F-DPA-714, a new TSPO positron emission tomography radioligand. Drug Metab Dispos Biol Fate Chem, 41:122-31

Phelps ME (2000) Positron emission tomography provides molecular imaging of biological processes. Proc Natl Acad Sci USA 97:9226-33

Pihlaja R, Takkinen JS, Eskola O, et al. (2015) Monoacylglycerol lipase inhibitor JZL184 reduces neuroinflammatory response in APdE9 mice and in adult mouse glial cells. J Neuroinflammation, 12:81

Pike VW (2009) PET Radiotracers: crossing the blood-brain barrier and surviving metabolism. Trends Pharmacol Sci, 30(8):431-40

Piomelli D (2003) The molecular logic of endocannabinoid signalling. Nat. Rev. Neurosci. 4:873-84

Piro JR, Benjamin DI, Duerr JM, et al. (2012) A dysregulated endocannabinoid-eicosanoid network supports pathogenesis in a mouse model of Alzheimer's disease. Cell Rep, (1):617-23

Pitt J, Wilcox KC, Tortelli V, et al. (2017) Neuroprotective astrocyte-derived insulin/IGF-1 stimulate endocytic processing and extracellular release of neuron-bound Aβ oligomers. Mol Biol Cell, 28:2623-36

Plassman BL, Langa KM, Fisher GG, et al. (2008) Prevalence of cognitive imapairment without dementia in the United states. Ann Intern Med, 148(6):427-34

Platt B, Drever B, Koss D, et al. (2011) Abnormal cognition, sleep, EEG and brain metabolism in a novel knock-in Alzheimer mouse, PLB1. PLoS One 6(11):e27068

Poisnel G, Hérard AS, El Tannir El Tayara, et al. (2012) Increased regional cerebral glucose uptake in an APP/PS1 model of Alzheimer's disease. Neurobiol Aging, 33(9):1995-2005

Popa-Wagner A, Buga AM, Popescu B, et al. (2015) Vascular cognitive impairment, dementia, aging and energy demand. A vicious cycle. J Neural Transm (Vienna) 122 Suppl, 1:S47-54

Rabiner EA (2018) Imaging synaptic density: a different look at neurologic disease. J Nucl Med, 59:380-1

Rabinovici GD, Furst AJ, O'Neil JP, et al. (2007) ^{11}C-PIB PET imaging in Alzheimer disease and frontotemporal lobar degeneration. Neurology, 68:1205-12

Radak Z, Suzuki K, Higuchi M, et al. (2016) Physical exercise, reactive oxygen species and neuroprotection. Free Radic Biol Med 98:187-96

Radde R, Bolmont T, Kaeser SA, et al. (2006) Abeta42-driven cerebral amyloidosis in transgenic mice reveals early and robust pathology. EMBO Rep, 7(9):940-6

Rademakers R, Cruts M, Sleegers K, et al. (2005) Linkage and association studies identify a novel locus for Alzheimer disease at 7q36 in a Dutch population-based sample. Am J Hum Genet, 77:643-52

Ramirez BG, Blazquez C, Gomez del Pulgar T, et al. (2005) Prevention of Alzheimer's disease pathology by cannabinoids: Neuroprotection mediated by blockade of microglial activation. J Neurosci, 25:1904-13

Rapic S, Backes H, Viel T, et al. (2013) Imaging microglial activation and glucose consumption in a mouse model of Alzheimer's disease. Neurobiol Aging, 34:351-4

Ray Sujata and Davidson Susan (2014) Dementia and cognitive decline – a review of the evidence. Age UK Research

Reddy PH, Mani G, Park BS, et al. (2005) Differential loss of synaptic proteins in Alzheimer's disease: Implications for synaptic dysfunction. J Alzheimers Dis, 7(2):103-17

Reddy PH (2011) Abnormal tau, mitochondrial dysfunction, impaired axonal transport of mitochondria, and synaptic deprivation in Alzheimer's disease. Brain Res, 1415:136-48

Reitz C and Mayeux R (2014) Alzheimer disease: Epidemiology, diagnostic criteria, risk factors and biomarkers. Biochemical Pharmacology 88(4):640-51

Reltz C (2011) Epidemiology of Alzheimer disease. Nat Rev Neurol, 7:137-52

Riaño Barros DA, McGinnity CJ, Rosso L, et al. (2014) Test-retest reproducibility of cannabinoid-receptor type 1 availability quantified with the PET ligand ^{11}C-MePPEP. Neuroimage, 97:151-62

Rice L and Bisdas S (2017) The diagnostic value of FDG and amyloid PET in Alzheimer's disease – a systemic review. European J Radiology, 94:16-24

Riebe CJ, Hill MN, Lee TT, et al. (2010) Estrogenic regulation of limbic cannabinoid receptor binding. Psychoneuroendocrinology, 35:1265-9

Riekse RG, Leverenz JB, McCormick W, et al. (2004) Effect of vascular lesions on cognition in Alzheimer's disease: a community-based study. J Am Geriatr Soc, 52(9):1442-8

Rodriguez-Vieitez E, Ni R, Gulyás B, et al. (2015) Astrocytosis precedes amyloid plaque deposition in Alzheimer APPswe transgenic mouse brain: a correlative positron emission tomography and *in vitro* imaging study. Eur J Nucl Med Mol Imaging, 42:1119-32

Rogaeva E, Meng Y, Lee JH, et al. (2007) The neuronal sortilin-related receptor SORL1 is genetically associated with Alzheimer's disese. Nature Genet, 39:168-77

Rojas S, Herance JR, Gispert JD, et al. (2013) *In vivo* evaluation of amyloid deposition and brain glucose metabolism of 5XFAD mice using positron emission tomography. Neurobiol Aging, 34(7):1790-8

Rokka J, Grönroos TJ, Viljanen T, et al. (2017) HPLC and TLC methods for analysis of ^{18}F-FDG and its metabolites from biological samples. J Chromatography B, 1048:140-9

Rowe CC, Ackerman U, Browne W, et al. (2008) Imaging of amyloid-β in Alzheimer's disease with ^{18}F-BAY94-9172, a novel PET tracer: proof of mechanism. Lancet Neurol, 7:129-35

Royall DR (2007) Location, location, location! Neurobiol. Aging, 28:1481-2

Rupp NJ, Wegenast-Braun BM, Radde R, et al. (2011) Early onset amyloid lesions lead to severe neuritic abnormalities and local, but not global neuron loss in APPPS1 transgenic mice. Neurobiol Aging, 32(12):2324.e1-6.

Saha GB (2016) Performance Characteristics of PET Scanners. In Basics of PET imaging, Physics, Chemistry, and Regulations, Saha GB, ed. Third Edition, Springer International Publishing Switzerland

Salthouse T (2012) Consequences of age-related cognitive declines. Annu Rev Psychol, 63:201-26

Sancheti H, Akopian G, Yin F, et al. (2013) Age-dependent modulation of synaptic plasticity and insulin mimetic effect of lipoic acid on a mouse model of Alzheimer's disease. PLoS One, 8:e69830

Santillo AF, Gambini JP, Lannfelt L, et al. (2011) *In vivo* imaging of astrocytosis in Alzheimer's disease: an ^{11}C-Ldeuteriodeprenyl and PIB PET study. Eur J Nucl Med Mol Imaging, 38:2202-8.

Scarmeas N, Stern Y, Tang MX, et al. (2006) Mediterranean diet and risk for Alzheimer's disease. Ann, Neurol, 59:912-21

Scheltens NME, van der Weijden K, Adriaanse SM, et al. (2018) Hypometabolism of the posterior cingulate cortex is not restricted to Alzheimer's disease. Neuroimage:Clinical 19:625-32

Schmidt-Nielsen K (1984) Metabolic rate and body size. In: Scaling: Why is animal size so important? Cambridge Univeristy Press; Cambridge:56-74

Schuitemaker A, Kropholler MA, Boellaard R, et al. (2013) Microglial activation in Alzheimer's disease: an (*R*)-^{11}C-PK11195 positron emission tomography study. Neurobiol Aging, 34:128-36

Sehlin D, Fang XT, Cato L, et al. (2016) Antibody-based PET imaging of amyloid beta in mouse models of Alzheimer's disease. Nat Commun, 7:10759

Selkoe DJ (2000) The genetics and molecular pathology of Alzheimer's disease: roles of amyloid and the presenilins. Neurol Clin, 18(4):903-22

Sérrière S, Tauber C., Vercouillie J, et al. (2015) Amyloid load and translocator protein 18 kDa in APP_{swe}-$PS1_{dE9}$ mice: a longitudinal study. Neurobiol Aging, 36:1639-52

Sherrington R, Rogaev EI, Liang Y, et al. (1995) Cloning of a gene bearing missense mutations in early-onset familial Alzheimer's disease. Nature, 375:754-60

Shukuri M, Mawatari A, Ohno M, et al. (2016) Detection of Cyclooxygenase-1 in activated microglia during amyloid plaque progression: PET Studies in Alzheimer's disease model mice. J Nucl Med, 57:291-6

Sibson N, Dhankhar A, Mason G, et al. (1998) Stoichiometric coupling of brain glucose metabolismand glutamatergic neuronal activity. Proc Natl Acad Sci USA, 95:316-21

Simpson IA, Chundu KR, Davies-Hill T, et al. (1994) Decreased concentrations of GLUT1 and GLUT3

glucose transporters in the brains of patients with Alzheimer's disease. Ann Neurol, 35:546-51

Skoog I and Gustafson D (2003) Hypertension, hypertension-clustering factors and Alzheimer's disease. Neurol Res, (6):675-80

Smith HL, Bourne JN, Cao G, et al. (2016) Mitochondrial support of persistent presynaptic vesicle mobilization with age dependent synaptic growth after LTP. eLife, 5:e15275

Snyder SE, Tluczek L, Jewett DM, et al. (1998) Synthesis of 1-^{11}C-methylpiperidin-4-yl propionate (^{11}C-PMP) for *in vivo* measurements of acetylcholinesterase activity. Nucl Med Biol, 25(8):751-4

Sochocka M, Koutsouraki ES, Gasiorowski K, et al. (2013) Vascular oxidative stress and mitochondrial failure in the pathobiology of Alzheimer's disease: a new approach to therapy. CNS Neurol Disord Drug Targets, 12(6):870-81

Sokoloff L, Reivich M, Kennedy C, et al. (1977) The ^{14}C-deoxyglucose method for the measurement of local cerebral glucose utilization: theory, procedure, normal values in the conscious and and anesthetized albino rat. J Neurochem, 28(5):897-916

Sokoloff L (1979) Mapping of local cerebral functional activity by measurement of local cerebral glucose utilization with ^{14}C-deoxyglucose. Brain, 102:653-68

Solas M, Francis PT, Franco R, et al. (2013) CB2 receptor and amyloid pathology in frontal cortex of Alzheimer's disease patients. Neurobiol Aging, 34:805-8

Sperling RA, Laviolette PS, O'Keefe K, et al. (2009) Amyloid deposition is associated with impaired default network function in older persons without dementia. Neuron, 63(2):178-88

Sperling RA, Aisen PS, Beckett LA, et al. (2011) Toward defining the preclinical stages of Alzheimer's disease: recommendations from the National Institute on Aging-Alzheimer's Association workgroups on diagnostic guidelines for Alzheimer's disease. Alzheimers Dement, 7(3):280-92

Stella N (2009) Endocannabinoid signaling in microglial cells. Neuropharmacology 56 (Suppl 1), 244-53

Stephens A (2017) Characterization of novel PET tracers for the assessment of tau pathology In Alzheimer's disease and other tauopathies. AD/PD 2017 Oral Presentation. https://www.acimmune.com/en/ad-pd-2017/. Accessed 9.11.2018.

Stewart CR, Stuart LM, Wilkinson K, et al. (2010) CD36 ligands promote sterile inflammation through assembly of a Toll-like receptor 4 and 6 heterodimer. Nat Immunol, 11(2):155-61

Stewart JB and Chinnery PF (2015) The dynamics of mitochondrial DNA heteroplasmy: implications for human health and disease. Nat Rev Genet, 16:530-142

Strittmatter WJ, Saunders AM, Schmechel D, et al. (1993) Apolipoprotein E: High-avidity binding to Beta-amyloid and increased frequency of type 4 allele in late-onset familial Alzheimer's disease. Proc Natl Sci, 90:1977-81

Strodant M, Mintun MA, Head D, et al. (2009) Cognitive decline and brain volume loss are signatures of cerebral Aβ deposition identified with PIB, Arch Neurol, 66(12):1476-81

Stumm C, Hiebel C, Hanstein R, et al. (2013) Cannabinoid receptor 1 deficiency in a mouse model of Alzheimer's disease leads to enhanced cognitive impairment despite of a reduction in amyloid deposition. Neurobiol Aging, 34(11):2574-84

Sturchler-Pierrat C, Abramowski D, Duke M, et al. (1997) Two amyloid precursor protein transgenic mouse models with Alzheimer disease-like pathology. Proc Natl Acad Sci USA, 94(24):13287-92

Sugiura T, Kondo S, Kishimoto S, et al. (2000) Evidence that 2-arachidonoylglycerol but not N-palmitoylethanolamine or anandamide is the physiological ligand for the cannabinoid CB2 receptor. Comparison of the agonistic activities of various cannabinoid receptor ligands in HL-60 cells. J Biol Chem, 275:605-12

Sultana R, Mecocci P, Mangialasche F, et al. (2011) Increased protein and lipid oxidative damage in mitochondria isolated from lymphocytes from patients with Alzheimer's disease: Insights into the role of oxidative stress in Alzheimer's disease and initial investigations into a potential biomarker for this dementing disorder. J Alzheimers Dis, 24:77-84

Suolinna E-M, Haaparanta M, Paul R, et al. (1986) Metabolism of 2-^{18}F-Fluoro-2-Deoxyglucose in Tumor-Bearing Rats: Chromatographic and Enzymatic Studies. Nucl Med Biol, 13(5):577-81

Surasi DS, Bhambhvani, P, Baldwin, JA., et al. (2014) ^{18}F-FDG PET and PET/CT Patient Preparation: A Review of the Literature. Journal of Nuclear Medicine Technology, 42:5-13

Suridjan I, Pollock BG, Verhoeff NP, et al. (2015) *In vivo* imaging of grey and white matter neuroinflammation in Alzheimer's disease: A positron emission tomography study with a novel radioligand, ^{18}F-FEPPA. Mol Psychiatry, 20:1579-87

Swerdlow RH and Khan SM (2004) A "mitochondrial cascade hypothesis" for sporadic Alzheimer's disease. Medical hypotheses, 63:8-20

Swerdlow RH (2007) Location, location, location! Neurobiol Aging, 28(10):1483

Swerdlow RH, Burns JM and Khan SM (2014) The Alzheimer's Disease Mitochondrial Cascade Hypothesis: Progress and Perspectives. Biochim Biophys Acta, 1842(8):1219-31

Syvänen S, Fang XT, Hultqvist G, et al. (2017) A bispecific Tribody PET radioligand for visualization of amyloid-beta protofibrils – a new concept for neuroimaging. Neuroimage, 148:55-63

Takahashi K, Rochford CD, and Neumann H (2005) Clearance of apoptotic neurons without inflammation by microglial triggering receptor expressed on myeloid cells-2. J Exp Med, 201:647-57

Takeda S, Sato N, Uchio-Yamada K, et al. (2010) Diabetes-accelerated memory dysfunction via cerebrovascular inflammation and abeta deposition in an Alzheimer mouse model with diabetes. Proc Natl Acad Sci USA, 107:7036-41

Talbot K, Wang H, Kazi H, et al. (2012) Demonstrated brain insulin resistance in Alzheimer's disease patients is associated with IGF-1 resistance, IRS-1 dysregulation, and cognitive decline. J Clin Invest, 122:1316-38

Tan MS, Yu JT, and Tan L (2013) Bridging integrator 1 (BIN1): form, function, and Alzheimer's disease. Trends Mol Med, 19(10):594-603

Tanzi R (2012) The Genetics of Alzheimer Disease. Cold Spring Harb Perspect Med, 2:a006296

Tashiro K, Hasegawa M, Ihara Y, et al. (1997) Somatodendritic localization of phosphorylated tau in neonatal and adult rat cerebral cortex. Neuroreport, 8:2797–801

Terni B, Boada J, Portero-Otin M, et al. (2010) Mitochondrial ATP-synthase in the entorhinal cortex is a target of oxidative stress at stages I/II of Alzheimer's disease pathology. Brain Pathol, 20:222-33

Terry GE, Liow JS, Chernet E, et al. (2008) Positron emission tomography imaging using an inverse agonist radioligand to assess cannabinoid CB1 receptors in rodents. Neuroimage, 41:690-8

Terry GE (2009a) *In vivo* imaging of the cannabinoid CB1 receptor using positron emission tomography. In: Thesis for doctoral degree. Stockholm Karolinska Institutet, Sweden.

Terry GE, Liow JS, Zoghbi SS, et al. (2009b) Quantitation of cannabinoid CB1 receptors in healthy human brain using positron emission tomography and an inverse agonist radioligand. Neuroimage, 48:362-70

Terry GE, Hirvonen J, Liow JS, et al. (2010) Imaging and quantitation of cannabinoid CB1 receptors in human and monkey brains using ^{18}F-labeled inverse agonist radioligands. J Nucl Med, 51:112–20

Thal D, Rüb U, Orantes M, et al. (2002) Phases of amyloid beta deposition in the human brain and its relevance for the development of AD. Neurology, 58(2):1791-800

THL Muistisairauksien yleisyys. Terveyden ja hyvinvoinnin laitos. https://thl.fi/fi/web/kansantaudit/muistisairaudet/muistisairauksien-yleisyys. Accessed 19.11.2018.

Toyama H, Ichisea M, Liowa JS, et al. (2004) Evaluation of anesthesia effects on ^{18}F-FDG uptake in mouse brain and heart using small animal PET. Nucl Med Biol, 31:251-6

Tsukada, H, Ohba H, Nishiyama S, et al. (2014) PET imaging of ischemia-induced impairment of mitochondrial complex I function in monkey brain. J Cereb Blood Flow Metab, 34(4):708-14

Tönnies E and Trushina E (2017) Oxidative Stress, Synaptic Dysfunction, and Alzheimer's Disease. J Alzheimer's Disease, 57:1105-21

Van Dam D and De Deyn PP (2011) Animal models in the drug discovery pipeline for Alzheimer's disease. Br J Pharmacol, 164(4):1285-300

Vandenberghe R, Van Laere K, Ivanoiu A, et al. (2010) ^{18}F-flutemetamol amyloid imaging in Alzheimer disease and mild cognitive impairment: a phase 2 trial. Ann Neurol, 68:319-29

Vandeputte C, Casteels C, Struys T, et al. (2012) Small-animal PET imaging of the type 1 and type 2 cannabinoid receptors in a photothrombotic stroke model. Eur J Nucl Med Mol Imaging, 39:1796-806

Van Laere K, Goffin K, Casteels C, et al. (2008) Gender-dependent increases with healthy aging of the human cerebral cannabinoid-type 1 receptor binding using ^{18}F-MK-9470 PET. Neuroimage, 39(4):1533-41

Varrone A, Mattsson P, Forsberg A, et al. (2013) *In vivo* imaging of the 18-kDa translocator protein (TSPO) with ^{18}F-FEDAA1106 and PET does not show increased binding in Alzheimer's disease patients. Eur J Nucl Med Mol Imaging, 40:921-31

Varrone A, Oikonen V, Forsberg A, et al. (2015) Positron emission tomography imaging of the 18-kDa translocator protein (TSPO) with ^{18}F-FEMPA in Alzheimer's disease patients and control subjects. Eur J Nucl Med Mol Imaging, 42:438-46

Varrone A and Nordberg A (2015) Molecular imaging of neuroinflammation in Alzheimer's disease. Clin Transl Imag, 3(6):437-47

Vasdev N, Cao P, van Oosten EM, et al. (2012) Synthesis and PET imaging studies of ^{18}F-2-fluoroquinolin-8-ol

(^{18}F-CABS13) in transgenic mouse models of Alzheimer's disease. MedChemComm, 3:1228-30

Veenman L, Papadopoulos V, and Gavish M (2007) Channel-like function of the 18-kDa translocator protein (TSPO): regulation of apoptosis and steroidgenesis as part of the host-defence response. Curr Pharm Des, 13(23):2385-405

Veerhuis R, Janssen I, De Groot CJ, et al. (1999) Cytokines associated with amyloid plaques in Alzheimer's disease brain stimulate human glial and neuronal cell cultures to secrete early complement proteins, but not C1-inhibitor. Exp Neurol, 160(1):289-99

Venneti S, Lopresti BJ, Wang G, et al. (2009a) PK11195 labels activated microglia in Alzheimer's disease and *in vivo* in a mouse model using PET. Neurobiol Aging, 30:1217-26

Venneti S, Lopresti BJ, and Wiley CA (2013) Molecular imaging of microglia/macrophages in the brain. Glia, 61:10-23

Vicidomini C, Panico M, Greco A, et al. (2015) *In vivo* imaging and characterization of ^{18}F-DPA-714, a potential new TSPO ligand, in mouse brain and peripheral tissues using small-animal PET. Nucl Med Biol, 42:309-16

Villemagne VL, Pike KE, Chételat G, et al. (2011) Longitudinal assessment of Aβ and cognition in aging and Alzheimer disease. Ann Neurol, 69(1):181-92

Villemagne VL, Burnham S, Bourgeat P, et al. (2013) Amyloid β deposition, neurodegeneration, and cognitive decline in sporadic Alzheimer's disease: a prospective cohort study. Lancet Neurol, 12:357-67

Villemagne VL, Doré V, Burnham SC, et al. (2018) Imaging tau and amyloid-β proteinopathies in Alzheimer disease and other conditions. Nat Rev Neurol, 14(4):225-36

Viswanathan A, Rocca WA, and Tzourio C (2009) Vascular risk factors and dementia: how to move forward? Neurology, 72(4):368-74

Vlaardingerbroek M and Boer J (2003) Magnetic Resonance Imaging: Theory and Practice. Springer Science & Business Media ISBN 3-540-43681-2, 3rd edition, Springer-Verlag Berlin Heidelberg, New York (Printed in Germany)

Vos SJB, Xiong C, Visser PJ, et al. (2013) Preclinical Alzheimer's disease and its outcome: a longitudinal cohort study. Lancet Neurol, 12(10):957-65

VSSHP Guidelines for PET/CT experiment. https://hoito-ohjeet.fi/OhjepankkiVSSHP/PET-TT-tutkimus.pdf. Accessed 12.11.2018.

Wadsworth H, Jones PA, Chau WF, et al. (2012) ^{18}F-GE-180: a novel fluorine-18 labelled PET tracer for imaging translocator protein 18 kDa (TSPO). Bioorg Med Chem Lett, 22:1308-13

Waldron AM, Wyffels L, Verhaeghe J, et al. (2015a) Quantitative μPET Imaging of Cerebral Glucose Metabolism and Amyloidosis in the TASTPM Double Transgenic Mouse Model of Alzheimer's Disease. Curr Alzheimer Res, 12(7):694-703

Waldron AM, Wintmolders C, Bottelbergs A, et al. (2015b) *In vivo* molecular neuroimaging of glucose utilization and its association with fibrillar amyloid-β load in aged APPPS1-21 mice. Alzheimers Res Ther, 7(1):76

Waldron AM, Wyffels L, Verhaeghe J, et al. (2017) Longitudinal Characterization of ^{18}F-FDG and ^{18}F-AV45 Uptake in the Double Transgenic TASTPM Mouse Model. J Alzheimers Dis, 55(4):1537-48

Walji AM, Hostetler ED, Selnick H, et al. (2016) Discovery of 6-(Fluoro-^{18}F)-3-(1H-pyrrolo[2,3-c]pyridin-1yl)isoquinolin-5-amine (^{18}F-MK6240): a positron emission tomography (PET) imaging agent for quantification of neurofibrillary tangles (NFTs). J Med Chem, 59:4778-89

Walter L, Franklin A, Witting A, Wet al. (2003) Nonpsychotropic cannabinoid receptors regulate microglial cell migration. J Neurosci, 23:1398-405

Wang L, Liu J, Harvey-White J, et al. (2003) Endocannabinoid signaling via cannabinoid receptor 1 is involved in ethanol preference and its age-dependent decline in mice. Proc Natl Acad Sci USA, 100:1393-8

Wang L, Benzinger TL, Su Y, et al. (2016) Evaluation of tau imaging in staging Alzheimer disease and revealing interactions between β-amyloid and tauopathy. JAMA Neurol, 73:1070-7

Watt G and Karl T (2017) *In vivo* evidence for therapeutic propertiesof cannabidiol (CBD) for Alzheimer's disease. Front Pharmacol, 8(20):1-7

Wenk GL, McGann K, Hauss-Wegrzyniak B et al. (2003) The toxicity of tumor necrosis factor-alpha upon cholinergic neurons within the nucleus basalis and the role of norepinephrine in the regulation of inflammation: implications for Alzheimer's disease. Neuroscience, 121(3):719-29

Westlake TM, Howlett AC, Bonner TI, et al. (1994) Cannabinoid receptor binding and messenger RNA expression in human brain: an *in vitro* receptor autoradiography and in situ hybridization histochemistry study of normal aged and Alzheimer's brains. Neuroscience, 63:637-52

WHO Dementia http://www.who.int/mental_health/neurology/dementia/en/ . accessed 27.06.2018

Whitmer RA, Sidney S, Selby J, et al. (2005) Midlife cardiovascular risk factors and risk of dementia in late life. Neurology, 64:277-81

Wilson AA, Garcia A, Parker J, et al. (2008) Radiosynthesis and initial evaluation of ^{18}F-FEPPA for PET imaging of peripheral benzodiazepine receptors. Nucl Med Biol, 35(3):305-14

Wilson RI and Nicoll RA (2001) Endogenous cannabinoids mediate retrograde signalling at hippocampal synapses. Nature, 410:588-92

Wingfield JC and Kitaysky AS (2002) Endocrine responses to unpredictable environmental events: stress or anti-stress hormones? Integrative and comparative biology, 42:600-9

World Alzheimer's Report 2014. https://www.alz.co.uk/research/world-report-2014. Accessed 15.11.2018.

Xia C, Makaretz SJ, Caso C, et al. (2017) Association of In Vivo ^{18}F-AV-1451 Tau PET Imaging Results With Cortical Atrophy and Symptoms in Typical and Atypical Alzheimer Disease. JAMA Neurol 74(4):427-36

Yao J, Irwin RW, Zhao L, et al. (2009) Mitochondrial bioenergetic deficit precedes Alzheimer's pathology in female mouse model of Alzheimer's disease. Proc Natl Acad Sci USA, 106:14670-5

Yasuno F, Ota M, Kosaka J, et al. (2008a), Increased binding of peripheral benzodiazepine receptor in Alzheimer's disease measured by positron emission tomography with ^{11}C-DAA1106. Biol Psychiatry, 64:835-41

Yasuno F, Brown AK, Zoghbi SS, et al. (2008b) The PET radioligand ^{11}C-MePPEP binds reversibely and with high specific signal to cannabinoid CB1 receptors in ninhuman primate brain. Neuropsychopharmacology, 33:259-69

Yin F, Sancheti H, Patil I, et al. (2016) Energy metabolism and inflammation in brain aging and Alzheimer's disease. Free Radic Biol Med, 100:108-22

Yoon SO, Park DJ, Ryu JC, et al. (2012) JNK3 perpetuates metabolic stress induced by Aβ peptides. Neuron, 75(5):824-37

Youmans KL, Tai LM, Nwabuisi-Heath E, et al. (2012) APOE4-specific changes in Aβ accumulation in a new transgenic mouse model of Alzheimer disease. J Biol Chem, 287(50):41774-86

Yu T, Robotham JL and Yoon Y (2006) Increased production of reactive oxygen species in hyperglycemic conditions requires dynamic change of mitochondrial morphology. Proc Natl Acad Sci USA, 103:2653-8

Zanotti-Fregonara P, Pascual B, Rizzo G, et al. (2018) Head-to-Head Comparison of ^{11}C-PBR28 and ^{18}F-GE180 for Quantification of the Translocator Protein in the Human Brain. J Nucl Med, 59:1260-6

Zhang L, Chen L, Dutra JK, et al. (2018) Identification of a Novel Positron Emission Tomography (PET) Ligand for Imaging β-Site Amyloid Precursor Protein Cleaving Enzyme 1 (BACE-1) in Brain. J Med Chem, 61(8):3296-308

Zhang MR, Maeda J, Ogawa M, et al. (2004) Development of a new radioligand, N-(5-fluoro-2-phenoxyphenyl)-N-(2 ^{18}F-fluoroethyl-5-methoxybenzyl)acetam ide, for PET imaging of peripheral benzodiazepine receptor in primate brain. J Med Chem, 47:2228-35

Zhang S, Han D, Tan X, et al. (2012) Diagnostic accuracy of ^{18}F-FDG and ^{11}C-PIB-PET for prediction of short-term conversion to Alzheimer's disease in subjects with mild cognitive impairment. Int J Clin Pract, 66:185-98

Zhang W, Cai Z, Li L, et al. (2016) Optimized and Automated Radiosynthesis of ^{18}F-DHMT for Translational Imaging of Reactive Oxygen Species with Positron Emission Tomography. Molecules, 9;21(12)

Zhang YW, Thompson R, Zhang H, et al. (2011) APP processing in Alzheimer's disease. Mol Brain 4:3

Zhou R, Yazdi AS, Menu P, et al. (2011) A role for mitochondria in NLRP3 inflammasome activation. Nature, 469:221-5

Öhrfelt A, Brinkmalm A, Dumurgier J, et al. (2016) The presynaptic vesicle protein synaptotagmin is a novel biomarker for Alzheimer's disease. Alzheimers Res Ther, 8(1):41

Annales Universitatis Turkuensis

UNIVERSITY OF TURKU

ISBN 978-951-29-7601-0 (PRINT)
ISBN 978-951-29-7602-7 (PDF)
ISSN 0355-9483 (Print) ISSN 2343-3213 (Online)

Painosalama Oy, Turku , Finland 2019